AD_____

Award Number: DAMD17-01-1-0490

TITLE: An Epigenetic Approach to Breast Cancer Treatment

PRINCIPAL INVESTIGATOR: Norbert R. Reich, Ph.D.

CONTRACTING ORGANIZATION: The University of California
Santa Barbara, California 93106-2050

REPORT DATE: August 2003

TYPE OF REPORT: Final

PREPARED FOR: U.S. Army Medical Research and Materiel Command
Fort Detrick, Maryland 21702-5012

REPORT DOCUMENTATION PAGE

Form Approved
OMB No. 074-0188

1. AGENCY USE ONLY (Leave blank)	2. REPORT DATE	3. REPORT TYPE AND DATES COVERED
	August 2003	Final (2 Jul 2001 - 1 Jul 2003)

4. TITLE AND SUBTITLE
An Epigenetic Approach to Breast Cancer Treatment

5. FUNDING NUMBERS
DAMD17-01-1-0490

6. AUTHOR(S)
Norbert R. Reich, Ph.D.

7. PERFORMING ORGANIZATION NAME(S) AND ADDRESS(ES)
The University of California
Santa Barbara, California 93106-2050

E-Mail: reich@chem.ucsb.edu

8. PERFORMING ORGANIZATION REPORT NUMBER

9. SPONSORING / MONITORING AGENCY NAME(S) AND ADDRESS(ES)
U.S. Army Medical Research and Materiel Command
Fort Detrick, Maryland 21702-5012

10. SPONSORING / MONITORING AGENCY REPORT NUMBER

11. SUPPLEMENTARY NOTES

12a. DISTRIBUTION / AVAILABILITY STATEMENT
Approved for Public Release; Distribution Unlimited

12b. DISTRIBUTION CODE

13. ABSTRACT (Maximum 200 Words)
DNA methylation is an epigenetic process that leads to normal and dysfunctional gene regulation. The latter is a well-documented pathway to tumorigenesis, particularly for certain tumors, such as those involved in breast cancer. We have identified several inhibitors of the mammalian DNA cytosine methyltransferase, and are trying to determine if such compounds are suitable for further development as cancer therapies.

14. SUBJECT TERMS
No subject terms provided.

15. NUMBER OF PAGES
67

16. PRICE CODE

17. SECURITY CLASSIFICATION OF REPORT	18. SECURITY CLASSIFICATION OF THIS PAGE	19. SECURITY CLASSIFICATION OF ABSTRACT	20. LIMITATION OF ABSTRACT
Unclassified	Unclassified	Unclassified	Unlimited

Table of Contents

INTRODUCTION: This project sought to determine if inhibitors of the mammalian DNA cytosine methyltransferase (Dnmt1) could form the basis of a novel therapy for cancer, and in particular, breast cancer. As part of this, we carried out detailed characterization of a well studied bacterial DNA cytosine methyltransferase (M.HhaI) as well as the Dnmt1. These efforts are summarized in the two manuscripts included in the appendix. We include another manuscript describing a potent Dnmt1 inhibitor; this published work was not directly supported by this Army grant, but is quite relevant.

BODY: The first part of this effort focused on M.HhaI, to provide a basis for understanding Dnmt1, and to develop novel inhibitors of the enzyme. We measured the tritium exchange reaction on cytosine C^5 in the presence of AdoMet analogs to investigate the catalytic mechanism of M.HhaI. Poly (dG-dC) and poly (dI-dC) substrates were used to investigate the function of the active site loop (residues 80-99), stability of the extra-helical base, base flipping mechanism, and processivity on DNA substrates. Based on several experimental approaches, we show that methyl transfer is the rate limiting presteady state step. Further, we show that the active site loop opening contributes to the rate limiting step during multiple cycles of catalysis. Target base activation and nucleophilic attack by $Cysteine^{81}$ is fast and readily reversible. Thus, the reaction intermediates involving the activated target base and the extrahelical base are in equilibrium and accumulate prior to the slow methyltransfer step. The stability of the activated target base depends on the active site loop closure, which is dependent on the hydrogen bond between $Isoleucine^{86}$ and the guanine 5′ to target cytosine. These interactions prevent the premature release of the extrahelical base and uncontrolled solvent access; the latter modulates the exchange reaction, and by implication, the mutagenic deamination reaction. The processive catalysis by M.HhaI is also regulated by the interaction between $Isoleucine^{86}$ and DNA substrate. Nucleophilic attack by $Cysteine^{81}$ is partially rate limiting when the target base is not fully stabilized in the extra-helical position, as observed during the reaction with the $Gln^{237}Trp$ mutant or in the cytosine C^5 exchange reaction in the absence of the cofactor.

In the second part of the effort, we characterized the murine Dnmt1. The cytosine C^5 proton exchange reaction catalyzed by murine Dnmt1 was measured with AdoMet analogs

to characterize how the formation and conversion of reaction intermediates differ with unmethylated and premethylated DNA. We also describe precautions and limitations in the design of Dnmt1 assays. Dnmt1 and the bacterial enzyme M.HhaI share many similarities but also differ in catalytic rates by 10-100 fold. The reaction intermediates prior to the rate limiting methyltransfer for Dnmt1 and M.HhaI are in rapid equilibrium. The slower rates observed with Dnmt1 relative to M.HhaI result from slower steps leading to the formation of the activated target base. Like M.HhaI, Dnmt1 interactions with the guanine 5' to the target cytosine can prevent the premature release of the target base and solvent access to the active site. Solvent access leads to an uncontrolled exchange reaction which is mechanistically related to the mutagenic deamination of cytosine and 5-methylcytosine. Placement of a single methylated cytosine within a span of 20 CpG sites is sufficient to allow Dnmt1 to differentiate between unmethylated and premethylated DNA. Premethylated DNA substrates show a pre-steady state burst and no substrate inhibition and unmethylated DNA shows an initial lag and substrate inhibition. The lag and allosteric inhibition are mechanistically related, indicating that the initiation of catalysis leads to a slow relief from allosteric inhibition. The faster rates with premethylated DNA are due to the more rapid accumulation of the activated target base.

KEY RESEARCH ACCOMPLISHMENTS:

1. Showed that the rate limiting step in DNA methylation for bacterial and mammalian enzymes is the methyltransfer step.
2. Showed that the well-characterized "activation" observed with the mammalian enzyme with DNA previously methylated, does not come from the deposition of methyl groups per se, but rather the catalytic process itself.
3. Dnmt1 is capable of carrying out multiple cycles of catalysis, as scored by the exchange reaction on cytosine, prior to delivering a methyl group.
4. Dnmt1 effectively carries out the cytosine C5 exchange reaction, which is mechanistically quite similar to the mutagenic deamination of cytosine. The latter is thought to be an important pathway towards commonly observed mutations which lead to cancer. Thus, our results suggest that Dnmt1-catalyzed deamination of

cytosine and 5-methyltcytosine may lead to the onset of tumorigenesis.

REPORTABLE OUTCOMES: Two manuscripts directly covering the results outlined above, are included in the appendix.

CONCLUSIONS: Our results provide a sound basis for developing assays and high through put screens for identifying inhibitors of Dnmt1 or related DNA cytosine methyltransferases. Such compounds are likely to be leads in the further development of epigenetically based cancer therapies.

APPENDICES:

DNA cytosine C^5 methyltransferase Dnmt1: modulation of the catalytic mechanism with premethylated DNA, Željko M. Svedružić and Norbert O. Reich, JBC, submitted.

The mechanism of target base attack in DNA cytosine C^5 methylation Željko Svedružić and Norbert O. Reich, JBC volume 43, 2004 11460-11473.

A potent cell-active allosteric inhibitor of murine DNA cytosine C5 methyltransferase.Flynn, J., Fang, JY, Mikovits, JA., Reich, NO, 2003, JBC, 278 8238-8243.

DNA cytosine C^5 methyltransferase Dnmt1: modulation of the catalytic mechanism with premethylated DNA

Running title: catalytic intermediates, rate limiting step, and allosteric regulation of Dnmt1

Željko M. Svedružić[#] and Norbert O. Reich*

From the Department of Chemistry and Biochemistry, University of California, Santa Barbara, California 93106

keywords: methylation spreading, maintenance methylation, epigenetics, presteady state kinetics, steady state kinetics, rate limiting steps, solvent kinetic isotope effect, allosteric regulation, mutagenic deamination, base flipping, pyrimidine methyltransferase

[#] Current address: School of Molecular Biosciences, Department of Biophysics and Biochemistry, Washington State University, Pullman, WA 99164

*To whom correspondence should be addressed, email reich@chem.ucsb.edu; Phone 805-893-8368

This work was supported by NIH GM56289 to N.O.R.

ABSTRACT: The cytosine C^5 proton exchange reaction catalyzed by murine Dnmt1 was measured with AdoMet analogs to characterize how the formation and conversion of reaction intermediates differ with unmethylated and premethylated DNA. We also describe precautions and limitations in the design of Dnmt1 assays. Dnmt1 and the bacterial enzyme M.HhaI share many similarities but also differ in catalytic rates by 10-100 fold. The reaction intermediates prior to the rate limiting methyltransfer for Dnmt1 and M.HhaI are in rapid equilibrium. The slower rates observed with Dnmt1 relative to M.HhaI result from slower steps leading to the formation of the activated target base. Like M.HhaI, Dnmt1 interactions with the guanine 5' to the target cytosine can prevent the premature release of the target base and solvent access to the active site. Solvent access leads to an uncontrolled exchange reaction which is mechanistically related to the mutagenic deamination of cytosine and 5-methylcytosine. Placement of a single methylated cytosine within a span of 20 CpG sites is sufficient to allow Dnmt1 to differentiate between unmethylated and premethylated DNA. Premethylated DNA substrates show a pre-steady state burst and no substrate inhibition and unmethylated DNA shows an initial lag and substrate inhibition. The lag and allosteric inhibition are mechanistically related, indicating that the initiation of catalysis leads to a slow relief from allosteric inhibition. The faster rates with premethylated DNA are due to the more rapid accumulation of the activated target base.

Abbreviations: **AdoMet**, *S*-adenosyl-L-methionine; **AdoHcy,** *S*-adenosyl-L-homocysteine; **bp** base pair, as two bases paired in Watson-Crick fashion; **C**, cytosine; $\mathbf{C^5}$ or $\mathbf{C^6}$ *etc.*, carbon 5 or carbon 6 in a pyrimidine ring; ^{5m}**C** - 5-methylcytosine, **dCTP**-deoxycytosine triphosphate; **dITP**-deoxyinosine triphosphate; **Dnmt1**-DNA methyltransferase type 1; **MEL** mouse erythroleukemia; **M.HhaI,** Methyltransferase, *Haemophilus haemolyticus* type I; **poly(dG-dC) or dGdC**, double stranded alternating polymer of deoxyguanine and deoxycytosine; **poly(dI-dC)**, double stranded polymer of alternating deoxyinosine-deoxycytosine; **pmpoly (dG-dC) or dGdC**, double stranded alternating polymer of deoxyguanine and deoxycytosine; **pmpoly(dI-dC)**, premethylated poly(dI-dC); **sin**, sinefungin; **SKIE** solvent kinetic isotope effect.

ACKNOWLEDGMENTS: We wish to thank UCSB undergraduate student Jamie Witham for help in these measurements. We are grateful to Prof. H. Olin Spivey from Oklahoma State University for advice on the initial lag analysis, and to Dr Sriharsa Pradhan at New England Biolabs, and Dr Albino Bacolla at Texas A&M University for their correspondence during these studies. We are grateful to Prof. Nancy C. Horton at University of Arizona for help in the molecular modeling studies. We gratefully acknowledge Ben Hopkins and Stephen Fiacco for their excellent help in these experiments, and Ana M. Ojeda and Dr Peter Vollmyer for help in Dnmt1 purification.

DNA methylation in eukaryotes occurs predominately at CpG dinucleotides and is essential for normal embryogenesis and cellular activity (1). The patterns of DNA methylation are tissue-specific and change dynamically throughout development. Inappropriate DNA methylation of tumor suppresser genes (2) and DNA repair genes (3-5) are non-mutagenic events which occur early in carcinogenesis (6). Dnmt1 is one of three predominant isoforms, and has both *de novo* and maintenance activity *in vitro* and *in vivo*. Dnmt1 is a large multi-domain protein that is structurally and functionally more complex than its smaller, bacterial counterparts (7-15). Mechanism-based inhibition of bacterial and mammalian DNA cytosine methyltransferases by 5-fluoro-cytosine (14,16), and the conserved sequence motifs observed in all DNA cytosine methyltransferases (17,18), suggest that Dnmt1 and its bacterial counterparts share similar catalytic mechanisms (Fig 1). However the sequence homology with the bacterial enzymes is found only in the small C terminal domain of Dnmt1 (18) and the large N terminal domain contains numerous regulatory sites, including a site of phosphorylation (Ser 514) (19), an allosteric DNA binding site (11,20), nuclear localization signal (21), PCNA binding sequence (22), replication foci homing sequence (23), and Zn-finger sequence motifs (20). The N-terminal allosteric site is believed to regulate the enzyme's preference for DNA containing a distribution of 5-methylcytosines (premethylated DNA) (11,20). An N-terminal allosteric site was postulated to cause potent cell-based, sequence-dependent Dnmt1 inhibition (8). The majority of the reported mechanistic studies on mammalian Dnmt1 use the murine (7-10,24) and human (11,12,14) enzymes, which share 78 % sequence identity.

Dnmt1's preference for premethylated DNA is frequently invoked as a key regulatory mechanism (7,10-13,25). Premethylated DNA includes sequences in which either cytosine within the CpG dinucleotide in duplex DNA is methylated (hemimethylated DNA), and in which the 5-methyl cytosine lies outside this recognition CpG, but within the enzyme's DNA footprint. Hemimethylated DNA occurs predominately following DNA replication and provides a basis for Dnmt1's propagation of methylation patterns, presumably through a multi-protein complex that assembles at

the sites of replication. 5-Methylcytosines (^{5m}C) positioned outside the target CpG dinucleotide are thought to be important for the allosteric regulation of the enzyme.

Dnmt1's catalytic preference for premethylated DNA derives in part from a faster methylation constant (7). Pedrali-Noy *et. al.* postulated that the enzyme's preference for premethylated DNA is due to the inhibitory action of unmethylated DNA (26), which was further elaborated by Bestor to function through an allosteric site on the N-terminal domain (20). A variety of studies have shown that the N-terminal domain is required for Dnmt1 function (11,27). Removal of the first 501 N-terminal residues results in a mutant Dnmt1 with higher than WT activities with both unmethylated and premethylated DNA (11). Thus, some form of allosteric inhibition is likely to be present with different DNA substrates. Surprisingly, the mutant still differentiates between premethylated and unmethylated DNA (11). We previously showed that Dnmt1 forms ternary enzyme:DNA:DNA complexes, that different DNA sequences vary in their binding affinity, and that the binding of a second DNA molecule most likely involves the N-terminal domain (8,9). In sum, previous studies (8,11,12,26) suggest that the N-terminal domain acts to inhibit the enzyme, and that a complex interplay between the enzyme's different DNA binding sites result in the enzyme's regulation. Our interest is to characterize the mechanisms of the enzyme's substrate preference and allosteric regulation.

We recently defined a kinetic approach for M.HhaI providing new insights into which steps limit catalysis and the nature of various reaction intermediates (28). Briefly, intermediate **2** (Fig 1) is readily protonated in the presence of a proton donor (pKa=11-18, (29)), so the ^{3}H exchange reaction in the presence of AdoMet analogues (i.e. proton donors, Fig 2), represents an opportunity to analyze this crucial stage of the catalysis (Fig 1, **1**→**2**). Here we use this approach with murine Dnmt1, by monitoring the cytosine C^5 exchange reaction with AdoMet analogs and poly (dG-dC) and poly (dI-dC) substrates. Our primary interest is of the Dnmt1:DNA complex involving the cognate site, as represented either by poly (dG-dC) or poly (dI-dC). These homogenous substrates cause each enzyme molecule to interact with the same DNA sequence, at both the active and allosteric sites (Fig 10). Further, all enzyme-DNA complexes are likely to be active since

every enzyme molecule bound to the DNA is bound at the recognition site, thereby increasing the sensitivity of the assay for an enzyme as slow as Dnmt1. These studies with poly (dG-dC) and poly (dI-dC) also provide a convenient comparison with prior studies of Dnmt1 (8,10,11,18,23,31).

Materials and Methods

S-adenosyl-L-[methyl^{14}C] methionine (59 mCi/mmol or 131 cpms/pmol), *S*-adenosyl-L-[methyl ^{3}H] methionine (66 to 82 Ci/mmol or 6100 to 7200cpms/pmol), deoxy[5-^{3}H] cytidine 5' triphosphate (19.0 Ci/mmol) ammonium salt, and Sequenase 2.0 were purchased from Amersham Corp. Poly poly(dI-dC) 1960 bp, dITP and dCTP were purchased from Pharmacia Biotech. DTT, Trizma, BSA fraction V and activated charcoal were purchased from Sigma Chemical Co. Some BSA batches were inhibitory, and each BSA batch was tested by showing that the reaction rate did not vary with BSA concentration (0.2 to 1.0 mg/ml). DE81 filters were purchased from Whatman, Inc. Sinefungin was purchased from Sigma Chemical Co. AdoMet 85% pure was purchased form Sigma Chemical Co (31). Dnmt1 was prepared from mouse erythroleukemia cells as previously described (32), and its concentration was determined by active site titration (7) and by titration with a potent Dnmt1 inhibitor (Kd $\approx$ 20 nM, (8)). The enzyme concentration determined by the presteady state burst is 40% lower than enzyme concentration determined by titration with the inhibitor. Because the presteady state burst is expected to give a lower measure of enzyme concentration (eqn. 1), we relied on the use of the oligonucleotide inhibitor to determine Dnmt1 concentration. M.HhaI was expressed using *E.coli* strain ER1727 containing plasmid pHSHW-5 (both provided by S. Kumar, New England Biolabs) and purified as previously described (15). AdoMet, sinefungin, poly(dI-dC) and pmpoly(dI-dC) concentrations were determined by absorbance at 260 nm. The respective molar absorptivity coefficients are: 15.0 10^3 M^{-1} cm^{-1} for AdoMet and sinefungin (Merck Index), 6.9 10^3 M^{-1} cm^{-1} for poly(dI-dC) bp (Pharmacia Tech. Info. Sheet).

Methods

Preparation of premethylated poly(dG-dC) and poly(dI-dC). The premethylated substrates were prepared with excess AdoMet and M.HhaI (Fig 10). The labeling reaction was run for only one or two turnovers (1.5 to 2 min) to limit the number of methylated cytosines (^{5m}C) to the number of initially bound M.HhaI molecules. For example, 30-40 μM M.HhaI and 100 μM of [methyl ^{14}C] AdoMet were incubated with 300 μM bp DNA (approximately 30μM of M.HhaI footprints, based on a 10 bp footprint, Fig 10 and (33)).

This reaction was quenched (90°C water bath for 3-5 min), followed by slow cooling (2-3 h) to room temperature to assure gradual DNA annealing. M.HhaI was removed by centrifugation and the remaining labeling mixture was dialyzed against 10 mM Tris/HCl pH (8.0) and 10mM EDTA. The extent of dialysis was determined with DE81 filter papers and washing the filters with 500 mM KPi buffer pH=6.8 as described above. Dialysis was continued until the washed and unwashed samples had the same counts. The final DNA concentration and extent of methylation were determined by measuring the absorbance at 260 nm and DNA specific activity, respectively. The substrates prepared by this procedure contain an average of one $5^{m}C$ every 7 to 20 bp, depending on the length of the labeling reaction and the ratio between total M.HhaI and DNA. All substrates prepared in this fashion showed a characteristic presteady state burst characteristic (7).

Preparation of [5-^{3}H] cytosine-poly(dG-dC) and poly(dI-dC). The labeling reactions for poly(dI-dC) were prepared by incubating 500 μM bp of poly(dI-dC) with 100 μM [5-^{3}H] dCTP, 1 mM CTP, 10 mM dITP with 0.62 U/μL of Sequenase 2.0 in 40 mM Tris/HCl (pH 7.5), 10 mM $MgCl_2$, 50 mM NaCl, 10mM DTT and 1.0 mg/ml BSA. The same approach was used in the labeling reactions with poly(dG-dC) except that poly(dI-dC) and 10 mM dITP were replaced by poly(dG-dC) and 1 mM dGTP. The labeling reactions were run for five hours at room temperature. Incorporation of [5-^{3}H] cytosine was determined by placing the reaction aliquots onto DE81 filter papers. Filters were washed twice for 5 min in 500 mM KPi buffer (pH, 6.8) and dried under a heat lamp. The high ionic strength (500 mM KPi) removes free nucleotides from the DE81 filters without impacting the bound DNA. The extent of label incorporation was calculated by comparing the counts from unwashed and washed papers. The procedure routinely results in approximately 30-60% label incorporation. The quenching, annealing, and dialysis procedures were as described for the premethylated substrates. The removal of reaction components was determined by comparing the radioactivity from unwashed and washed DE81 papers as indicated above. The labeling gives 13-40 cpms/pmol of base pairs for poly(dI-dC), and 60-105 cpms/pmol of base pairs for poly(dG-dC).

Methylation reactions. The methylation reactions were prepared by incubating M.HhaI, DNA substrate and radioactive AdoMet in 100 mM Tris/HCl (pH, 8.0), 10 mM

EDTA, 10 mM DTT and 0.5 mg/ml of BSA at 37 °C. The enzyme and DNA concentrations are specific for each assay and described in the figure legends. Incorporation of tritiated methyl groups into DNA was determined as previously described (31). Briefly, a typical reaction was followed by placing reaction aliquots onto DE81 paper, which allows the detection of intermediate **3A** and all products resulting from its formation (Fig. 2). The presteady state and steady state rates are determined by the steps that lead to and follow formation of intermediate **3A** (Fig. 1 and 2), respectively.

Tritium exchange reactions. The tritium exchange reaction was followed essentially as previously described (34). Briefly, tritium exchange is measured by quenching reaction aliquots in an acid suspension (HCl, pH=2.0-2.5) of activated charcoal. Because **3A** and **3B** (Fig. 2) rapidly degrade in acid, their formation can be detected prior to release from the enzyme, thereby allowing the determination of kinetic constants up to and including the formation of **3A** and **3B**. The enzyme concentration, DNA concentration, and cofactor concentration are specific for each assay and described in the figure legends. All reactions were saturated with the cofactor. The reaction buffer was 100 mM Tris/HCl (pH, 8.0), 10 mM EDTA, 10 mM DTT and 0.5 mg/ml of BSA.

Preparation of [5-^{3}H] cytosine pmpoly(dG-dC) and pmpoly(dI-dC). ^{3}H labeled premethylated DNA was prepared from [5-^{3}H] cytosine-poly(dI-dC) using the procedure described for the preparation of premethylated DNA.

Data Analysis. All reaction profiles were analyzed using the Microcal Origin 5.0 program. All rates were reported as the best fit values ± standard deviation. The burst profiles were fit to a two step irreversible mechanism (35):

$$[P](t) = \alpha \cdot E_t \cdot (1 - e^{-k_{pss} \cdot t}) + E_t \cdot k_{ss} \cdot t \qquad (1)$$

where *[P](t)* is product at time *t*, E_t is total enzyme in the assay, α is a constant that relates the burst magnitude and the actual enzyme concentration, k_{pss} is the presteady state rate, k_{ss} is the lag transition rate. All initial velocity lags were analyzed using a model equation that represents two enzymes forms with different catalytic activities (36):

$$[P](t) = E_t \cdot k \cdot t - \frac{E_t \cdot k}{k_l}(1 - e^{-k_l t}) \qquad (2)$$

where *[P](t)* is product at time t, E_t is total enzyme in the assay, k is the catalytic rate, k_l is the lag transition rate. Unless otherwise indicated all other profiles were analyzed using a linear equation ([P](t)=E_tk; [P](t) product at time t, E_t total enzyme, k turnover rate). Each experiment was repeated until shown to be reproducible; shown are representative examples.

SKIE measurements. All experiments in D_2O buffers were measured in parallel with the corresponding H_2O experiments, and were identical in all other parameters. The D_2O buffer was prepared as a ten fold concentrate, and its pH was adjusted taking into account the pD vs. pH correction (37) to be the same as in the corresponding H_2O buffer. H inventory profiles were analyzed using different forms of the Gross-Butler equation (37):

$$k_{\upsilon}^{D2O} = k^{H2O} \cdot \frac{(1+\upsilon-\upsilon\cdot\phi^{T})^{n}}{(1+\upsilon-\upsilon\cdot\phi^{G})^{m}} \qquad \text{(eqn. 3)}$$

Where $k_{\upsilon}^{D_2O}$ is the measured rate when the fraction of D_2O is equal υ, k^{H2O} is the rate measured in pure H_2O, υ is the fraction D_2O at which the rate was measured (i.e. 0.1 , 0.2, 0.3 etc), ϕ^T or ϕ^G are deuterium fractionation factors at the transition and the ground state respectively (37). Different forms of equation 4 can be produced by changing the values for parameters *n*, *m*, as we described earlier (28).

Fluorescence Measurements. The equilibrium dissociation constant for the Dnmt1 CRE $a^F b^m$ complex was measured in the presence and absence of AdoMet by following changes in the intrinsic protein florescence as a function of increasing DNA concentration. The fluorescence was measured using a Perkin Elmer LS50B instrument, with excitation at 290 nm (5 nm slits), and the emission at 340 nm (10 nm slits). The dissociation constant (K_d) was calculated using following equation:

$$\frac{Fo-Fi}{Fo-F_F} = \frac{(E_t - S_i + Kd) - \sqrt{(E_t - S_i + Kd)^2 - 4\cdot E_t \cdot S_i}}{2\cdot[E_t]} \qquad \text{(eqn. 4)}$$

where F_i is fluorescence at DNA concentration S_i, E_t is total Dnmt1 concentration, and F_O and F_F are the initial and the final fluorescence respectively. The experimental data were analyzed by nonlinear least squares using eqn. 4 and the Microcal Origin 5.0 program,

with K_d, F_O and F_F set as the free fit parameters. Prior to fitting using equation 4, the measured Dnmt1 fluorescence profiles were corrected for the inner filter effect that is caused by added DNA. The inner filter effect was measured by replacing Dnmt1 with free Trp at a concentration to get the same fluorescence as the initial Dnmt1 solution, using the following equation:

$$Fi = Fm + (Fo - Fw) \quad \text{(eqn 5)}$$

where F_i is the corrected florescence value that was used in the equation 4, F_m and F_w are measured Dnmt1 and free Trp fluorescence before the correction at a specific DNA concentration, and F_O is the initial fluorescence of the Dnmt1 (and free Trp) solution before addition of DNA or AdoMet. The correction curve showed that at the highest DNA concentration the inner filter effect was between 5-15% of the actual signal.

Results

Presteady state and initial steady state methylation reactions with poly(dI-dC) and pmpoly(dI-dC) (Fig 3 A, 4A, C), poly(dG-dC) and pmpoly(dG-dC) (Fig 3B, Fig. 4. B, C). Our initial interest was to characterize the methylation reaction (Fig 3 A-B, Fig 4 A-C) with premethylated and unmethylated poly(dI-dC) and poly(dG-dC) substrates to provide a basis for a direct comparison with our recent study of M.HhaI (28), and prior studies of Dnmt1 with different DNA substrates (Table 1). The relatively fast reactions with poly(dI-dC) and pmpoly(dI-dC) allow the measurement of both the presteady state and steady state parameters (Fig 3A, Table 1). In contrast, the slower reactions with poly(dG-dC) and pmpoly(dG-dC) limited our measurements to one or two turnovers (Fig 3B, Table 1). Both premethylated poly(dI-dC) and poly(dG-dC) show a mild presteady state burst (Figs. 3A and 3B) and no substrate inhibition (Fig 4C). Both unmethylated poly(dI-dC) and poly(dG-dC) show initial lags (Figs. 3A and 3B), and increasing DNA concentrations leads to longer lags (Figs. 3A and 3B) and greater substrate inhibition (Fig 4 A-B). In summary, the prepared premethylated and unmethylated substrates have distinct substrate inhibition characteristics and the initial rates (Table 1).

The premethylated substrate is similar to the substrate used in the original study which revealed differences in the initial lag and substrate inhibition (26). Modifications in the ratio of ^{5m}C to C ($^{5m}C/C$) greater than 1:20 do not cause changes in the kinetic parameters (data not shown). This density of ^{5m}C corresponds to approximately one ^{5m}C per enzyme:DNA footprint (supplement). Our results are consistent with our previous study showing that Dnmt1 has similar activities with premethylated substrates in which the distance between the target cytosine and ^{5m}C varies from 5 to 18 bp (24). The highest density between ^{5m}C and C sites was 1 to 7, to avoid problems associated with the potential depletion of the target cytosines.

Previous studies have used various premethylated substrates, including: (i) oligos with a single hemimethylated site (23); (ii) oligos with multiple hemimethylated sites (8,12,18); (iii) premethylated oligos with a single ^{5m}C at a fixed distance from the target C (24); (iv) premethylated oligos with multiple ^{5m}C and multiple target sites (8,12,18); (v) and polymeric poly(dI-dC) substrates with multiple target sites and multiple ^{5m}C groups

at varying distance from the target site (9,31). Like the hemimethylated oligo substrates ((7) and Table 1), the pm-poly(dG-dC) and pm-poly(dI-dC) substrates show a presteady state burst (Fig 3 A-B). The catalytic rates measured with the GC-rich premethylated substrates (12) are similar to the rates measured with the pm-poly(dG-dC) substrates studied here (Table 1). Finally, similar to the data in Fig 4C, prior studies of Dnmt1 and premethylated substrates did not show substrate inhibition at full saturation (10,26). In summary, the pm-poly(dG-dC) and pm-poly(dI-dC) substrates studied here show features similar to those described with diverse premethylated substrates.

The initial lag and substrate inhibition in the methylation reaction with poly(dI-dC) were reported earlier (26). In this study we analyze the initial lag to better understand the enzyme's allosteric regulation and the substrate inhibition. In general, features of both the assay design and inherent reaction mechanism can cause an initial lag during a normal reaction cycle (36,38). Many trivial explanations for the lag with Dnmt1 can be dismissed. Preincubation of Dnmt1 with DNA up to 10 minutes does not change the lag, suggesting that a slow transition involving ligand binding is not responsible. Changing the order of substrate addition (DNA and AdoMet) does not alter the lag. The lag correlates with the extent of substrate inhibition (Fig 3 and Fig 4, and (26)). A slow relief from enzyme inhibition is a well known mechanism leading to a kinetic lag (36,38). In summary, we propose that for Dnmt1, the start of the catalytic action with the unmethylated substrate results in a slow relief from the allosteric inhibition causing an initial lag in the catalytic activity.

The lag transition rate and the subsequent catalytic rate (Table 1) can be calculated using the equation modeled on two enzyme forms whose interconversion is initiated at the start of catalysis (eqn 2, (36,38)). The initial lag is only observed when the transition between the two enzyme forms (Fig 10 C) is slower than the catalytic rate (36,38). Thus, the lag is observed only in methylation (Fig 3) and during the exchange reaction with sinefungin (Fig. 5), but not during the slow exchange reaction with N-methyl-AdoMet (data not shown).

The methylation rates and reaction profiles (Fig 3A) measured with poly(dI-dC) are similar to previous studies (Fig 3A in (14); and Fig 1 in (7), Table 1). The methylation

rates with unmethylated poly(dG-dC) substrates are similar to the rates measured with other unmethylated GC-rich substrates (Table 1), and plasmid pRW3602 (Table 1). Saturation with poly(dG-dC) and poly(dI-dC) leads to partial inhibition (Fig 4 A-B), indicating that occupancy of the allosteric site leads only to modulation, rather than complete loss of catalytic activity. The lag is observed even at sub-saturating substrate concentration (Fig 3 and Fig 4), and the substrate dependency of the binding and inhibition profiles overlap (supplement). Thus, the active site and the allosteric site have a similar binding affinities for poly(dG-dC) and poly(dI-dC) (Fig 10C), consistent with the observation that the allosteric site mutant shows higher rates than the wild type even at subsaturating substrate concentrations (Fig 4A in (14) vs. Fig 4A in (11)).

The exchange reaction with AdoMet analogues and premethylated and unmethylated poly(dG-dC) substrates (Table 1 and Fig 4 A and B, Fig 6A). We show that Dnmt1 catalyzes the exchange reaction, supporting the idea that it is mechanistically related to other pyrimidine methyltransferases (Fig 1). The combined use of AdoMet analogs and the cytosine C^5 tritium exchange assay (Fig. 1, **2**→**3B**→**4B**) provides mechanistic insights into catalytic events that take place at the C^5 position (intermediate **2** Fig 1), the stability of intermediate **2**, and the rate limiting steps (28). The modulation of the exchange reaction by AdoMet analogs closely parallels our observations with M.HhaI. The AdoMet analogs used in this study differ only in the position of the active methyl group (Fig 2). The exchange rates are high with sinefungin, intermediate with N-methyl-AdoMet and low with AdoHcy, AdoMet and in the absence of the cofactor (Table 2). The high tritium release rates during methylation with poly(dG-dC) (Fig 6C) result exclusively from the methyltransfer reaction (Fig. 1, **2**→**3A**); thus, AdoMet does not support the exchange reaction (Fig 1, **2**→**3B**→**4B**) with poly(dG-dC) substrates (Fig 6 A-C). In summary, just as with M.HhaI, the AdoMet analogues control the exchange reaction by Dnmt1 by controlling the rate-limiting proton transfer at the activated target base (Fig, **2**→**3B**). Interestingly, the enzyme shows the same preference for DNA with AdoMet analogs that modulate the exchange reaction rate by over three-orders of magnitude: the fastest exchange rates are observed with pmpoly(dI-dC), followed by poly(dI-dC), pmpoly(dG-dC) and poly(dG-dC) (Table 2). Thus, differences between

premethylated and unmethylated DNA, or between poly(dI-dC) and poly(dG-dC), do not derive from differences in the methyltransfer (Fig 1, **2**→**3A**) or proton transfer rates (Fig 1, **2**→**3B**).

The exchange reaction with sinefungin is particularly revealing. First, an initial lag is observed in the absence of any production of ^{5m}C (Fig 5). Importantly, this shows that the increased rate following the initial lag in the methylation reaction (Fig 3 A-B) is unlikely to be due to self-activation through the AdoMet-dependent production of ^{5m}C at the start of catalysis. Also, the steady state exchange rates for poly(dI-dC) and pmpoly(dI-dC) (Fig 5, Table 2) differ by nine-fold, in contrast to the nearly identical AdoMet-dependent methylation rates (Fig 3A, Table 1). Furthermore, the apparent $K_m^{sinefungin}$ measured with poly(dI-dC) is nine times higher than with pmpoly(dI-dC) (5.1 ± 1.4 μM *vs.* 0.6 ± 0.1 μM). For comparison, K_m^{AdoMet} in the methylation reaction with poly(dI-dC) is two times higher than with pmpoly(dI-dC) (1.3 ± 0.21 μM *vs.* 2.7± 0.4 μM). In summary, the ^3H exchange reaction indicates that studying the steps prior to the methyltransfer step (Fig 1, **2**→**3A**) can reveal unique insights in the enzyme's preference for different DNA substrates.

Tritium release rates during the AdoMet-dependent methylation reaction with premethylated and unmethylated poly(dG-dC) and poly(dI-dC) substrates (Fig 6 A-C). We sought to determine the basis of Dnmt1's sinefungin-dependent preference for pm-poly(dI-dC), which is not revealed during methylation (Fig. 3 vs Fig. 5). Accordingly, we measured the methylation and accompanying tritium release reactions simultaneously (Fig 6 A-C) using ^{14}C-AdoMet and DNA substrates labeled with tritium at the C^5 position. Based on the reaction mechanism, every methyltransfer (Fig 1, **2**→**3A**) is expected to result in one tritium release (Fig 1, **3A**→**4A**) and the methylation and the accompanying tritium release rates are expected to be identical (28,34). We observe this one to one stoichiometry in both the presteady and steady state methylation reactions with poly(dG-dC) and pmpoly(dG-dC). Thus, intermediate **2** (Fig 1) leads only to methyltransfer (Fig 1, **2**→**3A**) with poly(dG-dC) and pmpoly(dG-dC) substrates. In contrast, Dnmt1 like M.HhaI, shows an excess release of tritium during the AdoMet-dependent methylation of poly(dI-dC) and pmpoly(dI-dC) (Table 2). The excess tritium

release in the methylation reaction during the first turnover indicates that proton transfer at C^5 (Fig 1, **2**→**3B**) can take place before the methyltransfer step (Fig 1, **2**→**3A**). Furthermore, since a single target base attack can result in only one tritium release (Fig. 1, **2**→**3B**→**4B**), the several fold difference between the tritium release and the methylation rates indicates that the enzyme can attack and release several bases prior to catalyzing one methyl transfer. Thus, the target base activation (Fig 1, **1**→**2**) is fast, and there is a direct competition between the target base release (i.e. breakdown of intermediate **1**) and the slow methyltransfer step (**2**→**3A**, Fig. 1). The difference between poly(dI-dC) and pmpoly(dI-dC) (Fig 6A vs 6B) indicates that intermediate **2** (Fig 1, **1**→**2**) is formed faster with pmpoly(dI-dC) as already indicated by the data in Figure 5.

H inventory studies (Fig 7 A-B). H inventory profiles are rate studies performed at varying D_2O and H_2O ratios (37). Earlier we used this approach to study the exchange reaction catalyzed by M.HhaI (28). Dnmt1 and M.HhaI show similar proton inventory profiles in the exchange reaction with sinefungin (Fig 7 A-B), although the reaction rates vary by orders of magnitude (Table 2). Proton inventory profiles can be described numerically using the Gross-Butler equation (eqn 5, (37)). For all four DNA substrates the transition state fractionation factors (ϕ^T) is between 0.32-0.35 (0.35 ±0.03 poly(dI-dC); 0.30 ± 0.05 pmpoly(dI-dC); 0.34 ± 0.04 poly(dG-dC); 0.30 ± 0.05 pmpoly(dG-dC)). The ground state fractionation factor (ϕ^G) is between 2.1 and 2.4 (2.5±0.2 poly(dI-dC); 2.5 ± 0.3 pmpoly(dI-dC); 2.3 ± 0.3 poly(dG-dC); 2.5 ± 0.3 pmpoly(dG-dC)). The similar ϕ^T values suggest that reactions with the four different DNA substrates share the same rate-limiting step, while the similar ϕ^G values suggest that the reactions also share similar intermediates (37). The measured ϕ^T values are expected for reactions involving N-H-C proton bridges in the transition state (p. 86 in (37)). A N-H-C proton bridge could form between the amino group on sinefungin (Fig 2) and intermediate **2** (C^5, Fig 1) if the rate limiting step is proton transfer from the cofactor to the carbon 5 (Fig 1, **2**→**3A**) as we suggested earlier (Table 2 and, (28)). Moreover, Dnmt1 and M.HhaI show similar proton inventory profiles in the exchange reaction with sinefungin, consistent with these enzymes having common intermediates and rate limiting steps (Fig 1 and 9). In summary, the proton inventory analysis indicates that the Dnmt1 exchange reaction with different

DNA substrates, as well as the exchange reaction by Dnmt1 and M.HhaI, share the same intermediates and the rate limiting step even though the catalytic rates can vary by orders of magnitude (Table 2).

Fluorescence titration of Dnmt1 *with CRE* $a^F b^m$ *oligo (Fig 8).* AdoMet binding by M.HhaI leads to a large conformational change (33), an increase in DNA binding affinity by three orders of magnitude (15), and a change in the mechanism of the target base attack by DNA methyltransferases (28). In contrast, we previously showed that Dnmt1's affinity for DNA is not modulated by the cofactor (7)(9). Moreover, the substrate inhibition (like in Fig 4A) is more pronounced at sub-saturating AdoMet concentrations (14), and with some DNA substrates an increase in AdoMet concentration does not lead to the expected increase in the catalytic rates (Fig 6B in (12) vs. Fig 3D in (11)). We sought to probe the importance of the cofactor towards DNA affinity further by using substrates containing 5-fluorocytosine. Catalysis with 5-fluorocytosine-containing substrates is limited by a slow methyltransfer rate (Fig 1, **2**→**3A**, rate < 0.1 h^{-1}, (16)). Thus, 5-fluorocytosine provides an opportunity to investigate how AdoMet alters Dnmt1-DNA interactions when the enzyme is trapped in the form of transient catalytic intermediates **1** and **2** (Fig. 1; (39)). The DNA substrate was a 30 bp long hemimethylated CRE ab^m oligo that was used in the previous studies (7), and the binding was measured by following changes in intrinsic protein florescence as a function of increasing DNA concentration (see methods). The best fit value for the Dnmt1-CRE$a^F b^m$ complex in the absence of the cofactor was 1.56 ± 0.03 μM, and the best fit value in the presence of AdoMet was 0.6 ± 0.01 μM. These values are very similar to the previous dissociation constants measured with Dnmt1 and CRE ab^m substrate (7,9). Thus, unlike M.HhaI, AdoMet binding by Dnmt1 has minimal effects on its DNA binding affinity.

Discussion

Substrate inhibition by Dnmt1 derives from the turnover-dependent activation of the enzyme. Premethylated and unmethylated DNA show differences in the substrate inhibition (Fig 4 A-C), the initial lag (Fig 3A-B), and catalytic rates (Table 1). The initial lag was not routinely described in prior kinetic studies of Dnmt1, in contrast to the various forms of substrate inhibition; however, a lag is apparent in some cases ((26); Fig 1 and Fig 3 in (7) ; and Fig 3A (14)). Our results indicate that the kinetic lag is not an assay artifact (36,38). The lag is observed only with unmethylated DNA (Fig 3A-B), and only when the catalytic rates are faster than the lag transition rates (Fig 3A and Fig 5), but not in the slow exchange reaction with N-methyl-AdoMet (data not shown). Furthermore, the duration of the lag is substrate-specific (Fig 3A vs. Fig 3B), and the lag does not depend on the order of addition of the reaction components, nor on Dnmt1 concentration (data not shown). The lag correlates with the extent of substrate inhibition (Fig 3A-B, Fig 4 A-C). Slow relief from enzyme inhibition induced by the start of catalysis was previously shown to lead to an initial lag (36,38). In summary, we propose that the start of catalysis on unmethylated DNA initiates a slow conformational change and a slow relief from allosteric inhibition.

Although the precise nature of this slow transition remains obscure, plausible driving forces include AdoMet binding, DNA release from the site of inhibition, a combination of these two processes, or some other slow conformational change. AdoMet binding is the most likely factor since DNA inhibition is more pronounced at subsaturating AdoMet concentrations (Fig 4A in (14)), indicating that AdoMet binding can affect the extent of substrate inhibition. Moreover, a comparison of Dnmt1 and its allosteric site mutant showed that changes in AdoMet concentration do not result in the expected increase in catalytic rates (Fig 6B in (12) vs. Fig 3D in (11)). These results are consistent with a slow step following the formation of the Dnmt1:DNA:AdoMet complex. The exceptionally slow exchange reaction in the absence of cofactor (Table 2) is also consistent with the proposal that AdoMet binding can facilitate the target base attack and the formation of intermediates **1** and **2** (Fig. 1). AdoMet binding to M.HhaI is known to cause a conformational change and a significant increase in DNA affinity

(15,33). Here we found that for Dnmt1, AdoMet binding does not lead to a drastic increase in DNA binding affinity (Fig 8). In summary, we propose that AdoMet binding to Dnmt1 initiates a slow relief from the allosteric inhibition; however, AdoMet binding does not lead to a change in binding affinity for DNA, as observed for M.HhaI (Fig. 8).

The reactions with the premethylated substrate show a presteady state burst as reported earlier (7). In general the initial burst indicates that steps leading to the detection step are faster than the steps following the detection step (p. 274 in (40)). Thus, a mild presteady state burst indicates that for premethylated substrates the steps leading to intermediate **3A** (Fig 1) are in part rate limiting during the initial target base attack, while the subsequent turnovers are partially controlled by the steps that come after intermediate **3A**. The burst and the fast formation of the intermediate **3A** can be attributed to the favorable steps that lead to the activated target base (Fig 1, **2**), as indicated by the ^{3}H exchange reaction (Fig 5 and Fig 6 A-B, see later in the text). The slow step following the presteady state burst is due to AdoHcy dissociation, since the fast ^{3}H exchange reaction does not show the burst, and does not require cofactor dissociation (Fig 3 vs. Fig 5, Fig 6 B, Table 2). With substrates that have multiple target sites the burst is relatively mild (Fig 3 A-B)(7)). The reactions with premethylated DNA do not show substrate inhibition (Fig 4C) and the initial lag (Fig 3 A-B). Thus, premethylated DNA either does not cause allosteric inhibition, or allosteric inhibition by the premethylated substrate does not result in the slow transition at the start of catalysis. The mutant lacking the functional allosteric site shows higher catalytic rates even with the premethylated DNA (Fig 3 C-D in (11) vs. Fig 6 A-B in (12)), indicating that the allosteric inhibition occurs with both premethylated and unmethylated DNA.

*Dnmt1 has similar reaction intermediates and rate-limiting steps as M.*Hha*I.* In our earlier work with M.HhaI we used the exchange reaction with AdoMet analogs and poly(dG-dC) and poly(dI-dC) to describe the reaction intermediates and the rate-limiting steps during catalysis (28). We sought to apply this approach to Dnmt1 to further characterize the enzyme's preference for premethylated substrates. The ability of Dnmt1 to catalyze the exchange reaction supports the results from sequence similarity studies (Fig 9), and 5-fluoro-cytosine inhibition studies (16), and shows that Dnmt1 has the same

catalytic mechanism as other pyrimidine methyltransferases (Fig 1). Dnmt1 and M.HhaI share similarities in key aspects of the cytosine C^5 exchange reaction, even though the catalytic rates can differ by 10 to 100 fold (Table 2). AdoMet analogs can modulate the exchange rates by orders of magnitude for both Dnmt1 and M.HhaI (Table 2), indicating that the availability of proximal proton(s) (Fig 2) in the position of the active methyl moiety is critical (Fig 1). Another key similarity between Dnmt1 and M.HhaI is the excess tritium release during the methylation reaction with poly(dI-dC) (and pmpoly(dI-dC), Fig 6 A-B), while no excess tritium release is observed in the reaction with poly(dG-dC) (and pmpoly(dG-dC), Fig 6C). Finally, we also found that Dnmt1 and M.HhaI show similar proton inventory profiles in the exchange reaction with sinefungin (Fig 7 A-B). Based on these similarities, and related interpretations for M.HhaI (28), we propose that the AdoMet analogs modulate the exchange rates by Dnmt1 by controlling the proton access at the C^5 on intermediate **2** (Fig 2 and solvent in Fig 9). For both Dnmt1 and M.HhaI, intermediates leading to the intermediates **1** and **2** accumulate as a dynamic equilibrium (Fig 1, **1**↔**2**), prior to the slow methyltransfer (Fig 1, **2**→**3A**), or proton transfer step (Fig1, **2**→**3B**). If Dnmt1 flips the target base like M.HhaI and other methyltransferases (41), the rapid equilibrium would include base flipping and base re-stacking steps, and the equilibrium between intermediates **1** and **2**. The intermediates form a rapid equilibrium, since the same intermediates are part of the target base attack and the product release steps (28).

In the case of a rapid equilibrium between the steps leading to intermediates **1** and **2**, the observed catalytic rates are not dependent on a single rate limiting event (28). Rather, the catalytic rates are simultaneously and independently regulated by factors which control the concentrations of intermediates **1** and **2** (Fig 1), and by factors that control the methyltransfer (Fig 1, **2**→**3A**) or proton transfer steps (**2**→**3B**). The methyl transfer rate (Fig 1, **2**→**3A**) is directly proportional to the lifetime of intermediate **2**, which in turn depends on the factors which control the equilibrium between intermediates **1** and **2**, like the pKa of the active site cysteine (28). The lifetime of intermediate **1** is dependent on the ratio between base flipping and the base re-stacking rates, and the ratio between the conversion rates **1**→**2** and **2**→**1**. In the next few paragraphs we use the

concept of a dynamic equilibrium preceding the slow methyl transfer step to describe the factors that control Dnmt1's catalytic rates. We describe the rate differences between premethylated and unmethylated substrates, the difference between poly(dI-dC) and poly(dG-dC) substrates, and the difference between Dnmt1 and M.HhaI

Difference in catalytic rates between unmethylated and premethylated DNA substrates. The methyltransfer step is rate limiting with both unmethylated and premethylated substrates (Fig 6 A-B), yet the two substrates have different catalytic rates (Table 2). The tritium exchange rates with sinefungin and premethylated and unmethylated substrates differ by 9 fold (Table 2), yet the proton inventory data shows that both reactions are limited by proton transfer at cytosine C^5 (Fig 7 A-B). The exchange rates with both premethylated and unmethylated substrates are modulated by orders of magnitude with various AdoMet analogs, yet the rates with the premethylated substrates are uniformly faster (Table 2). Thus, the difference between the unmethylated and premethylated substrates does not derive from the rate limiting events on intermediate **2** (Fig 1, **2**→**3A**, or **2**→**3B**). Rather, the difference derives from changes that favor the accumulation of intermediates **1** and **2** (Fig 6A-B).

Since each target base attack can lead to only one tritium release (Fig 1, **2**→**3B**→**4B**), the higher exchange rates with the premethylated substrates (Fig 5 and 6 A-B) indicate a higher frequency of target base attacks. In another words, the preference for the premethylated substrate must involve all steps leading to intermediates **1** and **2** (Fig 1). Interestingly, the exchange rates with unmethylated DNA are never as fast as with premethylated DNA (Fig 5 and Fig 6 A-B), even though the early lag indicates (Fig 3) a relief from the allosteric inhibition at the start of the catalysis. Thus, the allosteric site is not the only site that regulates the enzyme's preference for the premethylated substrate. This is consistent with earlier work showing that a dysfunctional regulatory domain does not affect Dnmt1's ability to differentiate between premethylated and unmethylated substrates (11).

The difference between poly(dI-dC) and poly(dG-dC), and the difference between Dnmt1 and M.HhaI. Dnmt1's preference for poly(dI-dC) is unusual, resulting in rates comparable to those observed for M.HhaI (Table 2), in contrast to the two orders of

magnitude difference in presteady state methylation rates with poly(dG-dC) (Table 2 and (7)) or other DNA substrates (15). The preference for poly(dI-dC) is unlikely to be caused by differences in the allosteric regulation since poly(dI-dC) shows faster rates than pmpoly(dG-dC), even though pmpoly(dG-dC) does not show substrate inhibition. Also, the Dnmt1 mutant lacking the functional allosteric site shows 3-18 fold slower rates with G:C rich substrates relative to the poly(dI-dC) substrate (11,12). The preference for poly(dI-dC) substrates is unlikely to result directly from faster catalytic processes at cytosine C^5 (Fig 1, **2**→**3A** or **2**→**3B**) since the reactions with poly(dI-dC) are uniformly faster, even though AdoMet analogues can modulate the exchange rates by three orders of magnitude (Table 2). Finally, the proton inventory studies (Fig 7 A-B) suggest that all four DNA substrates share the same rate limiting steps. In summary our results indicate that the higher catalytic rates with poly(dI-dC) vs. poly(dG-dC) (Table 1 and 2) are not due to the differences in allosteric regulation, or in the conversion of intermediates **2**→**3A** or **2**→**3B**. We therefore propose that differences in the accumulation of intermediate **1** and **2** (Fig 1) are most likely responsible. The structures of I:C and G:C base pairs can be superimposed (42); however, unlike the G:C base pair, the I:C base pair has only two hydrogen bonds (Fig 2). Thus, a disruption of the I:C base pair during the base flipping process requires less energy, so it is tempting to attribute the faster rates with poly(dI-dC) substrate to a more favorable base flipping process.

Similar to the differences between Dnmt1 reactions with poly(dG-dC) and poly(dI-dC), the difference between Dnmt1 and M.HhaI can be traced to the accumulation of intermediates **1** and **2**. The ^3H exchange reaction with AdoMet analogues (Fig 2) and the proton inventory studies (Fig 7) indicate that Dnmt1 and M.HhaI share the same mechanism with poly(dI-dC) and poly(dG-dC), once intermediates **1** and **2** are formed (Figs. 1 and 9). Thus, the uniformly faster rates with M.HhaI (Table 2) must come from early steps leading to intermediates **1** and **2**, rather than from methyltransfer or proton transfer rates. Unlike Dnmt1, M.HhaI shows similar catalytic rates with poly(dI-dC) and poly(dG-dC) substrates (28), indicating that two enzymes differ in the mechanism that leading to the accumulation of intermediates **1** and **2** (i.e. base flipping).

^3H exchange reaction and mutagenic deamination. DNA methylation sites are mutation hot spots, which frequently occur in critical cancer related genes (43), as a result of deamination of cytosine to uracil, and 5-methylcytosine to thymine (Fig 1). Bacterial DNA cytosine methyltransferases are known to catalyze mutagenic deamination (44), and deamination rates are affected by AdoMet analogues (45,46). The M.HhaI-catalyzed exchange and deamination reactions are affected by AdoMet analogs in the same fashion (28), supporting the idea that the two reactions share similar intermediates (Fig 1, **1**→**2**→**3B**→**3C**→**4C** and (44-48)). The deamination reaction is extremely slow and thus difficult to study mechanistically. We thus studied the Dnmt1-catalyzed exchange reaction to obtain insights into the enzyme's ability to catalyze this, and the related deamination reactions.

Cytosine C^5 methyltransferases need to balance the solvent access at the active site (Fig 9); the solvent forms part of the obligatory β-elimination step (Fig 1, **3B**→**3C**), and may be important for the mutagenic deamination (Fig 1, **1**→**2**→ **3B**→**3C**→**4C**). Intermediates **1** and **2** accumulate prior to the slow methyltransfer step (Fig 6 A-B, and (28)), thus enhancing the opportunity for solvent access to these intermediates. Intermediate **2** is readily protonated (Fig 1, **2**→**3B**, pKa=11-18, (29)), thereby increasing the chances of mutagenic deamination by at least 4 orders of magnitude (48). In the case of M.HhaI (28), the excess tritium released in the methylation reaction with poly(dI-dC) is enhanced by the positioning of the active site loop (residues 80-99) and enzyme-DNA interactions with guanine 5' to the target cytosine. Like M.HhaI, Dnmt1 shows excess tritium release in the methylation reaction with poly(dI-dC), but not with poly(dG-dC) (Fig 6 A-C). Thus, for both Dnmt1 and M.HhaI, enzyme interactions with the guanine within the recognition site limit the solvent access to the active site, the exchange reaction, and presumably the mutagenic deamination (Fig 1, **1**→**2**→**3B**→**3C**→**4C**). Aside from the active site loop, the cofactor can also protect intermediates **1** and **2** from solvent (Table 2 and Fig 9). The low ^3H exchange reaction with AdoHcy (Table 2), indicates that for both M.HhaI and Dnmt1, the β-elimination step (Fig 1, **3B**→**3C**) is unlikely to take place through a direct solvent access at intermediate **2** (49) or even prior to AdoHcy dissociation.

The exchange and mutagenic deamination reactions are likely slowed down by anything which decreases the lifetime of the extrahelical base. For example, the proposal that Dnmt1 is slower than M.HhaI because intermediates **1** and **2** accumulate to a lesser extent, would also result in Dnmt1 being less mutagenic than M.HhaI. In contrast to M.HhaI, the exchange reaction for Dnmt1 is very slow in the absence of cofactor (Table 2). Thus, Dnmt1 is unlikely to efficiently deaminate cytosine in the absence of the cofactor, which is precisely the condition that shows the most extensive deamination for the majority of bacterial enzymes (44-47).

Dnmt1 is not self-activated by the ^{5m}C groups deposited at the start of the methylation reaction on unmethylated substrate. It is unclear from the current literature whether Dnmt1's preference for premethylated substrates derives from activation by the premethylated substrates, inhibition by unmethylated substrates, or a combination of those two phenomena. The Dnmt1 mutant lacking a functional regulatory domain (11) shows higher catalytic rates with premethylated and unmethylated DNA substrates, indicating that allosteric inhibition is present with every DNA substrate. Here we show that Dnmt1's preference for premethylated substrates derives from allosteric inhibition by unmethylated substrates, rather than allosteric activation by premethylated substrates. First, our observation of the kinetic lag, and the resultant "activation" during the sinefungin-mediated exchange reaction (Fig 5) indicates that the faster catalysis following the initial lag is not due to activation caused by the deposition of methyl groups at the start of catalysis (Fig. 1). Second, premethylated DNA (Fig 4 C) does not show a sigmoidal curve which is characteristic of substrates that act as allosteric activators (pp. 21-29 in (38) or pp. 203-234 in (40)). Finally, we find that after 10 minutes of methylation (Fig 6A), the fraction of ^{5m}C becomes comparable to the fraction of ^{5m}C that is present in premethylated poly(dI-dC) (^{5m}C:C=1:12); yet, we do not see a gradual increase in the tritium release rates to that observed with premethylated poly(dI-dC) (Fig 5 B vs. Fig 5 A). In summary, it appears that the higher catalytic rates with premethylated substrates do not depend on the mere presence of ^{5m}C. We propose one mechanism to account for those observations in our study of Dnmt1 processivity and allosteric regulation (Svedružić and Reich, submitted). Briefly, the allosteric site and the active site

do not bind the same DNA molecules and the adjacent sites (Fig 10C). Since Dnmt1 is processive with poly(dI-dC), the new methylation sites remain near the active site and have no immediate access at the allosteric site. With distributive substrates, the new methylation sites get released in the bulk solution where it diluted by an excess of unmethylated DNA (Fig 10 C).

Fine Print Supplement: Kinetic Studies of mammalian DNA cytosine methyltransferases. A number of Dnmt1 studies have been published to this date; unfortunately it is difficult to integrate these results in a logical coherent mechanism. The nature of the assay design is the primary cause of the observed inconsistencies. Steady state studies require an excess of substrate over enzyme and multiple catalytic turnovers (40), both of which are often impossible, or very difficult to achieve in Dnmt1 reactions. Dnmt1 is exceptionally slow (Table 1); thus, limitations in the assay sensitivity determine the measurable catalytic rates, demanding relatively high enzyme concentrations (e.g. 5-40 nM). However, many DNA molecules show saturation kinetics in this same concentration range (7,8,10-12,14,24). Furthermore some substrates show saturation kinetics at higher concentration (e.g., Fig 1B in (8)); however, the slow catalytic turnover, as with many other oligo substrates (Table 1), makes the measurement of steady state rates in multiple turnovers practically unfeasible. Driven by these concerns we did not use Michaelis-Menten kinetics to analyze Figures 4 A-C, or the previously published results (Table 1 and (7,8,10-12,14,24,50)).

The rate profiles in Figure 4 A-C and the similar studies in the past, are not determined by the Michaelis-Menten parameters but rather by the particular enzyme and DNA concentrations. Several studies suggested that the allosteric site and the active sites can independently bind DNA ((8,11,20) and Fig 10 C). Thus, at low DNA concentration (i.e. less than one 30 bp segment per each Dnmt1 molecule, Fig 10), Dnmt1 is in excess (Fig 10 C). Under these conditions, the catalytic rates are low since only a small fraction of the total enzyme is present in the ES and SES forms (Fig 10C). Further increases in DNA concentration results in an increase in the catalytic rates, since more of the enzyme is present in the ES and SES forms (Fig 10C). The highest catalytic rates are achieved when the ES form of the enzyme predominates relative to the E, SE and SES forms (Fig 10C). Once the maximal rates are achieved, a further increase in DNA concentration results primarily in the conversion of the ES to SES form and the visible substrate inhibition phase (Fig 10C). Since Dnmt1 and DNA are present in a similar concentrations, a change in enzyme concentration results in a change in the substrate

concentration which gives the maximal rate (Fig 4 A-B), as shown previously (7-9,11,12,24,27,50).

An increase in Dnmt1 concentration (Fig 4 A-B) leads to apparent inhibition, (Fig 4 A-B; (8,51)) since the Dnmt1 concentration approaches the binding constant for the allosteric site. Thus, a smaller fraction of the total enzyme is present in the ES form relative to E, SE, and SES forms (Fig 10C). Use of a steady state approach to analyze Dnmt1 experiments in which the substrate is not in excess relative to Dnmt1 has contributed to the reporting of very unusual enzymatic properties of Dnmt1. For example, the large variations in reported k_{cat}, and k_{cat}/Km values for otherwise identical reactions are caused by such effects. The K_m, k_{cat} and K_i constants calculated from such studies reflect the enzyme:DNA ratios (Fig 4 A-B) rather than kinetic properties of Dnmt1. Also, using a steady state approach with enzyme and substrate present at similar concentrations can obscure competitive and noncompetitive inhibition features, and the patterns observed with varying AdoMet and DNA concentrations (7-9,11,12,24,27,50).

We do not know if Dnmt1 can be activated by fully methylated DNA (12,50); however, most prior studies do not support such a mechanism (Fig 4 and (8,11,20)). It is plausible that fully methylated DNA may displace DNA bound at the allosteric site (Fig 10 C), thereby causing a relief from inhibition, rather than true activation. This situation is particularly relevant at low DNA concentrations, in which the DNA displaced from the allosteric site (Fig 10C) may bind at the active site (ES) and lead to higher rates. The earlier studies that reported activation were not designed to distinguish between the effects coming from true activation or effects coming based on the relief from allosteric inhibition (Fig. 10C). Standard techniques used to detect allosteric activation ((40) pp. 204-237, and (38) pp 21-29) should be also the most reliable approach to test for allosteric activation by Dnmt1 (Fig 4C).

References:

1. Li, E., Bestor, T. H., and Jaenisch, R. (1992) *Cell* **69,** 915-26
2. Ahuja, N., Li, Q., Mohan, A. L., Baylin, S. B., and Issa, J. P. (1998) *Cancer Res* **58,** 5489-94
3. Cunningham, J. M., Christensen, E. R., Tester, D. J., Kim, C. Y., Roche, P. C., Burgart, L. J., and Thibodeau, S. N. (1998) *Cancer Res* **58,** 3455-60
4. Kane, M. F., Loda, M., Gaida, G. M., Lipman, J., Mishra, R., Goldman, H., Jessup, J. M., and Kolodner, R. (1997) *Cancer Res* **57,** 808-11
5. Veigl, M. L., Kasturi, L., Olechnowicz, J., Ma, A. H., Lutterbaugh, J. D., Periyasamy, S., Li, G. M., Drummond, J., Modrich, P. L., Sedwick, W. D., and Markowitz, S. D. (1998) *Proc Natl Acad Sci U S A* **95,** 8698-702
6. Egger, G., Liang, G., Aparicio, A., and Jones, P. A. (2004) *Nature* **429,** 457-463
7. Flynn, J., Glickman, J. F., and Reich, N. O. (1996) *Biochemistry* **35,** 7308-15
8. Flynn, J., Fang, J. Y., Mikovits, J. A., and Reich, N. O. (2003) *J Biol Chem* **278,** 8238-43
9. Flynn, J., Azzam, R., and Reich, N. (1998) *J Mol Biol* **279,** 101-16
10. Flynn, J., and Reich, N. (1998) *Biochemistry* **37,** 15162-9
11. Bacolla, A., Pradhan, S., Larson, J. E., Roberts, R. J., and Wells, R. D. (2001) *J Biol Chem* **276,** 18605-13
12. Bacolla, A., Pradhan, S., Roberts, R. J., and Wells, R. D. (1999) *J Biol Chem* **274,** 33011-9
13. Pradhan, S., and Roberts, R. J. (2000) *Embo J* **19,** 2103-14
14. Pradhan, S., Bacolla, A., Wells, R. D., and Roberts, R. J. (1999) *J Biol Chem* **274,** 33002-10
15. Lindstrom, W. M., Jr., Flynn, J., and Reich, N. O. (2000) *J Biol Chem* **275,** 4912-9
16. Yoder, J. A., Soman, N. S., Verdine, G. L., and Bestor, T. H. (1997) *J Mol Biol* **270,** 385-95
17. Pradhan, S., and Esteve, P. O. (2003) *Clin Immunol* **109,** 6-16
18. Lauster, R., Trautner, T. A., and Noyer-Weidner, M. (1989) *J Mol Biol* **206,** 305-12
19. Glickman, J. F., Pavlovich, J. G., and Reich, N. O. (1997) *J Biol Chem* **272,** 17851-7
20. Bestor, T. H. (1992) *EMBO J* **11,** 2611-7
21. Bestor, T. H., and Verdine, G. L. (1994) *Curr Opin Cell Biol* **6,** 380-9
22. Chuang, L. S., Ian, H. I., Koh, T. W., Ng, H. H., Xu, G., and Li, B. F. (1997) *Science* **277,** 1996-2000
23. Leonhardt, H., Page, A. W., Weier, H. U., and Bestor, T. H. (1992) *Cell* **71,** 865-73
24. Aubol, B. E., and Reich, N. O. (2003) *Biochem Biophys Res Commun* **310,** 209-14
25. Jones, P. A., and Takai, D. (2001) *Science* **293,** 1068-70
26. Pedrali-Noy, G., and Weissbach, A. (1986) *J Biol Chem* **261,** 7600-2
27. Pradhan, S., and Esteve, P. O. (2003) *Biochemistry* **42,** 5321-32
28. Svedruzic, Z. M., and Reich, N. O. (2004) *Biochem.* **43**(36), 11460-11473

29. Perakyla, M. (1998) *J. Am. Chem. Soc.* **120,** 12895-12902
30. Bolden, A., Ward, C., Siedlecki, J. A., and Weissbach, A. (1984) *J Biol Chem* **259,** 12437-43
31. Reich, N. O., and Everett, E. A. (1990) *J Biol Chem* **265,** 8929-34
32. Xu, G., Flynn, J., Glickman, J. F., and Reich, N. O. (1995) *Biochem Biophys Res Commun* **207,** 544-51
33. Klimasauskas, S., Kumar, S., Roberts, R. J., and Cheng, X. (1994) *Cell* **76,** 357-69
34. Wu, J. C., and Santi, D. V. (1987) *J Biol Chem* **262,** 4778-86
35. Johnson, K. A. (ed) (1992) *Transient-State Kinetic Analysis of Enzyme Reaction Pathways*, 3rd Ed. Vol. XX. The Enzymes. Edited by A., B. P. I-XX vols., Academic Press, Inc
36. Frieden, C. (1970) *J Biol Chem* **245,** 5788-99
37. Quinn, D. M., and Sutton, L. D. (1991) in *Enzyme Mechanisam from Isotope Effects* (Cook, P. F., ed), pp. 73-126, CRC Press, Boca Raton, FL
38. Tipton, K. F. (ed) (2002) *Enzyme Assays*, 2nd Edition Ed. Practical Approach. Edited by Eisenthal, R., and Danson, M. J., Oxford University Press
39. Klimasauskas, S., Szyperski, T., Serva, S., and Wuthrich, K. (1998) *Embo J* **17,** 317-24
40. Cornish-Bowden, A. (1999) *Fundamentals of Enzyme Kinetics*, Portland Press
41. Roberts, R. J., and Cheng, X. (1998) *Annu Rev Biochem* **67,** 181-98
42. Kumar, V. D., Harrison, R. W., Andrews, L. C., and Weber, I. T. (1992) *Biochemistry* **31,** 1541-50
43. Pfeifer, G. P., Tang, M., and Denissenko, M. F. (2000) in *DNA Methylation and Cancer* (Johns, P. A., and Vogt, P. K., eds) Vol. 249, pp. 1-19, Springer-Verlag
44. Shen, J. C., Rideout, W. M. d., and Jones, P. A. (1992) *Cell* **71,** 1073-80
45. Zingg, J. M., Shen, J. C., and Jones, P. A. (1998) *Biochem J* **332**(Pt 1)), 223-30
46. Zingg, J. M., Shen, J. C., Yang, A. S., Rapoport, H., and Jones, P. A. (1996) *Nucleic Acids Res* **24,** 3267-75
47. Gabbara, S., Sheluho, D., and Bhagwat, A. S. (1995) *Biochemistry* **34,** 8914-23
48. Ivanetich, K. M., and Santi, D. V. (1992) *Prog Nucleic Acid Res Mol Biol* **42,** 127-56
49. Lau, E. Y., and Bruice, T. C. (1999) *J Mol Biol* **293,** 9-18
50. Fatemi, M., Hermann, A., Pradhan, S., and Jeltsch, A. (2001) *J Mol Biol* **309,** 1189-99
51. Hitt, M. M., Wu, T. L., Cohen, G., and Linn, S. (1988) *J Biol Chem* **263,** 4392-9
52. O'Gara, M., Klimasauskas, S., Roberts, R. J., and Cheng, X. (1996) *J Mol Biol* **261,** 634-45
53. Kumar, S., Horton, J. R., Jones, G. D., Walker, R. T., Roberts, R. J., and Cheng, X. (1997) *Nucleic Acids Res* **25,** 2773-83
54. Kumar, S., Cheng, X., Klimasauskas, S., Mi, S., Posfai, J., Roberts, R. J., and Wilson, G. G. (1994) *Nucleic Acids Res* **22,** 1-10

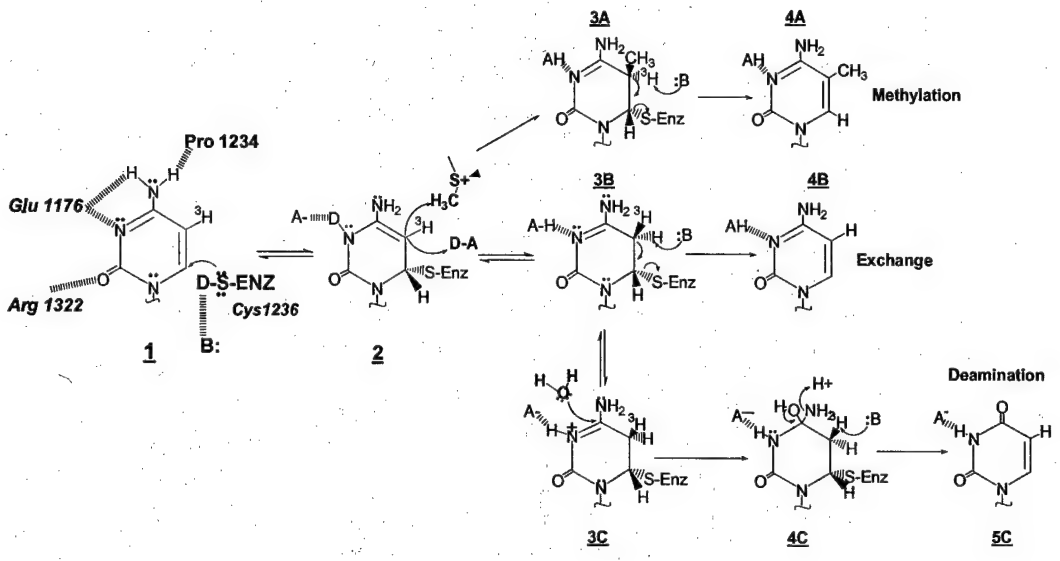

Figure 1: Reactions catalyzed by cytosine C^5 DNA methyltransferases: methylation (A) exchange (B) and deamination (C). The target cytosine interacts with active site residues (**1**) to facilitate cysteine nucleophilic attack at the C^6 position. Nucleophilic attack disrupts the pyrimidine's aromaticity, generating the reactive covalent adduct (**2**). Intermediate **2** can readily undergo electrophilic addition, either through methylation (**3A**) or protonation (**3B**). **3B** can lead to the exchange reaction (**4B**), or to mutagenic deamination (**3B**→**4C**→**5C**). Acidic groups are labeled as HA and basic groups as :B. All exchangeable protons that can result in a SKIE are shown as D in intermediates (**1** and **2**). The pre-steady state in the methylation reaction are all steps leading to intermediate **3A** (or **3B** for exchange), while the steady state are subsequent steps (see methods). Conserved active site residues are indicated.

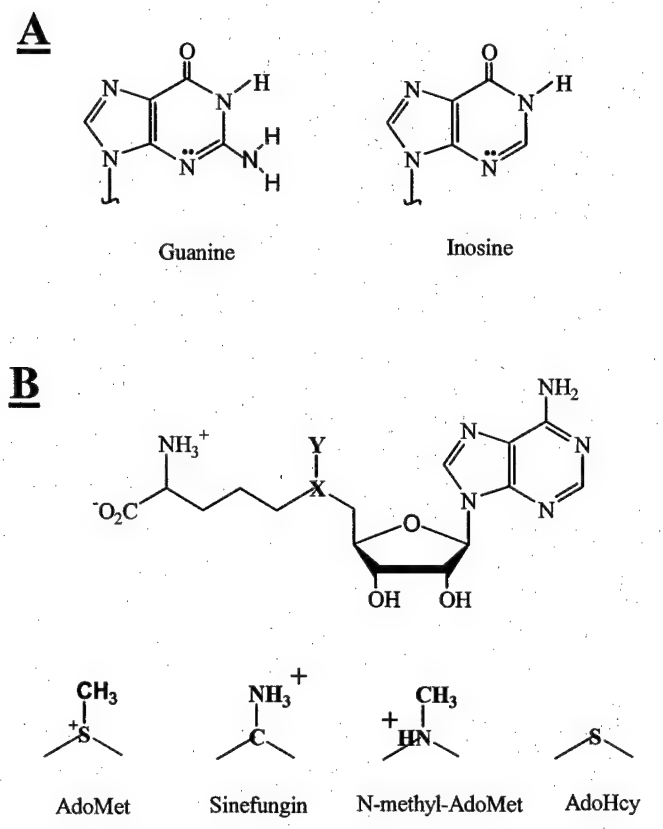

Figure 2: Inosine, guanine (A), AdoMet and its analogs (B).

Figure 3 (A-B): Dnmt 1 methylation reaction with different DNA substrates.

(A) Methylation profiles (■) with pmpoly(dI-dC) (12 μM bp) and with poly(dI-dC) (12 μM bp (○) and 260 μM (+) bp) in the presence of 145 nM Dnmt1. pmpoly(dI-dC) has an average of one out of eight cytosines methylated. **(B)** Methylation profiles (■) with pmpoly(dG-dC) (10 μM bp) and with poly(dG-dC) (4 μM bp (○) and 20 μM (+) bp) in the presence of 270nM and 350 nM Dnmt1 respectively. pmpoly(dG-dC) has an average of one out of seven cytosines methylated. All reactions were measured in the presence of 12.5 μM of AdoMet (6100 cpms/pmol).

Figure 4 (A-C): Methylation rate as a function of increasing concentration of substrate DNA. **(A)** poly(dG-dC) as the substrate and 80 nM (▽), 160 nM (•), and 250 nM (□) Dnmt1. **(B)** poly(dI-dC) as the substrate and 100 nM (▽), 200 nM (•), and 300 nM (□) Dnmt1. **(C)** pmpoly(dI-dC) (•) and pmpoly(dG-dC) (○) as substrates and 100 nM Dnmt1.

Figure 5: Tritium exchange reaction in the presence of sinefungin with different DNA substrates. **(A)** The exchange reaction with 105 nM Dnmt1, 20 μM of sinefungin and 10μM bp of ^{3}H-pmpoly(dI-dC) (•) 19 cpms/pmol, ^{5m}C:C=1:14, or ^{3}H-poly(dI-dC) (○), 33 cpms/pmol. **(B)** The exchange reaction with 160 nM Dnmt1, 20 μM of sinefungin and 8 μM bp of ^{3}H-pmpoly(dG-dC) (•) 56 cpms/pmol, ^{5m}C:C=1:15, or 8 μM bp of ^{3}H-poly(dG-dC) (○) (88 cpms/pmol).

Figure 6 (A-C): Methylation and tritium release profiles in the reaction with different DNA substrates. **(A)** Methylation (○) and tritium release (■) profiles with 12 μM bp ^{3}H-poly(dI-dC) (33 ± 2 cpms/pmol of bp) and 125 nM Dnmt1. **(B)** Methylation (○) and tritium release (■) with 12 μM bp ^{3}H-pmpoly(dI-dC) (19 ± 1.3 cpms/pmol of bp, ^{5m}C:C=1:14) and 125 nM Dnmt1. **(C)** Methylation (•) and tritium release (○) profiles with 8 μM bp ^{3}H-pmpoly(dG-dC) (76 ± 5 cpms/pmol of bp, ^{5m}C:C=1:17); methylation (■) and tritium release (□) profiles with 8 μM bp ^{3}H-poly(dG-dC) (102 ± 8 cpms/pmol of bp). The reactions with

poly(dG-dC) and pmpoly(dG-dC) had 250 nM Dnmt1. All of reactions had 12.5 μM [^{14}C-methyl] AdoMet (131 cpms/pmol).

Figure 7 (A-B): H inventory profiles during the exchange reaction with sinefungin and different DNA substrates. **(A)** The H inventory profiles for the exchange reaction with 10 μM bp poly(dG-dC) (○) and 10 μM bp premethylated poly(dG-dC) (●) in the presence of 20 μM sinefungin and 250 nM Dnmt1. The rates in H_2O and D_2O mixtures were measured during the first catalytic turnover (Fig 3B). **(B)** The H inventory profiles for the exchange reaction with 10 μM bp poly(dI-dC) (○) and 10 μM bp premethylated poly(dI-dC) (●) in the presence of 20 μM sinefungin and 250 nM Dnmt1. The rates in H_2O and D_2O mixtures were measured in the linear part of the reaction during multiple turnovers (Fig 3A). The data in both panels were analyzed using equation 3 as indicated in the text.

Figure 8: Fluorescence titration of Dnmt 1 with CRE a^Fb^M substrate

Equilibrium dissociation constant between 150 nM of Dnmt1 and increasing concentration of CRE a^Fb^m was measured in the presence of 12.5μM of AdoMet (■), and in the absence of the cofactor (□) (100 mM Tris/HCl pH=8.0, 10 mM EDTA, 10 mM DTT). Dnmt1 intrinsic fluorescence was measured in a micro cuvette (sample slot 2 mm wide, 10 mm long) using a Perkin Elmer LS50B fluorimeter at 25°C. The total sample volume was 220μl. The excitation was set at 290 nm with 5nm slit and the emission was monitored at 335 nm with 10 nm slits. The profiles were analyzed using the equations 4 and 5.

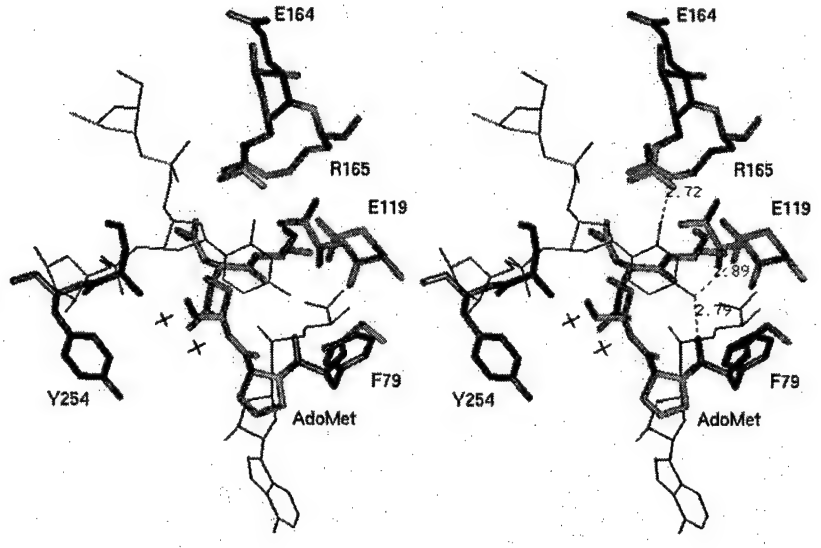

Figure 9: Active site sequence similarity between M.HhaI and Dnmt1. Stereo figure (Biosym, InsightII) of M.HhaI active site (pdb code 3MHT, (52)). The target base and AdoMet are shown as thin lines, the amino acids forming the catalytic pocket are in bold. The AdoMet structure is taken from pdb file 6MHT (53) and superimposed onto the backbone of AdoHcy present in the original structure. Water molecules are indicated as crosses (+). The image was generated in an attempt to construct the Dnmt1 active site by mapping the M.HhaI and Dnmt1 sequences to the M.HhaI structure. The amino acids colored red are identical between M.HhaI and Dnmt1 and belong to the highly conserved domains of the methyltransferase family (motifs IV, VI and X (54)). Four residues, R^{165}, E^{119}, F^{79}, and C^{81} make direct contact with the target base and mediate the methylation chemistry. Three of these four residues (R, E, and C) are found in M.HhaI and all known metazoan methyltransferases. F^{79} forms a hydrogen bond between the backbone carbonyl oxygen and the C^4 amine of the target base. F^{79} in M.HhaI is replaced by P^{1234} in Dnmt1.

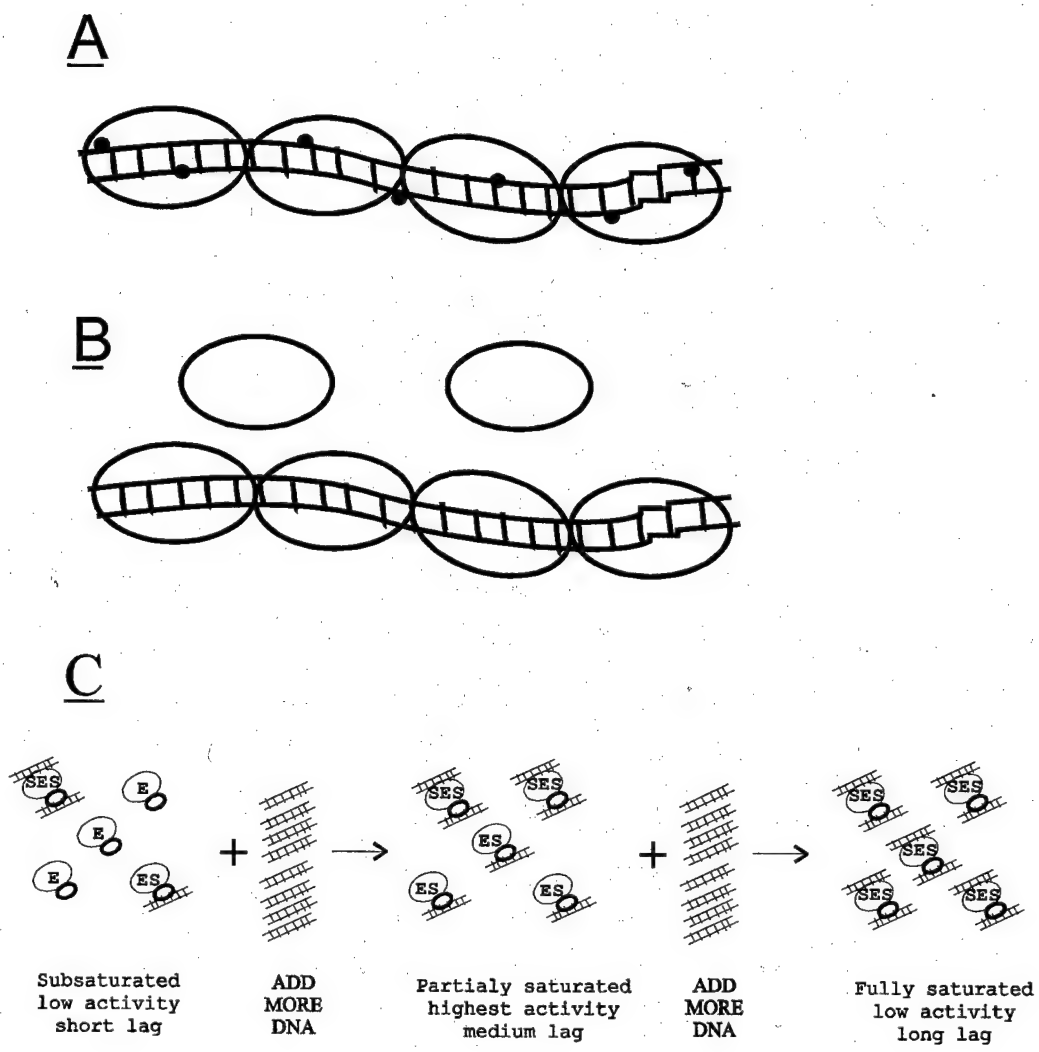

Figure 10 (A-C). Schematic for the interaction between Dnmt1 (oval) and its DNA substrate (rail).

(A) Dnmt1 bound on poly(dG-dC) or poly(dI-dC) with ^{5m}C groups (small filled circles) evenly distributed once or twice per enzyme footprint. **(B)** Given a DNA footprint of approximately 30 bp for Dnmt1 (7), a poly(dG-dC) substrate of 120 bp provides 120 CpG methylation sites, but only enough flanking DNA to afford the binding of approximately four Dnmt1 molecules. Thus, Dnmt1 and DNA are present in close stoichiometric concentrations (see supplement). Substrate concentrations are commonly represented in terms of

CpG or CpI sites (12-14), or in terms of total concentration of long DNA molecules (7,8,10). In both cases, the Dnmt1 to DNA ratios need to be considered (see supplement). The quantitative analysis of Dnmt1-DNA interaction stoichiometry is especially difficult with random DNA sequences longer than 30 bp. Due to non-specific binding, not all Dnmt1 molecules will have access to CpG sites, and different Dnmt1 molecules will have different DNA sequences bound at the active site and the regulatory site, leading to different activities (7,9). We used poly(dG-dC) and poly(dI-dC) substrates, a homogenous sequence of recognition sites, to assure that every Dnmt1 molecule is equally active when bound to DNA. (**C**) The active site (small oval) and the allosteric site (large oval) on Dnmt1 can bind DNA independently (8,11,27). Dnmt1 (**E**) with DNA bound at the active site (**ES**), allosteric site (**SE**), and the active site and the allosteric site (**SES**) at sub-saturating and saturating DNA substrate as in Figures 4 A-C.

Figure 3 A-B

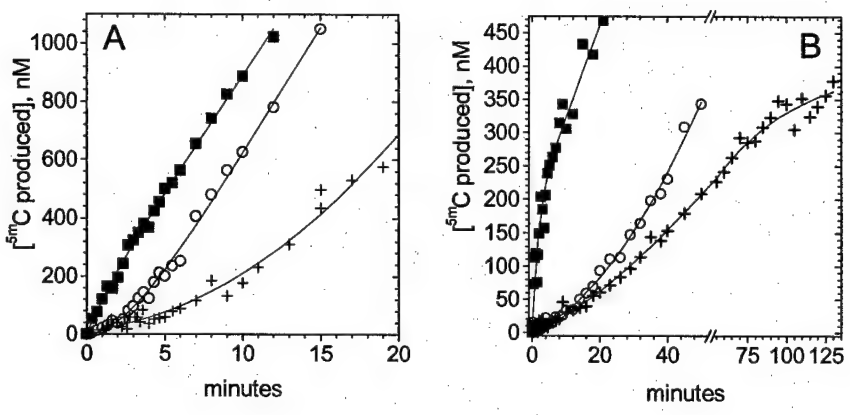

Figure 4 A-C

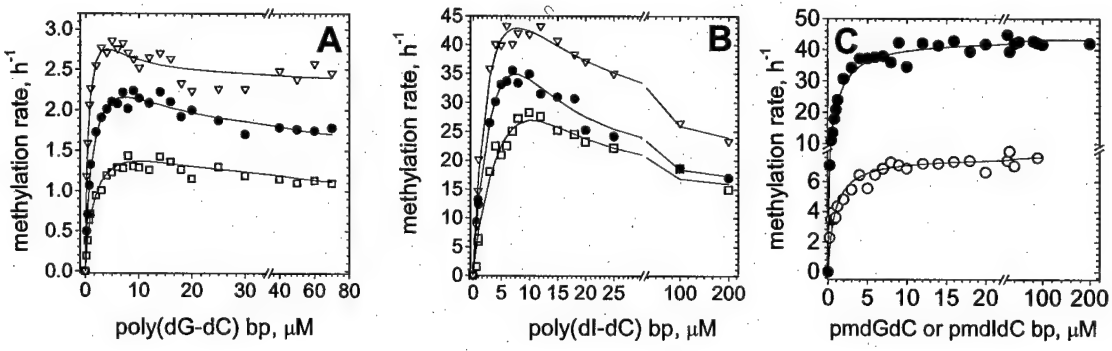

Figure 5 A-B

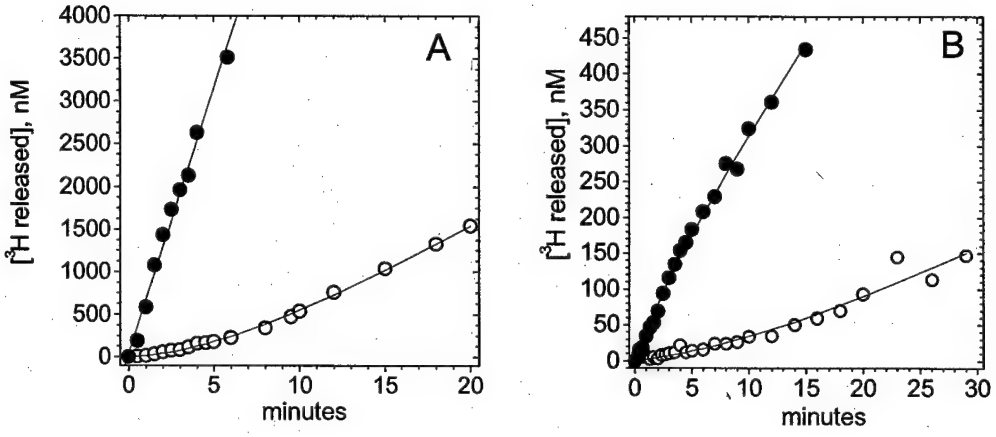

Figure 6 A-C

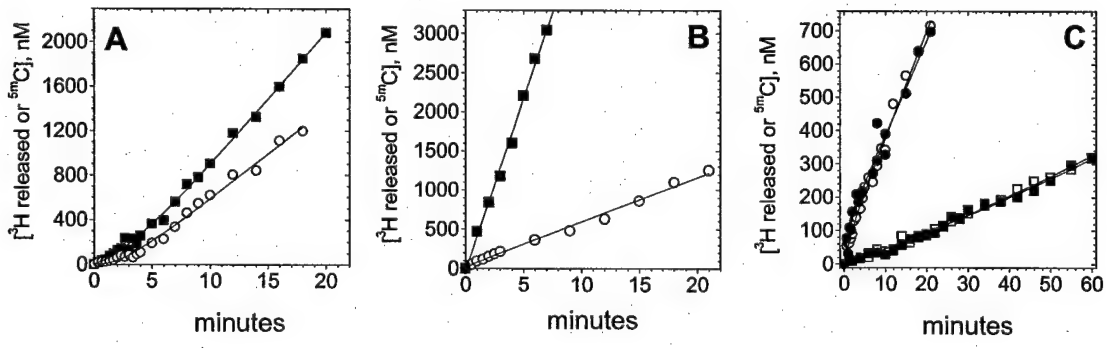

Figure 7 A-C

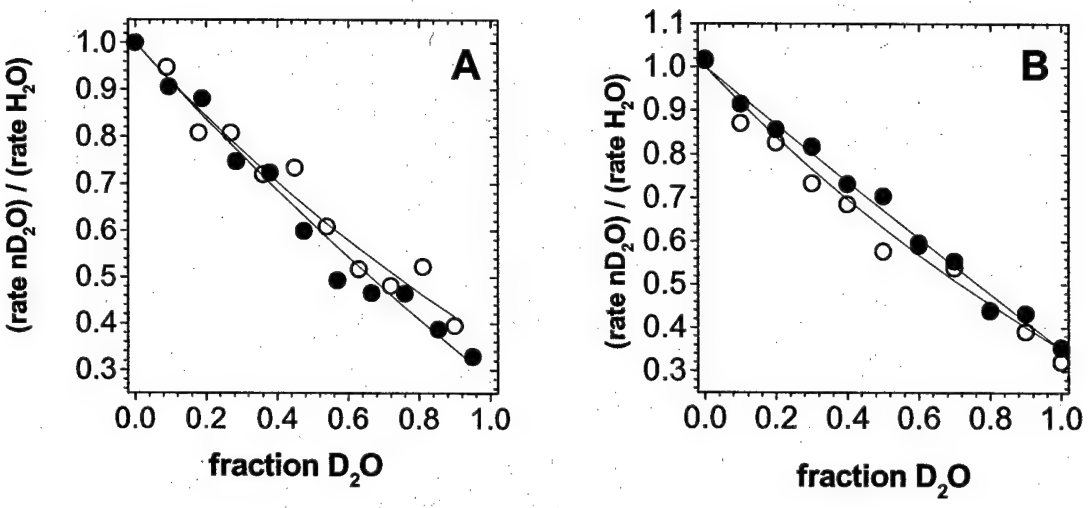

Figure 8

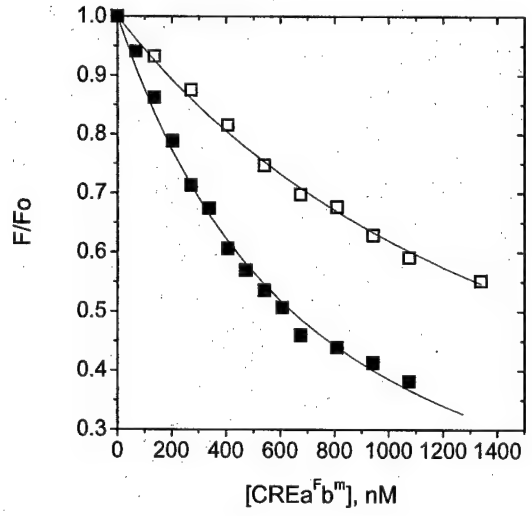

Table 1. Dnmt1 pre-steady state and steady state methylation rates with different DNA substrates [e].

Substrate	Pre steady state, h^{-1}	Steady state, h^{-1}	Conditions	References, and enzyme source	Comments
poly(dG-dC)	1.6 ± 0.6 1 ± 0.3	b 0.2 ± 0.02	@ 4 μM bp, 15 μM AdoMet @ 20 μM bp, 15 μM AdoMet	Fig 3B this study, mouse Fig 3B in this study, mouse	Lag transition rate: 1.2 ± 0.4 h^{-1} 0.7 ± 0.3 h^{-1}
pmpoly(dG-dC)	8.8 ± 0.6	5.1 ± 0.7	10 μM bp, 15 μM AdoMet	Fig 3B this study, mouse	Presteady state burst
poly(dI-dC)	a	37 ± 0.4 20.6 ± 0.3	@ 10 μM bp, 15 μM AdoMet @260 μM bp, 15 μM AdoMet	Fig 3A this study, mouse Fig 3A in this study, mouse	Lag transition rate: 19.2 ± 1.2 h^{-1} 9.6 ± 0.6 h^{-1}
pmpoly(dI-dC)	56 ± 11	36 ± 0.5	12 μM bp, 15 μM AdoMet	Fig 3A this study, mouse	Presteady state burst
poly(dI-dC) poly(dI-dC)	b	20 26	6.25 μM IC, 15 μM AdoMet 0.5 μM IC, 15 μM AdoMet	Fig 1 in (7), Fig 2A in (8), mouse	Dnmt1 concentration determined by a pre steady state burst
poly(dI-dC) poly(dI-dC)	b	70 36	10 μM AdoMet, 1 μM IC 10 μM AdoMet, 1 μM IC	Fig 4A in (14), human Fig 3A in (14), human	Dnmt1 concentration determined by Bradford
--CGG CGG CGG—[d] --GCC GCC GCC--	0.85[c]		50μM AdoMet, 1 μM CG, or 41 nM oligo	Fig 4A in (12), human	Unmethylated GC rich oligo 36 bp
--MGG MGG MGG—[d] --GCC GCC GCC--	3.0[c]		10 μM AdoMet, 1 μM CG, or 83 nM oligo	Fig 4C in (12), human	Hemimethylated GC rich oligo 36 bp
--CGG CGG CGG—[d] --GCM GCM GCM--	13.5[c]		10 μM AdoMet, 1 μM CG, or 41 nM oligo	Fig 6A in (12), human	Premethylated GC rich oligo 36 bp
PRW3602 plasmid	1.5		10 μM AdoMet, 25 μM GC	Fig 1A in (12), human	Unmethylated plasmid 2705 bp
-ATTGACGTCAAA-[d] -TAACTGCAGTTT-	0.59 ±0.02	b	15 μM oligo, 15 μM AdoMet	CRE ab in Table 3 in (7), mouse	Unmethylated 30 bp, oligo CG site in AT rich sequence
-ATTGAMGTCAAA-[d] -TAACTGCAGTTT-	3.0 ± 0.2	0.6 ± 0.05	15 μM oligo, 15 μM AdoMet	CRE ab[m] in Table 3 and Fig 4 in (7), mouse	Hemimethylated 30 bp, oligo CG site in AT rich sequence; presteady state burst
-AGGGGCGGGGCA-[d] -TCCCCGCCCCGT-	0.15 ± 0.02	b	15 μM oligo, 15 μM AdoMet	GC box ab in Table 3 in (7), mouse	Unmethylated 30 bp, oligo CG site in GC rich sequence
-AGGGGCGGGGCA-[d] -TCCCCGMCCCGT-	1.2 ± 0.1	b	15 μM oligo, 15 μM AdoMet	GC box ab[m] in Table 3, (7), mouse	Hemimethylated 30 bp, oligo CG site in GC rich sequence; presteady state burst

a can not be calculated due to the initial lag; **b** not measured; **c** not enough information available to differentiate between steady state and presteady state. The values were calculated from the actual data figures, and thus we cannot show error; **d** M stands for ^{5m}C, and methylation target sites are shown in bold; **e** The reported rates are measured at DNA and AdoMet concentrations that give the highest values. In compiling the table, we did not use reported k_{cat} values, since different publications used different procedures to calculate those values, which can led to large variations in otherwise comparable reactions (see supplement). The table shows results only from Dnmt1 studies that gave enough experimental description (enzyme and substrate concentration, product concentration) to allow independent evaluation.

Table 2 (A-B). **(A)** Exchange rates with unmethylated and premethylated poly(dG-dC) and poly(dI-dC), with AdoMet analogs and in the absence of the cofactor, for Dnmt1 and small bacterial enzyme M.HhaI (28). **(B)** Methylation and accompanying tritium release rates for Dnmt1 and bacterial enzyme M.HhaI (28).

(A)

Dnmt1 exchange rates, this study				
	Sinefungin rates, h^{-1}	**N-methyl-AdoMet rates h^{-1}**	**AdoHcy rates, h^{-1}**	**No cofactor Rates, h^{-1}**
poly(dG-dC)	3.5 ± 0.8	0.1 ± 0.02	< 0.01	0.02 ± 0.001
poly(dI-dC)	42 ± 6	0.9 ± 0.1	0.1 ± 0.02	0.18 ± 0.02
Pmpoly(dG-dC)	21 ± 4	0.5 ± 0.2	0.2 ± 0.05	0.08 ± 0.01
Pmpoly(dI-dC)	438 ± 18	9 ± 0.8	2 ± 0.4	4.4 ± 0.5

M.HhaI exchange rates [a]				
	Sinefungin rates, h^{-1}	**N-methyl-AdoMet rates h^{-1}**	**AdoHcy rates, h^{-1}**	**No cofactor Rates, h^{-1}**
poly(dG-dC)	500 ± 200 44 ± 3[b]	33 ± 5	0.1 ± 0.02	650 ± 200 105 ± 10[b]
poly(dI-dC)	165 ± 20	145 ± 15	0.5 ± 0.005	10 ± 1

(B)

	Dnmt1		**M.HhaI**	
	Methylation rates, h^{-1}	**Exchange rates, h^{-1}**	**Methylation rates, h^{-1}**	**Exchange rates, h^{-1}**
poly(dG-dC)	1.7 ± 0.4	1.5 ± 0.3	140 ± 20 40 ± 4[b]	146 ± 15 43 ± 4[b]
poly(dI-dC)	37 ± 0.4	60 ± 2	65 ± 8	230 ± 25
Pmpoly(dG-dC)	8 ± 0.6	8.4 ± 0.6		
Pmpoly(dI-dC)	36 ± 0.5	257 ± 8		

a, M.HhaI shows no difference between premethylated and unmethylated substrates prepared for this study

b, presteady state and the steady state values respectively

11460 *Biochemistry* **2004,** *43,* 11460−11473

The Mechanism of Target Base Attack in DNA Cytosine Carbon 5 Methylation†

Željko M. Svedružić‡ and Norbert O. Reich*

Department of Chemistry and Biochemistry, University of California, Santa Barbara, California 93106

Received February 12, 2004; Revised Manuscript Received July 1, 2004

ABSTRACT: We measured the tritium exchange reaction on cytosine C^5 in the presence of AdoMet analogues to investigate the catalytic mechanism of the bacterial DNA cytosine methyltransferase M.HhaI. Poly(dG-dC) and poly(dI-dC) substrates were used to investigate the function of the active site loop (residues 80−99), stability of the extrahelical base, base flipping mechanism, and processivity on DNA substrates. On the basis of several experimental approaches, we show that methyl transfer is the rate-limiting pre-steady-state step. Further, we show that the active site loop opening contributes to the rate-limiting step during multiple cycles of catalysis. Target base activation and nucleophilic attack by cysteine 81 are fast and readily reversible. Thus, the reaction intermediates involving the activated target base and the extrahelical base are in equilibrium and accumulate prior to the slow methyl transfer step. The stability of the activated target base depends on the active site loop closure, which is dependent on the hydrogen bond between isoleucine 86 and the guanine 5′ to the target cytosine. These interactions prevent the premature release of the extrahelical base and uncontrolled solvent access; the latter modulates the exchange reaction and, by implication, the mutagenic deamination reaction. The processive catalysis by M.HhaI is also regulated by the interaction between isoleucine 86 and the DNA substrate. Nucleophilic attack by cysteine 81 is partially rate limiting when the target base is not fully stabilized in the extrahelical position, as observed during the reaction with the $Gln^{237}Trp$ mutant or in the cytosine C^5 exchange reaction in the absence of the cofactor.

Enzymatic pyrimidine methylation is essential for diverse biological pathways including gene regulation, DNA and RNA biosynthesis, DNA repair, and protection against foreign DNA (*1*−*3*). Not surprisingly, the folate- and *S*-adenosylmethionine-dependent methyltransferases involved in these processes are the targets of antibiotics, cancer chemotherapies, and other drugs (*4*, *5*). Enzymatic activation of the pyrimidine ring occurs by various mechanisms, with the single common feature being formation of a covalent intermediate between the enzyme and the pyrimidine C^6 position. *S*-Adenosylmethionine-dependent DNA cytosine methyltransferases represent a broad, structurally and mechanistically characterized family of enzymes (*4*). M.HhaI[1] (methyltransferase *Haemophilus haemolyticus* type I) was the first AdoMet-dependent enzyme to be structurally characterized (*6*, *7*) and provides a paradigm not only for AdoMet-dependent enzymes but for enzymes that induce dramatic conformational changes within their duplex DNA substrate (*8*, *9*). M.HhaI methylates the underlined cytosine in duplex DNA (GCGC), stabilizing the cytosine into an extrahelical position residing within the active site of the enzyme (Figure 1).

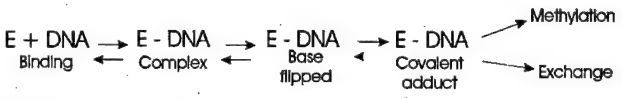

FIGURE 1: Four steps leading to methylation or exchange by DNA cytosine methyltransferases. The exchange reaction is proposed to share all steps up to the transfer of a proton in place of a methyl moiety. The equilibrium steps up to and including covalent adduct formation are implied by the results in this work.

Formation of the ternary M.HhaI·DNA·AdoMet complex is followed by at least three steps leading to product formation, outlined in Figure 1: base flipping, covalent adduct formation, and methyl transfer. We and others have studied this process in detail for M.HhaI (*9*, *10*), as well as other DNA methyltransferases (*11*, *12*). In contrast to the detailed structural information available for M.HhaI (*8*), little is known about the kinetics of these steps. For example, the flipping and methyl transfer kinetics have been directly measured for M.EcoRI (*11*−*13*), an adenine methyltransferase, but other than similar experiments with mismatched DNA (*14*), no such measurements have been made for M.HhaI. ^{19}F NMR and gel shifting evidence support the existence of two M.HhaI·DNA intermediates involving an extrahelical cytosine, one of which is stabilized by the presence of the cofactor (*15*); however, these experiments provide limited mechanistic insights since they represent largely static descriptions and use 5-fluorocytosine, which

† This work was supported by NIH Grant GM 463333 and NSF Grant MCB-9983125 to N.O.R.

* To whom correspondence should be addressed: e-mail, reich@chem.ucsb.edu; tel, 805-893-8368; fax, 805-893-4120.

‡ Current address: School of Molecular Biosciences, Department of Biophysics and Biochemistry, Washington State University, Pullman, WA 99164.

[1] Abbreviations: AdoMet, *S*-adenosyl-L-methionine; AdoHcy, *S*-adenosyl-L-homocysteine; bp, base pair; C^5, C^2, C^4, etc., carbon 5, carbon 2, carbon 4, etc. of the target base ring; ^{5m}C, 5-methyl-2′-deoxycytosine; dCTP, deoxycytosine triphosphate; poly(dG-dC) or dGdC, double-stranded alternating polymer of deoxyguanine and deoxycytosine; dITP, deoxyinosine triphosphate; M.HhaI, methyltransferase *Haemophilus haemolyticus* type I; M.SssI, methyltransferase *Spiroplasma* sp. type I; poly(dI-dC) or dIdC, double-stranded alternating polymer of deoxyinosine and deoxycytosine; pss, pre steady state: ss, steady state; sin, sinefungin; WT, wild type; N-AdoMet, *N*-methyl-AdoMet.

10.1021/bi0496743 CCC: $27.50
Published on Web 08/19/2004

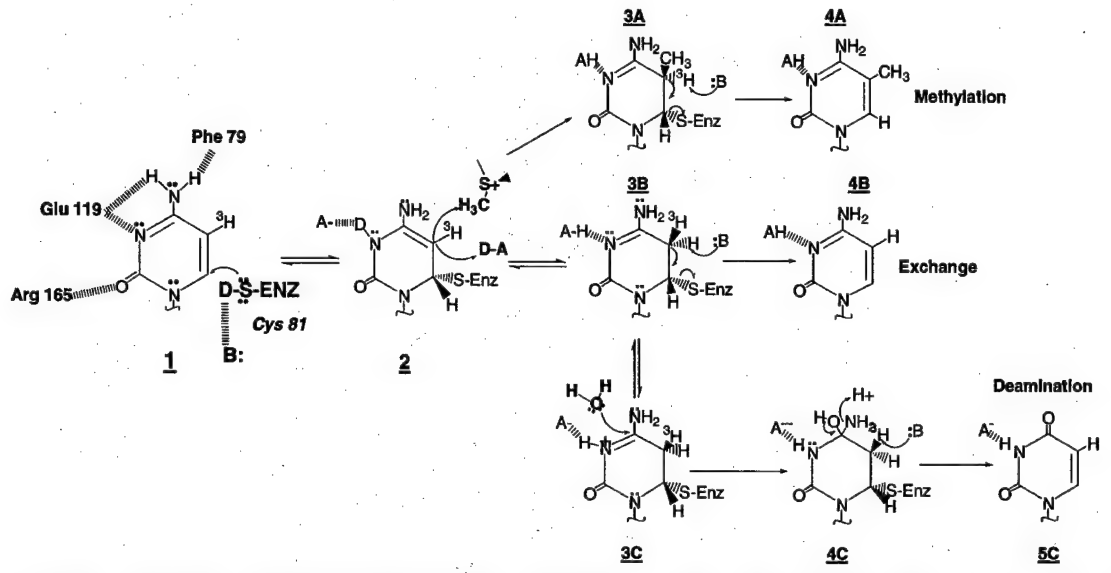

FIGURE 2: Reactions catalyzed by cytosine methyltransferases: methylation (A), ^3H exchange (B), and deamination (C). The extrahelical cytosine interacts with active site amino acids that facilitate cysteine 81 nucleophilic attack at cytosine C^6 (intermediate **1**). Nucleophilic attack disrupts the pyrimidine's aromaticity, forming intermediate **2**. Intermediate **2** can readily undergo electrophilic addition, either through methylation (**3A**) or protonation (**3B**). The 5,6-dihydropyrimidine adduct (**3B**) can lead to the exchange reaction (**4B**) or be attacked by water to form intermediate **4C**, which can lead to elimination of NH_3 and mutagenic deamination (**5C**). Acidic groups are labeled as HA and basic groups as :B. All exchangeable protons that can cause SKIE are shown as D in the intermediates (**1** and **2**). ^3H exchange rates are measured by acid quench; thus the ^3H exchange reaction is detected as soon as intermediate **3A** or **3B** is formed. The methylation reaction is detected as soon as intermediate **3A** is formed. For both reactions the pre steady states are steps that lead to intermediate **3A** (and **3B** for exchange), while the steady-state rates include the subsequent steps (see Methods).

severely perturbs the kinetics of attack and methyl transfer (*10*). Single-turnover measurements with M.HhaI show that the methyl transfer step, or some prior transition, has a rate constant of 0.14−0.26 s^{-1} (*9*, *10*), and the methylation reaction shows a pre-steady-state burst, suggesting that methyl transfer is followed by slow product release steps (*9*, *10*).

We refer to the base flipping and covalent adduct formation as the "target base attack" steps which serve to activate the cytosine to displace the electrophilic methylsulfonium on AdoMet (Figure 2). The proposed mechanism in Figure 2 is based largely on three lines of evidence: (1) structural and mechanistic parallels with the well-studied folate-dependent thymidylate synthetase (*16*), (2) structure−function studies of M.HhaI (*7*, *17*) and other DNA cytosine methyltransferases (*8*), and (3) theoretical studies (*18*). However, details involving individual steps, the identity of the functionalities involved, and the relative contribution to rate-limiting steps remain uncertain. For example, Arg^{165}, Glu^{119}, and Phe^{79} are clearly positioned to interact with the cytosine as shown in Figure 1. Yet, the proposal that the nucleophilic attack by cysteine 81 is assisted by protonation at the cytosine N^3, rather than the cytosine O^2 (*18*) (or both), has no experimental support. Similarly, there is little evidence for the existence, identity, or importance of moieties involved in acid- and base-assisted catalysis to facilitate the β-elimination step (Figure 2). Protein engineering efforts to determine the mechanisms of base flipping and stabilization include the interaction between glutamine 237 and the orphan guanosine (*19*); although the mutants retained function, albeit reduced ~50-fold, the underlying mechanisms were not determined.

M.HhaI catalyzes the exchange of the cytosine C^5 hydrogen (*17*), which is compelling evidence for the proposed mechanism and cysteinylcytosine covalent intermediate (Figure 2). Moreover, because this reaction occurs in the absence of cofactors and is inhibited by *S*-adenosylhomocysteine (*17*), it supports methods of study not suitable for the methylation reaction itself. No evidence for the exchange reaction during AdoMet-dependent steady-state methylation was described for M.HhaI (*17*) or for M.EcoRII, the only other DCMTase studied by this method (*20*); rather, M.HhaI simply replaces the C^5 proton with a methyl group (Figure 2). Bacterial DCMTases catalyze the deamination of cytosine to uracil and of 5-methylcytosine to thymine (Figure 2 and refs *21*−*23*). This mutagenic reaction, if catalyzed by human DCMTases, is postulated to account in part for the high level of CG to TG mutations that occur within critical genes in human cancers (*24*).

We describe pre-steady-state, steady-state, pH, and solvent kinetic isotope effect (SKIE) studies of the methylation and ^3H exchange reactions using structural analogues of the DNA and cofactor, AdoMet. The exchange reaction provides unique opportunities because the mechanistic importance of the cofactor can be readily probed with analogues. We used poly(dI-dC) and poly(dG-dC) in our analysis because (i) these substrates allow a quantitative analysis since every enzyme molecule can bind a recognition site and proceed with catalysis, and (ii) the preparation of DNA substrates containing a single radiolabeled [5-^3H]cytosine is problematic and provides a less sensitive measure of catalysis (*20*). Poly(dI-dC) and the $Gln^{237}Trp$ mutant provide unique opportunities to study the base flipping step and stabilization of the extrahelical cytosine. Pre-steady-state kinetic, pH, and SKIE studies were used to determine the importance of cysteine 81 toward the rate-limiting events during target base attack, methylation, and exchange.

EXPERIMENTAL PROCEDURES

Materials

S-Adenosyl-L-[*methyl*-^{14}C]methionine (59 mCi/mmol or 131 cpm/pmol), *S*-adenosyl-L-[*methyl*-^{3}H]methionine (66−82 Ci/mmol or 6100−7200 cpm/pmol), deoxy[5-^{3}H]cytidine 5′-triphosphate (19.0 Ci/mmol) ammonium salt, and Sequenase 2.0 were purchased from Amersham Corp. Poly(dI-dC), 1960 bp, dITP, and dCTP were purchased from Pharmacia Biotech. DTT, Trizma, and acid-washed activated charcoal were purchased from Sigma Chemical Co. BSA was purchased from Boehringer Mannheim, and it was DNA free on the basis of the absorbance ratio at 280 and 260 nm. DE81 filters were purchased from Whatman, Inc. Sinefungin was purchased from Sigma Chemical Co. AdoMet (85% pure) was purchased form Sigma Chemical Co. and HPLC purified as described earlier (*25*). WT M.HhaI and the Gln^{237}Trp^{237} mutant were expressed using *Escherichia coli* strain ER1727 containing plasmids pHSHW-5 and pHSH0-1, respectively (generously provided by Dr. S. Kumar, New England Biolabs), and purified as previously described (*9*). The M.HhaI concentration at the end of the preparation was determined by pre-steady-state burst. AdoMet, sinefungin, poly(dI-dC), and poly(dG-dC) concentrations were determined by absorbance at 260 nm. The respective molar absorptivity coefficients are 15.0×10^3 M^{-1} cm^{-1} for AdoMet and its analogues, 6.9×10^3 M^{-1} cm^{-1} for poly(dI-dC) (per bp), and 8.4 10^3 M^{-1} cm^{-1} for poly(dG-dC) (per bp) (Pharmacia Technical Infomation Sheet).

Methods

Preparation of [5-^{3}H]Cytosine−Poly(dI-dC). Labeling reactions were prepared by incubating 500 μM bp poly(dI-dC) with 100 μM [5-^{3}H]dCTP, 1 mM CTP, 10 mM dITP with 0.62 unit/μL Sequenase 2.0 in 40 mM Tris-HCl (pH 7.5), 10 mM $MgCl_2$, 50 mM NaCl, 10 mM DTT, and 1.0 mg/mL BSA. Labeling reactions for [5-^{3}H]cytosine−poly(dG-dC) used the same approach except that poly(dI-dC) was replaced with poly(dG-dC) and 10 mM dITP was replaced by 1 mM dGTP. Reactions were run for 5 h at room temperature. Incorporation of [5-^{3}H]cytosine was followed by spotting the reaction aliquots onto DE81 paper. Spotted papers were washed twice for 5 min in 500 mM KP_i buffer (pH = 6.8) and dried under a heat lamp. The extent of label incorporation was calculated by comparing the counts from unwashed and washed papers. This procedure gives approximately 60% label incorporation. The reaction was stopped by incubating the sample for 5 min at 90 °C followed by slow cooling (2−3 h^{-1}) to room temperature. The cooled sample was centrifuged and the supernatant dialyzed against 10 mM Tris-HCl (pH 8.0) and 10 mM EDTA. The removal of reaction components was determined by comparing the radioactivity from unwashed and washed DE81 papers. The [5-^{3}H]cytosine-labeled poly(dI-dC) and poly(dG-dC) prepared in the described procedure was between 13 and 40 cpm/pmol of base pairs for dIdC,and between 60 and 105 cpm/pmol of base pairs for dGdC.

Methylation Reactions. The methylation reactions were prepared by incubating M.HhaI, DNA substrate, and radioactive AdoMet in 100 mM Tris-HCl (pH 8.0), 10 mM EDTA, 10 mM DTT, and 0.5 mg/mL BSA at 37 °C. The enzyme and DNA concentrations are specific for each assay and are described in the figure legends. Incorporation of [^{3}H]-methyl groups in the DNA substrate was determined as previously described (*25*, *26*). Briefly, the reaction is followed by spotting reaction aliquots on DE81 paper, leading to the detection of intermediate **3A** and all products resulting from its formation (Figure 2). Thus, the pre-steady-state rates are determined by the steps that lead to intermediate **3A** (Figures 1 and 2), while the steady-state rates are determined by steps that follow formation of intermediate **3A**.

Tritium Exchange Reactions. The tritium exchange reaction was followed essentially as previously described (*17*). Briefly, tritium exchange is measured by quenching reaction aliquots in an acid suspension (HCl, pH = 2.0−2.5) of activated charcoal. Because **3A** and **3B** (Figure 2) rapidly degrade in acid, their formation can be detected prior to release from the enzyme, thereby allowing the determination of kinetic constants up to and including the formation of **3A** and **3B** as a part of the pre-steady-state rate. The enzyme concentration, DNA concentration, and cofactor concentration are specific for each assay and are described in the figure legends. All reactions were saturated with the cofactor. The reaction buffer was 100 mM Tris-HCl (pH, 8.0), 10 mM EDTA, 10 mM DTT, and 0.5 mg/mL BSA.

Data Analysis. All reaction rates were calculated using Microcal Origin 5.0. All rates were reported as the best fit values ± standard deviation. The burst profiles were fit to a two-step irreversible mechanism (*27*):

$$[P](t) = \alpha E_t(1 - e^{-k_{pss}t}) + E_t k_{ss} t \qquad (1)$$

where $[P](t)$ is the product concentration generated at time t, E_t is the total enzyme concentration, α is the factor that correlates stoichiometry between burst amplitude and enzyme concentration, k_{pss} and k_{ss} are pre-steady-state and steady-state rates, respectively, and t is the time from the start of the reaction. Unless otherwise indicated, all other profiles were analyzed using a linear equation. Each experiment was repeated in several independent measurements until the reproducibility of observed phenomena was established. The presented data show representative examples of analyzed phenomena.

pH Measurements. pH measurements between 6.5 and 7.5 were measured in 100 mM Bis-Tris-HCl ($pK_a = 6.5$ at 25°C), EDTA (10 mM), DTT (10 mM), and BSA (0.5 mg/mL). The pH profiles between 7.5 and 9.0 were measured in 100 mM Tris-HCl ($pK_a = 8.1$ at 25°C), EDTA (10 mM), DTT (10 mM), and BSA (0.5 mg/mL). The catalytic rates were within 10% when measured in Bis-Tris and Tris at pH 7.5. The pH profiles were analyzed using a single acidic and basic site (*28*):

$$v = \frac{V_{max}}{1 + 10^{-pH}/K_1 + K_2/10^{-pH}} \qquad (2)$$

where V_{max} is the maximal rate observed in the pH profile, K_1 is the acidic constant, and K_2 is the basic constant. The expected SKIE at the given pH and pK_a for the active site cysteine was calculated using the relations (*29*):

$$10^{pH-pK_a} = [cys\text{-}]/[Hcys]$$

and

$$2 = \frac{[cys_D\text{-}]/[Dcys]}{[cys_H\text{-}]/[Hcys]} \quad (3)$$

where [cys-] is the concentration of unprotonated cysteine, [cys_D-] and [cys_H-] are the concentrations of unprotonated cysteine in D_2O and H_2O buffer, [Dcys] and [Hcys] are the concentrations of protonated cysteine in D_2O and H_2O buffer, and the ratio of unprotonated and protonated cysteine in D_2O is two times higher than the ratio of unprotonated and protonated cysteine in H_2O. The sum of [cys_D-] and [Dcys] or [cys_H-] and [Hcys] equals the total cysteine concentration.

SKIE Measurements. All experiments in D_2O buffers were measured in parallel with corresponding H_2O experiments, and except for the solvent difference the two reactions are identical. The D_2O buffer was prepared as 10×, and its pH was adjusted, taking into account the pD vs pH correction (*29*) to be the same as in the corresponding H_2O buffer. Proton inventory profiles were analyzed using different forms of the Gross−Buttler equation (*29*):

$$k_\nu^{D_2O} = k^{H_2O}\frac{(1+\nu-\nu\phi^T)^n}{(1+\nu-\nu\phi^G)^m}Z^{-\nu} \quad (4)$$

where $k_\nu^{D_2O}$ is the measured rate at the given fraction of D_2O, k^{H_2O} is the rate measured in 100% H_2O, ν is the fraction of D_2O at which the rate was measured (i.e., 0.1, 0.2, 0.3, etc.), ϕ_T and ϕ_G are deuterium fractionation factors at the transition and the ground state, respectively, and Z is a cumulative fractionation factor for multiple small sites (*29*). Different forms of eq 4 can be produced by changing the values for parameters n, m, and Z as described in the Results section. Each form of eq 4 represents a unique mechanism with a distinct shape. Accordingly, each proton inventory profile was analyzed using several forms of eq 4, and the best fits were chosen on the basis of error in the best fit parameters, random distribution of the best fit residuals, and resolution between the fit parameters.

RESULTS

Methylation and Proton Exchange Reactions with ^{3}H-Poly-(dG-dC) (Figure 4). We measured the proton exchange rates in the presence of AdoMet and AdoMet analogues and in the absence of cofactors to focus on the catalytic events involving the cytosine C^5 (Figure 2, conversions **2** → **3A** or **2** → **3B**). The experiments were inspired by previous studies which showed that the cofactor can modulate the exchange (*17*) and cytosine deamination rates (*21*−*23*). The AdoMet analogues used in this study differ only at the position of the active methyl group (Figure 3). The exchange rates vary by over 3 orders of magnitude when measured in the presence of different cofactor analogues or in the absence of the cofactor (Table 1). The exchange rates are low in the presence of AdoMet (Figure 4A) and AdoHcy, intermediate with *N*-methyl-AdoMet, and high with sinefungin and in the absence of the cofactor (Figure 4B, Table 1). The relatively high tritium release rates in the presence of AdoMet result from the methylation reaction (Figure 2, **3A** → **4A**); thus no net exchange occurs with AdoMet (Figure 2, **3B** → **4B**). A stoichiometric proton release during the steady-state methylation reaction was shown before (*17*). Here we show that

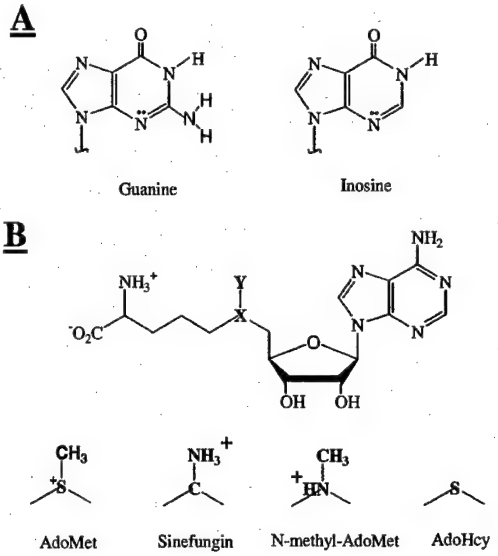

FIGURE 3: Structures of inosine and guanine (A) and AdoMet and its analogues (B).

Table 1: Pre-Steady-State and Steady-State Rate Constants for Methylation and ^{3}H Exchange Reactions[a]

	poly(dG-dC)		poly(dI-dC)[b]
	pss	ss	ss
wild type			
methylation (AdoMet)	140 ± 20	40 ± 4	65 ± 8
exchange (AdoMet)	146 ± 15	43 ± 4	230 ± 25
exchange (sinefungin)	500 ± 200	44 ± 3	165 ± 20
exchange (no cofactor)	650 ± 200	105 ± 10	10 ± 1
exchange (N-AdoMet)	33 ± 5	33 ± 5	145 ± 15
exchange (AdoHcy)	0.1 ± 0.02	NM	0.5 ± 0.005
$Gln^{237}Trp$			
methylation (AdoMet)	1.10 ± 0.05	NM	1.15 ± 0.1
exchange (AdoMet)	1.06 ± 0.04	NM	1.15 ± 0.05
exchange (no cofactor)	0.045 ± 0.008	NM	0.047 ± 0.006
exchange (sinefungin)	0.31 ± 0.02	NM	NM
exchange (N-AdoMet)	0.23 ± 0.03	NM	NM

[a] All rates are expressed as h^{-1} ± best fit error. NM, not measured. All values below the $Gln^{237}Trp$ row are for this mutant. [b] The reactions with poly(dI-dC) do not show a pre-steady-state (pss) burst, so the rates measured during the first turnover and the subsequent turnovers are all indicated as the steady-state (ss) rates.

the methylation and proton release reactions have identical pre-steady-state rates. Thus, in the presence of AdoMet, intermediate **2** leads exclusively to methyl transfer (Figure 2, **2** → **3A**). A pre-steady-state burst is observed during AdoMet-dependent methylation and exchange (Figure 4A), in the exchange reaction in the presence of sinefungin (Figure 4B), and in the ^{3}H exchange reaction without cofactors (Figure 4B). The relatively large errors for the reported pre-steady-state rates (Table 1) are caused by the fast rates, allowing only for measurements of the burst and later stages of the reaction (Figure 4B). The pre-steady-state burst in the methylation reaction indicates that the steps leading to methyl transfer (Figure 2, **2** → **3A**) are faster than the subsequent steps, while the pre-steady-state burst in the exchange reaction indicates that the proton transfer (Figure 2, **2** → **3B**) at C^5 is faster than the subsequent steps. In summary, this study shows that the ability of different cofactor analogues to support or inhibit the exchange rates is dependent on the availability of a proton proximal to the C^5 moiety of the target cytosine (Figure 3).

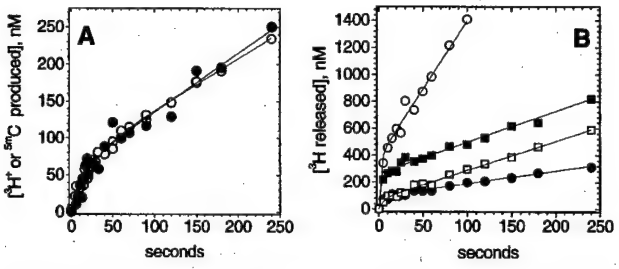

FIGURE 4: ^{3}H exchange and methylation reaction with ^{3}H-poly-(dG-dC). (A) ^{3}H exchange (○) and methylation rates (●) were measured in parallel by using M.HhaI (75 nM), ^{3}H-poly(dG-dC) (10 μM bp, 80 cpm/pmol), and ^{14}C-AdoMet (12 μM, 130 cpm/pmol). The rates were calculated using eq 1. (B) All reactions were measured in the presence of M.HhaI (285 nM) and ^{3}H-poly(dG-dC) (8 μM bp, 88 cpm/pmol). The reactions with sinefungin (10 μM) at pH = 8.0 (■) and pH = 6.5 (●) are shown. The reactions in the absence of the cofactor at pH = 8.0 (○) and pH = 6.5 (□) are also shown.

Analysis of pH and Solvent Kinetic Isotope Effects (SKIE) during Methylation and Exchange Reactions with Poly(dG-dC) (Figure 5). Previous studies suggested that nucleophilic attack by the active site Cys^{81} is rate limiting during methylation (*10*, *18*). Because cysteine has a unique 2-fold preference for hydrogen vs deuterium (*29*), pH/SKIE studies can be used to probe if the rate-limiting step in methylation or any of the exchange reactions depends on nucleophilic attack by Cys^{81} (*30*−*33*). If Cys^{81} attacks the target base as the thiolate, the observed reactions will give an inverse SKIE with the ground state ϕ_G close to 0.5 (eq 4 and ref *29*). If Cys^{81} attacks as the thiol and is deprotonated during nucleophilic attack, the reaction will give a normal SKIE and the transition state ϕ_T will be close to 0.5 (eq 4 and ref *29*). Both effects should disappear as the pH increases above the pK_a for the active site cysteine. We measured the pH profiles for the pre-steady-state rates during methylation and different exchange reactions (e.g., in the absence of cofactors and in the presence of sinefungin) to determine the number of pH-sensitive steps and the corresponding pK_a values (Figure 5). In reactions without cofactor analogues and with sinefungin we show that changes in pH affect the intercept in the pre-steady-state burst (Figure 4B), since the pre-steady-state rates were too fast to allow accurate determination of the kinetic constants. The pH profiles were analyzed using eq 2 and can be best described assuming a single protonation site with pK_as ranging from 7.4 to 7.8 (Table 2). Interestingly, the pH profiles are similar even though the catalytic rates vary by 3 orders of magnitude, suggesting that a similar residue(s) is (are) critical for the pH-sensitive step. The observed SKIE is specific for each reaction and principally pH-independent, unlike the pH−activity profiles. Thus, the pH and SKIE profiles are at least in part caused by different groups, and it is thus unlikely that a single rate-limiting step is being probed by these methods. We used eq 3 to generate the predicted SKIE profiles for a reaction limited by a nucleophilic cysteine, the medium value for the measured pK_a range (Table 2), and the known fractionation factor for cysteine $\phi = 0.5$ (*29*).

The exchange reaction without cofactor has an inverse SKIE, and the SKIE increases with increasing pH (Figure 5B). This pH-induced change in the SKIE indicates that the SKIE is at least in part a result of a pH-sensitive step. If the pH response is controlled by the active site Cys^{81}, a pH-induced change in the SKIE suggests that conversion between intermediates **1** and **2** contributes to the rate-determining step. The observed pH/SKIE profiles are different from the pH/SKIE profiles expected for a reaction that is *primarily* controlled by a cysteine nucleophilic attack with the measured pK_a (Figure 5B, upper panel). However, the observed SKIE may be caused by the nucleophilic cysteine and some other group, which is consistent with dome-shaped proton inventory studies (Figure 10A).

Methylation and Tritium Exchange Reaction with Poly-(dI-dC) and AdoMet Analogues (Figures 6 and 7). We

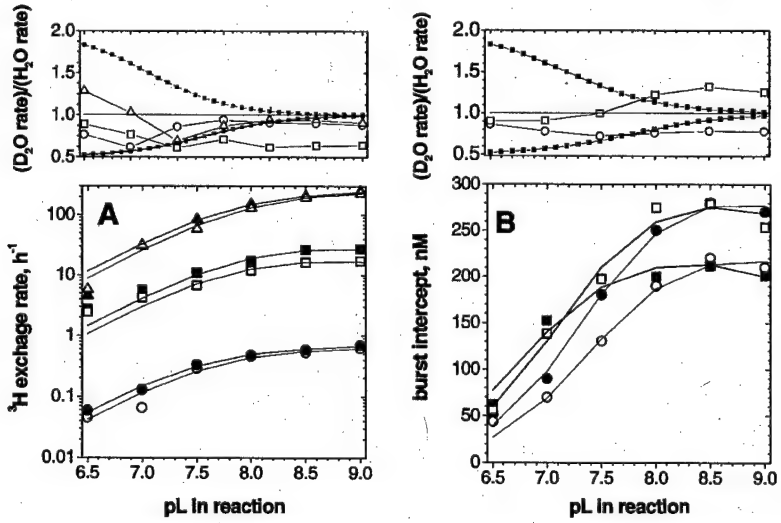

FIGURE 5: pH profiles and SKIE analysis of the ^{3}H exchange reaction with ^{3}H-poly(dG-dC). (A) pH profile for the ^{3}H exchange reaction with AdoMet (▲, △), *N*-methyl-AdoMet (■, □), and AdoHcy (●, ○) in H_2O and D_2O, respectively. Each profile was analyzed using eq 2, and the best fit values are listed in the Table 2. In the upper panel the symbols represent AdoMet (△), *N*-methyl-AdoMet (□), and AdoHcy (○). The dashed line is calculated using eq 3 and shows the expected SKIE if the rate-limiting step is primarily dependent on a nucleophilic cysteine with pK_a = 7.5. (B) pH profile for the burst intercept in the ^{3}H exchange reaction with sinefungin (●, ○) and in the absence of the cofactors (■, □) in H_2O and D_2O. Each profile was analyzed using eq 2, and the best fit values are listed in Table 2. In the upper panel the symbols represent sinefungin (○) and the reaction in the absence of the cofactor (□). The dashed line is calculated using eq 3 and represents the expected SKIE if the rate-limiting step is primarily dependent on a nucleophilic cysteine with pK_a = 7.5.

Table 2: Summary of the pH and SKIE Analysis of the Presented Reactions

	apo	sinefungin	AdoMet	N-AdoMet	AdoHcy
			Wild Type with ^{3}H-Poly(dG-dC) Substrate		
SKIE type and shape[a]	inverse and dome shape	normal and bowl shape	none	normal and dome shape	none
ϕ_T	3.2 ± 1	0.42 ± 0.07		0.34 ± 0.04	
ϕ_G	2.1 ± 0.7	1.8 ± 0.2		1.4 ± 0.2	
pK_a(H_2O)	7.7 ± 0.08	7.3 ± 0.05	7.8 ± 0.06	7.8 ± 0.2	7.5 ± 0.07
pK_a(D_2O)	7.1 ± 0.08	7.3 ± 0.07	7.9 ± 0.04	7.4 ± 0.3	7.6 ± 0.1
comments				$Z = 1 \pm 0.03$	
			Wild Type with ^{3}H-Poly(dI-dC) Substrate		
SKIE type and shape[a]	inverse and almost linear	normal and bowl shape	normal and linear when reciprocal	normal and linear when reciprocal	none
ϕ_T	3.7 ± 0.5	0.47 ± 0.05	1.08 ± 0.32	0.94 ± 0.33	NM[b]
ϕ_G	1.1 ± 0.2	1.7 ± 0.12	2.04 ± 0.66	2.15 ± 0.7	NM[b]
pK_a(H_2O)		7.4 ± 0.07	7.6 ± 0.04	7.5 ± 0.08	7.6 ± 0.06
pK_a(D_2O)		7.5 ± 0.05	7.4 ± 0.06	7.7 ± 0.07	7.5 ± 0.08
comments	no pH response	slower than GC in pss[c] and faster in ss[c]	exchange faster than methylation	5 times faster with IC relative to GC	5 times faster with IC relative to GC
			Gln^{237}Trp with ^{3}H-Poly(dG-dC) Substrate		
SKIE type and shape[a]	inverse and mild dome shape	normal and linear when reciprocal	inverse and mild dome shape	inverse and mild dome shape	
ϕ_T	2.4 ± 0.5	1.1 ± 0.3	2.2 ± 0.8	1.8 ± 0.04	
ϕ_G	1 ± 0.5	2.1 ± 0.6	1.1 ± 0.4	0.96 ± 0.2	
pK_a(H_2O)	NM[b]	7.3 ± 0.06	7.4 ± 0.12	7.4 ± 0.07	
pK_a(D_2O)		7.5 ± 0.1	7.5 ± 0.1	7.6 ± 0.1	
comments		SKIE type and shape changes with pH	SKIE changes with the pH	SKIE type and shape changes with pH	

[a] To describe the shape, we used the nomenclature described in ref *29*; inverse means the reaction is faster in D_2O, and normal means the reaction is slower in D_2O. [b] NM, not measured. [c] pss stands for pre steady state; ss stands for steady state.

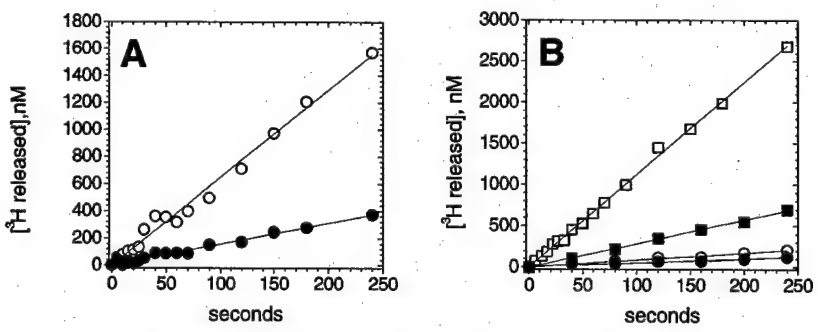

FIGURE 6: ^{3}H exchange and methylation reaction of ^{3}H-poly(dI-dC). (A) ^{3}H exchange (○) and methylation rates (●) were measured in parallel using M.HhaI (100 nM), ^{3}H-poly(dI-dC) (10 μM bp, 13 cpm/pmol), and ^{14}C-AdoMet (12 μM, 130 cpm/pmol). The rates were calculated by linear regression. (B) ^{3}H exchange reaction with sinefungin (□, ■) and in the absence of the cofactor (○, ●) at pH = 8.0 and 6.5, respectively. All reactions with ^{3}H-poly(dI-dC) were analyzed using linear equations.

compared the methylation and proton exchange reactions with ^{3}H-poly(dG-dC) and ^{3}H-poly(dI-dC) to understand how enzyme−DNA interactions alter catalysis. Poly(dI-dC) is a good substrate for the methylation and exchange reactions (Table 1 and Figure 6). Except for the exchange reaction in the absence of the cofactor (Table 1), the rate for poly(dI-dC) and the pre-steady-state and steady-state rate for poly(dG-dC) are quite similar. The reaction with poly(dI-dC) is slightly faster with AdoHcy and *N*-methyl-AdoMet and slightly slower with sinefungin (Table 1). The AdoMet-dependent methylation reaction and the sinefungin-dependent exchange reactions have 2-fold slower rates with poly(dI-dC), but the steady-state rates are 4-fold faster than with poly(dG-dC) (Table 1). We observe no burst with poly(dI-dC) during methylation (Figure 4A vs Figure 6A), nor in the exchange reactions with sinefungin (Figure 4B vs Figure 6B), indicating that the product release steps are faster and thus no longer rate limiting. Surprisingly, AdoMet-dependent methylation with poly(dI-dC) shows exchange rates which are four times faster than the methylation rates (Figure 6A and Table 1). The excess tritium released in the methylation reaction during the first turnover indicates that proton transfer at cytosine C^5 (Figure 2, **2** → **3B**) occurs prior to methyl transfer (Figure 2, **2** → **3A**). In addition, since a single target base attack can result in only one tritium release (Figure 2, **2** → **3B** → **4B**), the excess tritium released during the multiple catalytic turnovers in the methylation reaction indicates that the enzyme rapidly attacks and releases several target bases before catalyzing methyl transfer from the bound AdoMet. Such a rapid interchange between different bases indicates that there is a dynamic equilibrium between intermediates **1** and **2** (i.e., Figure 2, **1** ↔ **2**) and that the base restacking is fast and in a direct competition with the covalent adduct formation (**1** → **2**, Figure 2) and methyl transfer (**2** → **3A**, Figure 2). Crystallographic studies (*34*), ^{19}F NMR studies (*15*), and fluorescent studies (*14*) showed

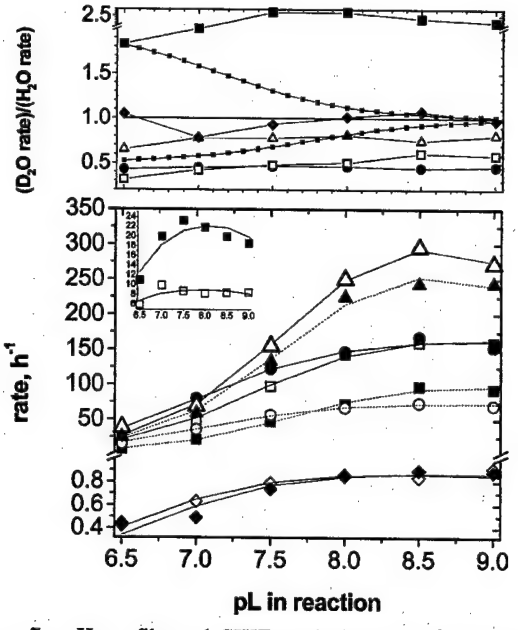

FIGURE 7: pH profile and SKIE analysis of the ^{3}H exchange reaction with ^{3}H-poly(dI-dC). The pH profiles for the ^{3}H exchange reaction with AdoMet (▲, △), sinefungin (●, ○), *N*-methyl-AdoMet (□, ■), and AdoHcy (◆, ◇) in H_2O and D_2O, respectively, are shown. The insert shows the pH profile for the reaction without cofactors (■, □) in D_2O and H_2O, respectively. All profiles were analyzed using eq 2, and the best fit values are listed in the Table 2. The upper panel shows the ratios between the rates measured in D_2O and H_2O in the presence of AdoMet (○), sinefungin (●), *N*-methyl-AdoMet (□), AdoHcy (△), and apoenzyme (■). The dashed lines are calculated using eq 3 and show the expected SKIE if the rate-limiting step is primarily dependent on a nucleophilic cysteine with $pK_a = 7.5$ as described in the text.

that the extrahelical base can exist as a stable and distinct intermediate. Our results show that with poly(dI-dC) the extrahelical base is a short-lived intermediate. Our observation that the exchange rate is much faster with poly(dI-dC) than methylation supports the idea that the methyl transfer step is limiting.

The pH profiles (Figure 7) for the exchange reaction with AdoMet and poly(dI-dC) and different analogues are very similar and closely resemble the profiles in similar reactions with poly(dG-dC) (Table 2 and Figure 5). Thus, any differences between poly(dG-dC) and poly(dI-dC) do not affect the pH-sensitive step. The SKIE for each reaction with poly(dI-dC) is unique and pH-independent. Thus, as with poly(dG-dC), the SKIE and pH profiles are at least in part caused by different phenomena. The most significant distinction between these two substrates is observed in the exchange reaction without cofactor (Figures 6B and 7, insert), with the poly(dI-dC) reaction being 2 orders of magnitude slower, is largely pH-independent, and has a large inverse SKIE. These observations suggest that in the absence of the cofactor the exchange reaction with poly(dI-dC) has a unique rate-limiting step and mechanism.

Processivity on Poly(dG-dC) and Poly(dI-dC) Substrates (Figure 8). To measure the processivity on DNA substrates, we prepared two identical exchange reactions, one containing only labeled DNA (called the *free* reaction) and one having ^{3}H-labeled DNA plus an *n*-fold excess (usually $n = 10$) of unlabeled DNA (called the *dilute* reaction). Both reactions are started simultaneously by adding equal amounts of enzyme. As expected, the ^{3}H release rate in the free reaction is *n*-fold higher than in the dilute reaction. By the end of the first turnover (Figure 8, arrow), an aliquot from the free reaction is mixed with an *n*-fold excess of unlabeled DNA (*chase* reaction). If the enzyme is fully processive, addition of the 10-fold excess of unlabeled substrate in the chase reaction will not affect the tritium release rates. If the enzyme is not processive, the ^{3}H release rates in the chase reaction will be immediately identical to the tritium release rates in the dilute reaction. A partially processive enzyme in which only a fraction of the enzyme molecules stay on the original substrate will result in the ^{3}H release rates in the chase reaction being between the tritium release rates for the free and dilute reactions. The rate will gradually decrease with each turnover until the chase and dilute reactions become

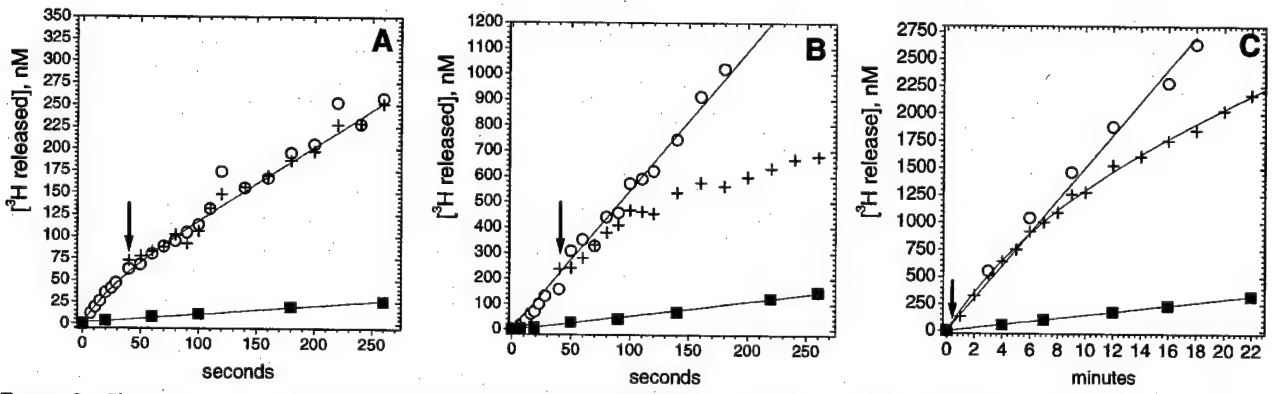

FIGURE 8: Chase processivity assay with M.HhaI and ^{3}H-poly(dG-dC) (A) or ^{3}H-poly(dI-dC) (B) and M.SssI with ^{3}H-poly(dI-dC) (C). (A) The free (○) reaction had M.HhaI (50 nM), ^{3}H-poly(dG-dC) (8 μM bp, 102 cpm/pmol), and AdoMet (10 μM). The dilute reaction (■) was prepared from a free reaction aliquot by adding a 10-fold excess of unlabeled poly(dG-dC). Free and dilute reactions were started simultaneously; the chase reaction (+) was started 40 s later (after the first turnover) by adding unlabeled poly(dG-dC) (80 μM bp) to the free reaction aliquot. (B) The free (○) reaction had M.HhaI (100 nM), AdoMet (10 μM), and ^{3}H-poly(dI-dC) (8 μM bp, 24 cpm/pmol). The dilute reaction (■) was prepared from a free reaction aliquot by adding a 10-fold excess of unlabeled poly(dI-dC). Free and dilute reactions were started simultaneously; the chase reaction (+) was started 45 s after the free reaction (after the second turnover) by adding unlabeled poly(dI-dC) (100 μM bp) to the free reaction aliquot. (C) The free (○) reaction had M.SssI (30 nM), ^{3}H-poly(dI-dC) (10 μM bp, 24 cpm/pmol), and AdoMet (10 μM). The dilute reaction (■) was prepared from a free reaction aliquot by adding a 10-fold excess of unlabeled poly(dI-dC). The chase reaction (+) was started 45 s after the free reaction by adding 100 μM bp unlabeled poly(dI-dC) to a free reaction aliquot.

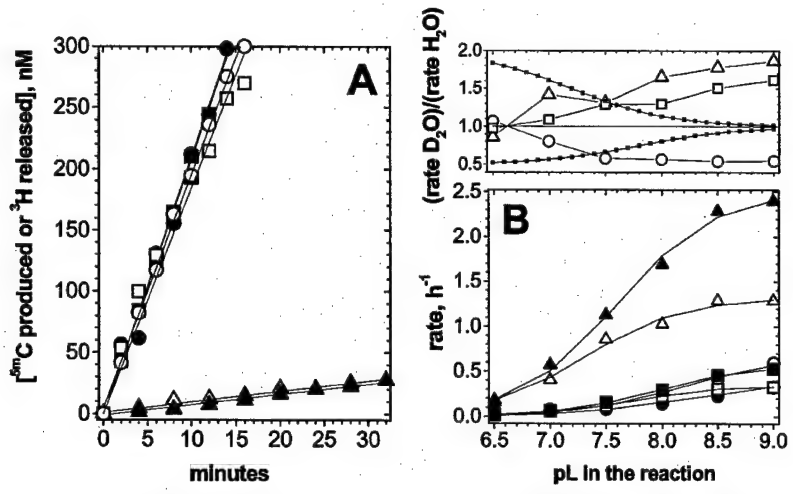

FIGURE 9: (A) Gln^{237}Trp mutant exchange and methylation reactions with ^{3}H-poly(dG-dC) and ^{3}H-poly(dI-dC) and (B) pH/SKIE profiles in the reaction with ^{3}H-poly(dG-dC). (A) Methylation and the ^{3}H exchange rates with the Gln^{237}Trp mutant (1000 nM) were measured in parallel using ^{14}C-AdoMet (12 μM, 131 cpm/pmol) and ^{3}H-poly(dG-dC) (12 μM bp, 88 cpm/pmol) or ^{3}H-poly(dI-dC) (12 μM bp, 25 cpm/pmol). The symbols represent the ^{3}H exchange (○, □) and methylation (●, ■) reaction with ^{3}H-poly(dG-dC) and ^{3}H-poly(dI-dC), respectively, and the ^{3}H exchange reaction without cofactor and ^{3}H-poly(dG-dC) (▲) and ^{3}H-poly(dI-dC) (△). All profiles were analyzed using a linear equation, and the best fit values are listed in the Table 1. (B) The lower panel shows pH profiles for exchange reactions measured with AdoMet (▲, △), sinefungin (○, ●), and *N*-methyl-AdoMet (■, □) in D_2O and H_2O, respectively. The pH profiles were analyzed using eq 2, and the best fit values are given in Table 2. The upper panel shows the ratios between the rates measured in D_2O and H_2O in the presence of AdoMet (△), sinefungin (●), and *N*-methyl-AdoMet (□) in D_2O and H_2O, respectively. The dashed lines are calculated according to eq 3 and represent the expected SKIE for a reaction that is primarily limited by cysteine nucleophilic attack with $pK_a = 7.5$ as described in the text.

identical. We find that M.HhaI is fully processive for five turnovers in the methylation reaction with poly(dG-dC) substrate. M.HhaI is only partially processive in the methylation reaction with the poly(dI-dC) substrate for about three to four turnovers. Since processivity experiments measure tritium release rates rather than the methyl transfer rates, the small processivity on poly(dI-dC) substrates can be attributed to excess tritium released during the methylation reaction with the poly(dI-dC) substrate (Figure 6A). A positive control was included in the form of M.SssI since this enzyme was previously shown to be processive (*35*). Here we show that M.SssI catalyzes 30 turnovers on the same DNA molecule.

Exchange Reaction with the Gln^{237}Trp Mutant (Figure 9). Gln^{237} interacts with the amino group on the C^2 of the orphan guanine; this interaction forms part of the network of hydrogen bonds that stabilize intermediates **1** and **2** (Figure 2 and ref *36*). The Gln^{237}Trp mutant is one of the least active Gln^{237} mutants (*19*). We were interested in using the kinetic analyses presented for the wild-type M.HhaI to identify which step(s) during catalysis is (are) significantly altered in the mutant. The Gln^{237}Trp mutant has methylation and exchange rates with poly(dG-dC) and poly(dI-dC) that are more than 10-fold slower than those of the wild-type enzyme (Table 1). The exchange rates are slowest in the absence of the cofactor, and there is little difference in catalytic rates with AdoMet, sinefungin, and *N*-methyl-AdoMet. Unlike the WT enzyme, we observe identical rates for the methylation and tritium release kinetics during AdoMet-dependent methylation of poly(dI-dC) (Figure 9A), and the mutant shows identical methylation and exchange kinetics for the two DNA substrates (Figure 9A).

The pH profiles with the mutant (Figure 9B) closely resemble the pH profiles in similar reactions with the WT enzyme (Figure 5 and Table 2). Since reactions with the mutant and the WT enzyme show very different rates, the observed similarity in the pH profiles further supports the idea that the ionization state of similar residues carries out similar functions in the two proteins. The mutant and the wild-type enzymes show distinct SKIE (Figures 5, 7, and 9B). For example, all reactions with the mutant show pH-dependent changes in the SKIE (Figure 9B); thus, the SKIE is at least in part caused by the pH-sensitive step.

Proton Inventory Experiments (Figure 10). Proton inventory profiles are measured at varying ratios of D_2O and H_2O (*29*). This approach represents a sensitive strategy to describe and compare the rate-limiting step in enzyme-catalyzed reactions (*29*). We measured proton inventories with the exchange reactions to determine if different reactions share similar intermediates and rate-limiting steps. For those reactions showing a pre-steady-state burst, the proton inventories were measured in the pre steady state; reactions showing linear profiles were measured in the first and subsequent turnovers. Proton inventories are usually described according to their shape and fractionation factors, i.e., ϕ_T and ϕ_G (*29*). The shape of the proton inventory profile indicates the number of steps or groups controlling the SKIE and whether the observed SKIE is caused in the ground state, transition state, or both (*29*). The fractionation factors can help to identify the group that causes the SKIE (i.e., $\phi = 0.5-0.6$ indicates cysteine) and also to compare proton inventory profiles from different reactions. The proton inventory profile is fit by using different forms of eq 4 involving different values and combinations of the *n*, *m*, and *Z* parameters. We used eq 4 to identify the simplest form that describes the proton inventory profiles based on the following options and parameters: (i) two SKIE-sensitive steps in the transition state ($n = 2$, $m = 0$, $Z = 1$); (ii) two SKIE-sensitive steps in the ground state ($n = 0$, $m = 2$, $Z = 1$); (iii) one SKIE-sensitive step in the ground state and one in the transition state ($v = 1$, $v = 1$, $Z = 1$). We also

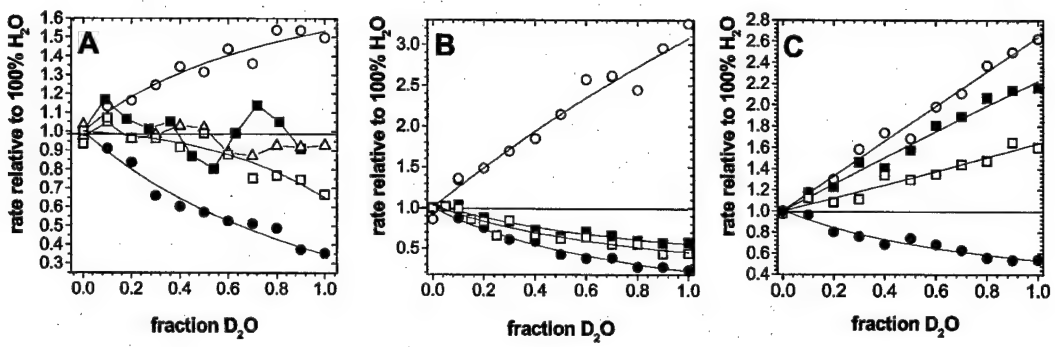

FIGURE 10: Proton inventory for the ^3H exchange reaction with (A) ^3H-poly(dG-dC), (B) ^3H-poly(dI-dC), and (C) the $Gln^{237}Trp$ mutant and ^3H-poly(dG-dC). In all three panels the symbols indicate proton inventory profiles for reaction without cofactors (○), AdoMet (■), *N*-methyl-AdoMet (□), and sinefungin (●). Panel A also has data for AdoHcy (△). The profiles represent rates measured in the pre steady state or in the steady state as described in the text. All profiles were analyzed using the Gross−Butler equation (eq 4), and the best fit values are given in the Table 2.

considered a situation involving contributions from multiple sites; i.e., the *Z* factor was allowed to float and $n = 1$, $m = 0$ or $n = 0$, $m = 1$. On the basis of the best fit residuals, the proton inventory profiles are best described as one SKIE-sensitive step in the transition state and one in the ground state (i.e., $n = 1$, $m = 1$, $Z = 1$). The calculated best fit fractionation factors are summarized in Table 2, and the best fit profiles are presented in Figure 10.

Different proton inventory profiles are observed during methylation with poly(dG-dC), methylation with poly(dI-dC), and methylation with the $Gln^{237}Trp$ mutant. Therefore, these reactions depend on different relative contributions from several steps, implicating distinct mechanisms. In contrast, the proton inventories and fractionation factors for the exchange reactions with sinefungin and poly(dG-dC) or poly(dI-dC) are within experimental error identical (Table 2), indicating that they have very similar mechanisms. All reactions with the wild-type enzyme have a ground state fractionation factor (ϕ_G) between 1.8 and 2, while the transition state fractionation factor ϕ_T is unique for each reaction (Table 2). The proton inventory analysis shows that the exchange reactions with both DNA substrates in the absence of cofactor are similar to the reactions catalyzed by the $Gln^{237}Trp$ mutant (Table 2): an inverse SKIE, an increase in SKIE with an increasing pH, and a transition state fractionation factor ϕ_T close to 2 (Table 2). The dome-shaped proton inventory profiles for the proton exchange reaction without cofactor (Figure 10A) suggest that the SKIE and multiple steps are rate limiting and determine the SKIE (*29*).

DISCUSSION

Despite a wealth of information regarding DNA cytosine methyltransferases, and in particular M.*Hha*I, there is little experimental evidence regarding three fundamental aspects of enzyme catalysis: the identity and roles of critical active site groups other than Cys^{81}, the identity and roles of reaction intermediates, and the rate constants associated with their interconversion (Figure 2). Our goals were to (1) understand which steps are rate limiting (Figure 2), (2) characterize the relative stabilities of intermediates **1** and **2**, (3) characterize the interconversion kinetics involving intermediates **1** and **2**, (4) investigate the extent to which solvent molecules gain access to intermediate **2**, and (5) characterize how protein−DNA interactions alter the stability of intermediates **1** and **2**. Our approach uses both base and cofactor analogues (Figure 3) in conjunction with several kinetic strategies.

Stabilization of the extrahelical cytosine (base flipping, Figure 1) within the enzyme's active site (Figure 2, intermediate **1**) has been proposed to activate the ring for nucleophilic attack at the C^6 position by protonation at N^3 (Figure 2, **1**, and refs *18* and *37*). Nucleophilic attack to form the covalent intermediate (Figure 2, **2**) is an essential feature of all DNA cytosine methyltransferases, including the enzymes involved in epigenetic regulation in humans (*38*). Indeed, nucleophilic attack at the pyrimidine C^6 position is core to all C^5 pyrimidine methyltransferases and the basis of drug action for several clinically used mechanism-based cancer treatments (*5*, *39*). Formation of intermediate **2** disrupts the aromaticity of the pyrimidine, while the insertion of electron density deriving from the thiolate enables the normally unreactive pyrimidine to attack a proximal electrophile. Experiments demonstrating that M.HhaI catalyzes the exchange of tritium placed at the cytosine C^5 position provided the first definitive evidence for the formation of intermediate **2** (*17*). This cytosine C^5 exchange reaction provides a unique opportunity to expand our ability to analyze the target base attack beyond the limitations of routine methylation assays. Like methylation, the exchange reaction requires that the enzyme forms a covalent adduct with the target base. Both reactions are the result of electrophilic addition at the cytosine C^5, and both reactions end with the β elimination involving proton removal at the cytosine C^5 position (Figure 2, **3A** → **4A** and **3B** → **4B**).

In this study we find that the tritium exchange rates vary by 3 orders of magnitude when measured in the presence of different cofactor analogues or in the absence of the cofactor (Table 1). The AdoMet analogues used in this study differ only at the position of active methyl group (Figure 3), and the analogues' ability to support the exchange reaction correlates with the proton presence at the position of the active methyl group (Figure 3). Possible mechanisms by which AdoMet and AdoHcy can inhibit the exchange reaction were previously described (*17*, *20*, *40*). Briefly, AdoMet and AdoHcy can inhibit the exchange reaction (i) by controlling the stereochemistry of the β elimination step (Figure 2, **3B** → **4B**), (ii) by affecting the enzyme's ability to form intermediates **1** or **2**, or (iii) by affecting proton access at the C^5 of the activated target base (Figure 2, **2** →

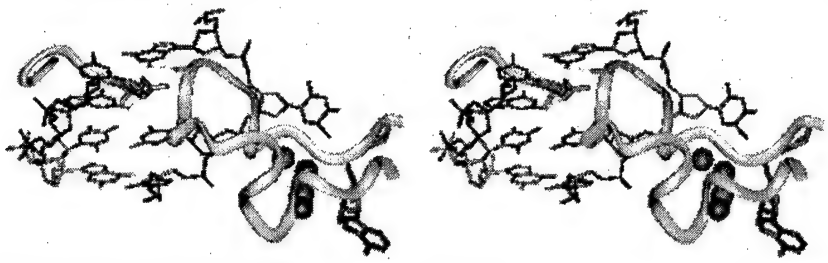

FIGURE 11: Structure of the active site loop, the Gln^{237} site, and the GCGC recognition sequence with an extrahelical base (*7*). DNA is shown in thin gray lines. The gray ribbon in the front represents the active site loop (amino acids 80−99) in the closed position when Ile^{86} (green) can make a hydrogen bound with the C^2 amino group (green) on guanine that is in the 5′ position relative to target cytosine. The background gray ribbon represents the peptide backbone with Gln^{237} (red) which makes a hydrogen bond with the C^2 amino group (red) on the orphan guanine. The cofactor is shown in red in the lower right corner, while the four solvent molecules near the target base are shown as gray spheres. The C^2 amino groups (green) on two of guanine residues are exposed to solvent and make no contacts with enzyme.

3B). Our exchange assay detects tritium exchange upon delivery of the proton to the cytosine C^5 position (Figure 2, **3A**) and the pre-steady-state rates do not depend on the stereochemistry of proton release (Figure 2, **3B** → **4B**). Thus, stereochemical control of the proton release step by the different analogues seems unlikely. It is equally unlikely that the analogues interfere with enzyme's ability to form intermediates **1** and **2** because (i) we observe different exchange rates with poly(dG-dC) and poly(dI-dC) in the presence of AdoMet (Figures 4A and 6A), (ii) AdoMet does not support the exchange reaction with poly(dG-dC) (Figure 4A), (iii) our pH/SKIE studies (Figures 5 and 8) are inconsistent with a rate-limiting step involving nucleophilic attack by Cys^{81}, and (iv) the subtle structural differences within the different cofactor analogues would seem unlikely to cause such dramatic changes in the enzyme's ability to form intermediate **2**, since high exchange rates in the absence of any cofactor involving well-studied and large conformational changes in the enzyme (*7*) have minimal effects on the exchange process.

The observed pattern in modulation of the exchange rates by AdoMet analogues and the crystal structures of M.HhaI (*7*, *40*, *41*) suggest that the exchange rates depend on the proton access to the C^5 of the target base. The four analogues (Figure 3) are likely to bind the active site in the same fashion since the cocrystal structures of the two most diverse forms involving AdoMet (*41*) and AdoHcy (*7*) reveal similar cofactor binding orientations. We suggest that the most likely candidate for the proton donor is the cofactor and/or the solvent molecules that are frequently observed in the active site (Figure 11 and ref *42*). The high exchange rates in the absence of the cofactor can be attributed to solvent which has ready access to the C^5 on the activated target base [pK_a = 18 (*18*)]. The low exchange rates in the presence of AdoMet and AdoHcy are to be expected since their proximity to the cytosine C^5 (*7*, *18*, *40*) can block solvent access. Although sinefungin and *N*-methyl-AdoMet can also block solvent access to the cytosine C^5 position, the relatively high exchange rates may derive from the proximal amino groups found within these analogues. The exchange rates are higher with sinefungin than *N*-methyl-AdoMet, since sinefungin's three protons are most likely closer to the cytosine C^5.

In summary, our study of AdoMet analogues and the exchange reaction extends the previous study (*17*) which showed that AdoMet and AdoHcy inhibit the exchange reaction when compared to the same reaction without cofactors. We show that the ability of the cofactors to support the exchange reaction correlates with the proton access and proximity (Figure 3) at the C^5 on the target base. These insights allow us to describe the catalytic events following the formation of the covalent intermediate **2** (Figure 2, **2** → **3A** → **4A** and **2** → **3B** → **4B**) and the rate limiting step as described further in the text. Furthermore, the exchange reaction shows a similar cofactor dependency as was previously reported for the mutagenic deamination reaction (*23*). The similar trends are reasonable since C^5 protonation is known to increase deamination rates by at least 4 orders of magnitude (*37*). Because the deamination reaction is difficult to study mechanistically, the exchange reaction provides a convenient mechanistic probe of the common features of these reactions. For example, the exchange reaction could be used to investigate the extent to which eukaryotic cytosine methyltransferases (e.g., Dnmt1) support the deamination reaction[2] or to investigate the basis for any differences in the deamination kinetics observed with different bacterial enzymes (*22*).

pH/SKIE Studies. We used pH and SKIE studies (Figures 5 and 7) to probe if the rate-limiting step in methylation or any of the exchange reactions depends on nucleophilic attack by Cys^{81} involving the transition between intermediates **1** and **2** (Figure 2). Based on theoretical studies (*18*), nucleophilic attack by Cys^{81} is thought to be rate limiting during methylation (*10*, *42*). Our pH/SKIE analysis showed no evidence that the cysteine nucleophilic attack is rate limiting during methylation or any of the exchange reactions in the presence of the cofactor. Interestingly, we find that even though the relative exchange rates vary by orders of magnitude (Table 1), all exchange reactions have very similar pH profiles (Table 2), and in the majority of the reactions the SKIE (ratio between the rates measured in D_2O and H_2O) is pH-independent and unique for each reaction (Figures 5 and 7). To understand how the conversion between intermediates **1** and **2** (Figure 2) might affect catalytic rates, it is necessary to realize that this conversion is in principle reversible and that reversion back to intermediate **1** is expected if methyl transfer (**2** → **3A**) or proton transfer (**2** → **3B**) is relatively slow. If the rate of reversal (**2** → **1**) is at least severalfold faster than the specific catalytic process at cytosine C^5, intermediates **1** and **2** will be in equilibrium (i.e., Figure 2, **1** → **2**, and Figure 1). Several experimental observations support a rapid equilibrium between intermediates **1** and **2**. First we observe an excess release of tritium

[2] Ž. M. Svedružić and N. O. Reich, manuscript in preparation.

during the methylation reaction involving poly(dI-dC) (Figure 6A). Second, the pre-steady-state exchange kinetics with sinefungin and poly(dG-dC) (Table 1) show that the conversion between intermediates **1** and **2** can be severalfold faster than the subsequent methyl transfer step. Finally, the results of the pH/SKIE studies (Figures 5 and 7) are also compatible with the rapid equilibrium proposal. A decrease in pH results in protonation of Cys^{81} and a shift in the equilibrium between **1** and **2** in favor of intermediate **1**, which leads to a decrease in the catalytic rates. We observe that solvent changes (e.g., replacement of H_2O with D_2O) have little effect on the pK_a of Cys^{81} (*43*) but do affect hydrogen-bonding interactions and proton transfer steps that lead to the exchange reaction. Hence, pH/SKIE studies (Figures 5 and 7) reveal that a change in the pH does affect catalytic rates, while the SKIE is pH-independent and specific for the particular mechanism of the proton transfer at the C^5 on the target base. In summary, the most important consequence of our proposed rapid equilibrium mechanism is that the catalytic rates are dependent on the steps that control the concentration of intermediate **2** *and* the steps that control the conversion to intermediate **3A** (Figure 2, **2** → **3A**) or **3B** (Figure 2, **2** → **3B**); this is in contrast to the circumstance in which only the formation of intermediate **2** is rate limiting (Figure 2, **1** → **2**).

The exchange reaction in the absence of the cofactor is unique in several features. High exchange rates without cofactors in the presence of poly(dG-dC) (Figure 4B and ref *17*) indicate that conformational changes associated with the cofactor binding are not necessary for a successful target base attack (Table 1). An increased SKIE with increasing pH suggests that nucleophilic attack by Cys^{81} (Figure 2, **1** → **2**, and Figure 5) is at least partially rate limiting in the exchange reaction. Once intermediate **2** is formed, the proton transfer to cytosine C^5 is likely to be relatively efficient since the target base is fully accessible to solvent molecules in the absence of bound cofactor (Figure 11 and ref *42*). Thus, it appears unlikely that intermediates **1** and **2** are in rapid equilibrium in the absence of cofactor and that proton transfer at cytosine C^5 is rate limiting. Further support for these conclusions is presented below in the exchange reaction with poly(dI-dC), in our studies with the Gln^{237}Trp mutant and in the analysis of various M.HhaI structures. The cofactor binding increases the enzyme's affinity for DNA by orders of magnitude (*9*). Cofactor binding is believed to induce active site loop movement (amino acids 80−99 (*7*)) and extensive conformational changes in protein structure (*7*).

Methylation and Exchange with Poly(dI-dC). Crystallographic studies with different DNA sequences (*8*), theoretical analysis (*36*), and various M.HhaI mutants (*10*, *19*, *44*) suggest how M.HhaI:DNA interactions can affect DNA binding, target sequence recognition, and the base flipping process. Investigation of various proposed mechanisms requires suitable assays, and we sought to apply our exchange assays to this end. Poly(dI-dC) has several unique features that provide an opportunity to probe the importance of the active site loop (residues 80−99, Figure 11, and ref *7*), the base flipping mechanism, and the functional distinctions between M.HhaI and the more complex mammalian enzyme Dnmt1.[2] Poly(dI-dC) cannot form a hydrogen bond with Ile^{86} within the active site loop. Closure of this loop appears to be crucial for the stabilization of the extrahelical base (Figure 11 and ref *7*); however, its dynamics and precise function cannot be completely understood from the static crystal structures. Poly(dI-dC) is a unique probe for interactions between the active site loop and Ile^{86} since the hydrogen bond is between the C^2 amino group on guanine and the protein backbone (Figure 11 and ref *7*). We also used poly(dI-dC) as a probe of the interactions that may contribute to the base flipping process since, in contrast to the G·C pair, the I·C base pair has only two hydrogen bonds (Figure 3 and ref *45*). Finally, the studies with poly(dI-dC) provide a basis for investigating the mammalian enzyme, Dnmt1, which has a strong preference for poly(dI-dC) (*26*).[2]

Poly(dG-dC) and poly(dI-dC) substrates show similar methylation and exchange rates (Table 1), and methylation rates with poly(dG-dC) and poly(dI-dC) are similar to the catalytic rates previously reported with different DNA substrates (*9*, *10*, *17*, *44*). The similar catalytic rates (Table 1) indicate that any structural differences between poly(dG-dC) and poly(dI-dC), or other DNA substrates used in the past, have negligible impacts on the enzyme's ability to form intermediates **3A** and **3B** (Figure 2, **1** → **2** → **3A** or **1** → **2** → **3B**). This is consistent with the available structures of M.HhaI complexed to DNA, which show that the majority of the M.HhaI·DNA interactions involve the phosphate backbone (ref *7* and Figure 11) and numerous base contacts involve the major groove. Poly(dG-dC) and poly(dI-dC) have identical functional groups in the major groove (Figure 3), and the I·C and G·C base pairs share the same conformation (*45*).

The poly(dI-dC) substrate revealed insightful changes in the stability of intermediates **1** and **2** (Figures 4A and 6A), in the partitioning of intermediate **2** toward proton or methyl transfer (Figures 4A and 6A), and in catalytic processivity (Figure 8A,B). The main difference between poly(dG-dC) and poly(dI-dC) is in the potential hydrogen-bonding interactions involving Gln^{237} or Ile^{86} (ref *7* and Figure 11). The hydrogen bonds involving Gln^{237} and Ile^{86} are most likely important for different steps in the target base attack (refs *7* and *36* and Figure 11). Gln^{237} interacts with the orphan guanine and is thought to regulate the early steps in the base flipping process and the formation of intermediates **1** and **2** (*7*, *36*). Thus, alterations in interactions involving Gln^{237} may affect steps leading to intermediates **3A** and **3B** (Figure 2). Our observation that the pre-steady-state methylation rates with poly(dI-dC) are 2-fold slower than with poly(dG-dC) may therefore result from this missing hydrogen bond between Gln^{237} and the orphan inosine. In contrast, the enzyme−DNA interactions at Ile^{86} require that the active site loop is closed (ref *7* and Figure 11) with the cytosine positioned in the active site (i.e., intermediates **1** and **2** are formed (ref *7* and Figure 11)). Thus, a lack of interaction with Ile^{86} should not affect the steps leading to intermediates **3A** and **3B** but rather the stability of this active site loop in the closed position. The release of the active site loop is part of the product release process and the accompanying proton elimination steps (Figure 2, **3A** → **4A** and **3B** → **4B**). Thus, loop opening before methyl transfer may lead to uncontrolled solvent access to intermediate **2** (Figure 11 and ref *42*) and/or premature release of intermediates **1** and **2**. The excess tritium released during the methylation reaction with poly(dI-dC) (Figure 6A) is fully consistent with this scenario. The premature loop release prior to methyl transfer

can lead to uncontrolled protonation of intermediate **2**, and/or premature release of intermediates **1** and **2**, without the methyl transfer step. Similarly, loop release and uncontrolled solvent access to intermediate **2** are likely causes of the faster exchange rates with poly(dI-dC) in the presence of AdoHcy and *N*-methyl-AdoMet relative to poly(dG-dC (Table 1). In summary, comparison of poly(dG-dC) and poly(dI-dC) substrates is consistent with the stabilization of the active site loop through a hydrogen bond between Ile^{86} and guanine (ref *7* and Figure 11). Since intermediates **1** and **2** tend to accumulate prior to the slow methyl transfer step, the closure of the active site loop prevents premature release of the target base and uncontrolled solvent access at the reactive intermediate **2** (Figure 2). Blocking uncontrolled solvent access to intermediate **2** is important for minimizing both the exchange reaction and the mutagenic deamination (Figure 2, **1** → **2** → **3B** → **4B**).

The reactions with the poly(dI-dC) substrate also indicate that the loop closure can contribute to the slow steady-state step and to the early steps in target base recognition. The faster steady-state rates with no pre-steady-state burst in the reaction with poly(dI-dC) relative to poly(dG-dC) (Figure 4A vs Figure 6A and Figure 4B vs Figure 6B) are most likely caused by unstable active site loop, leading to faster product release (ref *7* and Figure 11). Moreover, the differences between poly(dG-dC) and poly(dI-dC) during processive catalysis (Figure 8A) suggest that the active site loop is partially closed with poly(dG-dC) after AdoHcy release, retaining the enzyme on the DNA. This is somewhat surprising since structural studies (ref *7* and Figure 11) suggest that the loop closure is primarily dependent on cofactor binding. In contrast, the relative instability of the loop and thus the M.HhaI·DNA complex with poly(dI-dC) results in the enzyme leaving prematurely and is thus less processive. Similarly, the large difference between poly(dG-dC) and poly(dI-dC) in the exchange rates in the absence of the cofactor is in a sharp contrast to the similar exchange rates in the presence of the cofactor (Table 1). We suggest that the low exchange rates with poly(dI-dC) in the absence of cofactor are due to the lack of both factors that control the closure of the active site loop: interaction at the Ile^{86} site and the cofactor binding (ref *7* and Figure 11).

Finally, these studies with poly(dG-dC) and poly(dI-dC) substrates offer some insights into the enzyme's role in the base flipping process (*8*, *15*, *34*). A passive mechanism involves the protein simply stabilizing the extrahelical target base which spontaneously becomes unstacked from the duplex DNA, while an active mechanism invokes participation of the enzyme in the unstacking process itself. The loss of one of the three hydrogen bonds per base pair in poly(dI-dC) should result in faster formation of intermediate **1** and **2**, if these intermediates are formed largely by a passive mechanism. Our observation of similar rates with poly(dI-dC) and poly(dG-dC) argues against a passive mechanism. Interestingly, we find the reverse is true with the mammalian enzyme (Dnmt1), which shows at least 10-fold higher catalytic rates with poly(dI-dC) than poly(dG-dC).[2]

Methylation and Exchange with the Gln^{237}Trp Mutant. Gln^{237} makes hydrogen bonds that are considered to be crucial for the base flipping process and stabilization of the extrahelical cytosine (Figure 11 and refs *7* and *36*). Earlier analysis (*19*) of 19 different Gln^{237} mutants showed that the methylation rates can be 2−33-fold slower than wild-type M.HhaI. The Gln^{237}Trp mutant is one of the least active (*19*), and based on the crystal structures (Figure 11 and refs *7* and *36*) these substitutions are thought to impact the enzyme's ability to form intermediate **1**. We were interested to see if the exchange reactions could be used to probe this prediction. We find that, similar to the exchange reaction in the absence of the cofactor (Figure 5B), the mutant clearly shows a pH-dependent change in SKIE. This is expected if the pH profiles and the measured pK_a are caused by the active site Cys^{81}, and if the reactions are limited by the cysteine nucleophilic attack and the conversion between intermediates **1** and **2**. None of the reactions with the mutant show a pH/SKIE response expected for a reaction that is *primarily* limited by the cysteine nucleophilic attack with the measured pK_a (dashed line, upper panel, in Figures 5, 7, and 9B). This is understandable since the conversion between intermediates **1** and **2** depends on a specific set of hydrogen bonds (Figure 2 and refs *7* and *18*) which may contribute to the SKIE (*46*). In summary, our results with the Gln^{237} mutant support our proposal that the pH/SKIE studies can be used to study the relationship between base flipping and catalysis. For a comparison, crystallographic (*34*) and fluorescence studies (*14*) reveal the extent of DNA deformation but do not monitor catalysis by Cys^{81}. ^{19}F NMR studies (*15*) do provide insights into intermediates **1** and **2** (Figure 2); however, the methyl transfer step at 5-fluorocytosine is exceptionally slow, which obscures the actual rates of conversion between intermediates. The pH/SKIE studies can be measured with any DNA substrate using routine methyltransferase assays.

In contrast to the wild-type enzyme, the exchange reaction with the mutant shows a notably decreased dependence on the cofactor analogues (Table 1). Thus, the mutation affects not only interactions with the orphan guanine but also interactions between intermediate **2** and the cofactor that take place in the active site. Since the enzyme's active site is 15 Å away from Gln^{237} (Figure 11), substitutions of Gln^{237} indirectly alter the network of hydrogen bonds (*36*) that position intermediates **1** and **2** in the active site. The results with the mutant also support our conclusions from poly(dI-dC) studies using the wild-type enzyme. The mutant shows no difference between the poly(dI-dC) and poly(dG-dC) substrates (Table 1 and Figure 9A), and both substrates show identical methylation and accompanying tritium release rates. As suggested above, the excess tritium release which occurs with the wild-type enzyme (Figure 6A) results from the destabilization of the active site loop and increased solvent access to reactive intermediate **2** (Figure 2) that accumulates prior to the slow methyl transfer step. Accumulation of intermediates **1** and **2** does not occur with the mutant since formation of intermediates **1** and **2** is the slow step (Figure 1).

Proton Inventory Studies. We used proton inventory analysis (Figure 10) in an attempt to further determine if different reactions share similar rate-limiting steps and catalytic intermediates. Proton inventory profiles are usually described according to their shape and calculated fractionation factors (eq 4 and ref *29*). The overall shape can indicate the number of steps controlling the rate-limiting step and SKIE and whether the SKIE is caused in the ground state, transition state, or both. The fractionation factors provide insights into functionalities causing the SKIE and can support

a comparison of different proton inventory profiles with numerical precision. While proton inventory results can be difficult to interpret precisely, we are primarily interested in their application to determine if the exchange reaction under different conditions follows similar mechanisms.

The proton inventory results support our earlier proposal that the methylation reactions with poly(dG-dC), poly(dI-dC), and $Gln^{237}Trp$ depend on different rate-limiting steps. The pre-steady-state methylation rates with poly(dG-dC) depend on the methyl transfer step (Figure 2, **2** → **3A**), and no SKIE is observed (Figure 10A). The proton inventory for the methylation reaction with poly(dI-dC) (Figures 10B and 6A) results from the combined steps of methyl and proton transfer (Figure 2, **2** → **3A** and **2** → **3A**). The methylation reactions with the $Gln^{237}Trp$ mutant and the wild-type enzyme without cofactor show similar proton inventory profiles, consistent with our earlier proposal that in both reactions the rate-limiting step is the nucleophilic attack by Cys^{81} (Figure 2, **1** → **2**).

The proton inventory profiles for the exchange reaction with sinefungin and poly(dI-dC) and poly(dG-dC) appear to be identical (Figure 10A,B and Table 2), indicating that the rate-limiting steps and catalytic mechanism are similar for these two reactions. The ϕ_T measured with sinefungin (Table 2) can be found in reactions where the rate-limiting step involves a proton bridge (N−H−C) in the transition state (ref *29*, pp 85 and 86). This is consistent with our proposal that the exchange reaction with sinefungin and both DNA substrates involves a direct interaction between the amino group on the cofactor and the C^5 on the target base. Moreover, similar proton inventory profiles are observed in the same reaction with Dnmt1,[2] indicating that M.HhaI and Dnmt1 follow very similar mechanisms with sinefungin.

The ϕ_T is similar in magnitude for the exchange reaction with *N*-methyl-AdoMet and sinefungin with poly(dG-dC) but not with poly(dI-dC) (Table 2). This is consistent with our proposal that the slow exchange reaction with *N*-methyl-AdoMet and poly(dG-dC) depends on the cofactor amino moiety, while the high exchange rates in the reaction with poly(dI-dC) and *N*-methyl-AdoMet (Table 1) result in part from the premature release of the active site loop, exposing intermediate **2** (Figure 2) to solvent molecules. The similar proton inventory profiles for the exchange reactions with AdoMet and *N*-methyl-AdoMet with poly(dI-dC) (Table 2) suggest that both reactions result from uncontrolled solvent access to intermediate **2**, caused by premature active site loop release. In summary, the proton inventory results support the proposed mechanism that tritium release by sinefungin and *N*-methyl-AdoMet is controlled by the cofactor and the active site loop.

The proton inventory profiles in the exchange reaction without cofactor and poly(dG-dC) and the exchange reactions with the $Gln^{237}Trp$ mutant are dome shaped at pH 6.5 (data not shown) and partially curved (Figure 10C) at pH 8.0. Dome-shaped proton inventories which change with pH (Figures 5B and 9B) suggest that more than one step determines the rate-limiting step in those reactions (*29*), and that at least one is pH sensitive. This is consistent with our suggestion that nucleophlic attack by Cys^{81} is partially rate limiting in these reactions. If the pH-sensitive component of the SKIE is cysteine nucleophilic attack, the increase in SKIE caused by the increase in pH suggests that the nucleophilic cysteine is deprotonated in the transition state during the conversion between intermediates **1** → **2** (eq 4, ϕ_T, $n = 1$, $m = 0$). Thus, deprotonation of Cys^{81} occurs during the attack step, not prior. The pH-independent component of the SKIE shows an inverse SKIE which may involve one or more of the hydrogen bonds which activate intermediate **1** (*46*), since none of the functionalities on intermediates **1** and **2** are likely to cause such a fractionation factor when present alone (*29*). Finally, the reactions proposed to be limited by the **1** → **2** transition (Figure 10C), and reaction without cofactor and with poly(dG-dC), show an inverse SKIE and an apparent transition state fractionation factor (ϕ_T) of about 2 (Table 2). The reactions that are limited by proton transfer at intermediate **2** (**2** → **3B**) show a ground state fractionation factor ϕ_G around 2 (Figure 10A,B).

ACKNOWLEDGMENT

We gratefully acknowledge Ben Hopkins and Stephen Fiacco for their excellent help in these experiments and Drs. R. J. Roberts and S. Kumar from New England Biolabs for their generous gift of mutant M.HhaI plasmids.

REFERENCES

1. Jones, P. A., and Laird, P. W. (1999) Cancer epigenetics comes of age, *Nat. Genet. 21*, 163−167.
2. Jones, P. A., and Takai, D. (2001) The role of dna methylation in mammalian epigenetics, *Science 293*, 1068−1070.
3. Robertson, K. D., and Jones, P. A. (2000) DNA methylation: past, present and future directions, *Carcinogenesis 21*, 461−467.
4. Cheng, X., and Blumnethal, R. M. (1999) *S-Adenosylmethionine-Dependent Methyltransferases: Structures and Functions*, pp 1−400, World Scientific, Singapore, New Jersey, London, and Hong Kong.
5. Douglas, K. T. (1987) The thymidylate synthesis cycle and anticancer drugs, *Med. Res. Rev. 7*, 441−475.
6. Cheng, X., Kumar, S., Posfai, J., Pflugrath, J. W., and Roberts, R. J. (1993) Crystal structure of the HhaI DNA methyltransferase complexed with S-adenosyl-L-methionine, *Cell 74*, 299−307.
7. Klimasauskas, S., Kumar, S., Roberts, R. J., and Cheng, X. (1994) HhaI methyltransferase flips its target base out of the DNA helix, *Cell 76*, 357−369.
8. Cheng, X., and Roberts, R. J. (2001) AdoMet-dependent methylation, DNA methyltransferases and base flipping, *Nucleic Acids Res. 29*, 3784−3795.
9. Lindstrom, W. M., Jr., Flynn, J., and Reich, N. O. (2000) Reconciling structure and function in HhaI DNA cytosine-C-5 methyltransferase, *J. Biol. Chem. 275*, 4912−4919.
10. Vilkaitis, G., Merkiene, E., Serva, S., Weinhold, E., and Klimasauskas, S. (2001) The mechanism of DNA cytosine-5 methylation. kinetic and mutational dissection of Hhai methyltransferase, *J. Biol. Chem. 276*, 20924−20934.
11. Allan, B. W., Beechem, J. M., Lindstrom, W. M., and Reich, N. O. (1998) Direct real time observation of base flipping by the EcoRI DNA methyltransferase, *J. Biol. Chem. 273*, 2368−2373.
12. Allan, B. W., and Reich, N. O. (1996) Targeted base stacking disruption by the EcoRI DNA methyltransferase, *Biochemistry 35*, 14757−14762.
13. Allan, B. W., Garcia, R., Maegley, K., Mort, J., Wong, D., Lindstrom, W., Beechem, J. M., and Reich, N. O. (1999) DNA bending by EcoRI DNA methyltransferase accelerates base flipping but compromises specificity, *J. Biol. Chem. 274*, 19269−19275.
14. Holz, B., Klimasauskas, S., Serva, S., and Weinhold, E. (1998) 2-Aminopurine as a fluorescent probe for DNA base flipping by methyltransferases, *Nucleic Acids Res. 26*, 1076−1083.
15. Klimasauskas, S., Szyperski, T., Serva, S., and Wuthrich, K. (1998) Dynamic modes of the flipped-out cytosine during HhaI methyltransferase-DNA interactions in solution, *EMBO J. 17*, 317−324.
16. Finer-Moore, J. S., Santi, D. V., and Stroud, R. M. (2003) Lessons and conclusions from dissecting the mechanism of a bisubstrate

enzyme: thymidylate synthase mutagenesis, function, and structure, *Biochemistry 42*, 248−256.
17. Wu, J. C., and Santi, D. V. (1987) Kinetic and catalytic mechanism of HhaI methyltransferase, *J. Biol. Chem. 262*, 4778−4786.
18. Perakyla, M. (1998) A model study of the enzyme-catalyzed cytosine methylation using ab initio quantum mechanical and density functional theory calculations: pK_a of the cytosine N3 in the intermediates and transition states of the reaction, *J. Am. Chem. Soc. 120*, 12895−12902.
19. Mi, S., Alonso, D., and Roberts, R. J. (1995) Functional analysis of Gln-237 mutants of HhaI methyltransferase, *Nucleic Acids Res. 23*, 620−627.
20. Gabbara, S., Sheluho, D., and Bhagwat, A. S. (1995) Cytosine methyltransferase from *Escherichia coli* in which active site cysteine is replaced with serine is partially active, *Biochemistry 34*, 8914−8923.
21. Shen, J. C., Rideout, W. M. d., and Jones, P. A. (1992) High-frequency mutagenesis by a DNA methyltransferase, *Cell 71*, 1073−1080.
22. Zingg, J. M., Shen, J. C., and Jones, P. A. (1998) Enzyme-mediated cytosine deamination by the bacterial methyltransferase M.MspI, *Biochem. J. 332*, 223−230.
23. Zingg, J. M., Shen, J. C., Yang, A. S., Rapoport, H., and Jones, P. A. (1996) Methylation inhibitors can increase the rate of cytosine deamination by (cytosine-5)-DNA methyltransferase, *Nucleic Acids Res. 24*, 3267−3275.
24. Pfeifer, G. P., Tang, M., and Denissenko, M. F. (2000) in *DNA Methylation and Cancer* (Johns, P. A., and Vogt, P. K., Eds.) pp 1−19, Springer-Verlag, Berlin.
25. Reich, N. O., and Mashhoon, N. (1991) Kinetic mechanism of the EcoRI DNA methyltransferase, *Biochemistry 30*, 2933−2939.
26. Flynn, J., Glickman, J. F., and Reich, N. O. (1996) Murine DNA cytosine-C5 methyltransferase: pre-steady- and steady-state kinetic analysis with regulatory DNA sequences, *Biochemistry 35*, 7308−7315.
27. Johnson, K. A. (1992) in *The Enzymes* (Boyer, P. A., Ed.) Academic Press, New York.
28. Cornish-Bowden, A. (1999) *Fundamentals of Enzyme Kinetics*, Portland Press, Colchester, U.K.
29. Quinn, D. M., and Sutton, L. D. (1991) in *Enzyme Mechanism from Isotope Effects* (Cook, P. F., Ed.) pp 73−126, CRC Press, Boca Raton, FL.
30. Born, T. L., and Blanchard, J. S. (1999) Enzyme-catalyzed acylation of homoserine: mechanistic characterization of the *Escherichia coli* metA-encoded homoserine transsuccinylase, *Biochemistry 38*, 14416−14423.
31. Brocklehurst, K., Kowlessur, D., Patel, G., Templeton, W., Quigley, K., Thomas, E. W., Wharton, C. W., Willenbrock, F., and Szawelski, R. J. (1988) Consequences of molecular recognition in the S1-S2 intersubsite region of papain for catalytic-site chemistry. Change in pH-dependence characteristics and generation of an inverse solvent kinetic isotope effect by introduction of a P1−P2 amide bond into a two-protonic-state reactivity probe, *Biochem. J. 250*, 761−772.
32. Kinch, L. N., and Phillips, M. A. (2000) Single-turnover kinetic analysis of *Trypanosoma cruzi* S-adenosylmethionine decarboxylase, *Biochemistry 39*, 3336−3343.
33. Scheuring, J., and Schramm, V. L. (1997) Pertussis toxin: transition state analysis for ADP-ribosylation of G-protein peptide alphai3C20, *Biochemistry 36*, 8215−8223.
34. O'Gara, M., Horton, J. R., Roberts, R. J., and Cheng, X. (1998) Structures of HhaI methyltransferase complexed with substrates containing mismatches at the target base, *Nat. Struct. Biol. 5*, 872−877.
35. Renbaum, P., and Razin, A. (1992) Mode of action of the Spiroplasma CpG methylase M.SssI, *FEBS Lett. 313*, 243−247.
36. Huang, N., Banavali, N. K., and MacKerell, A. D., Jr. (2003) Protein-facilitated base flipping in DNA by cytosine-5-methyltransferase, *Proc. Natl. Acad. Sci. U.S.A. 100*, 68−73.
37. Ivanetich, K. M., and Santi, D. V. (1992) 5,6-dihydropyrimidine adducts in the reactions and interactions of pyrimidines with proteins, *Prog. Nucleic Acid Res. Mol. Biol. 42*, 127−156.
38. Yoder, J. A., Soman, N. S., Verdine, G. L., and Bestor, T. H. (1997) DNA (cytosine-5)-methyltransferases in mouse cells and tissues. Studies with a mechanism-based probe, *J. Mol. Biol. 270*, 385−395.
39. Szyf, M. (1996) The DNA methylation machinery as a target for anticancer therapy, *Pharmacol. Ther. 70*, 1−37.
40. O'Gara, M., Klimasauskas, S., Roberts, R. J., and Cheng, X. (1996) Enzymatic C5-cytosine methylation of DNA: mechanistic implications of new crystal structures for HhaL methyltransferase-DNA-AdoHcy complexes, *J. Mol. Biol. 261*, 634−645.
41. O'Gara, M., Zhang, X., Roberts, R. J., and Cheng, X. (1999) Structure of a binary complex of HhaI methyltransferase with S-adenosyl-L-methionine formed in the presence of a short nonspecific DNA oligonucleotide, *J. Mol. Biol. 287*, 201−209.
42. Lau, E. Y., and Bruice, T. C. (1999) Active site dynamics of the HhaI methyltransferase: insights from computer simulation, *J. Mol. Biol. 293*, 9−18.
43. Schowen, R. L. (1977) Isotope effects on enzyme-catalyzed reactions, in *Proceedings of the Sixth Annual Harry Steenbock Symposium* (Cleland, W. W., Northrop, D. B., and O'Leary, M. H., Eds.) Madison, WI, June 4 and 5, 1976, pp 64−99, University Park Press, Baltimore, MD.
44. Vilkaitis, G., Dong, A., Weinhold, E., Cheng, X., and Klimasauskas, S. (2000) Functional roles of the conserved threonine 250 in the target recognition domain of HhaI DNA methyltransferase, *J. Biol. Chem. 275*, 38722−38730.
45. Kumar, V. D., Harrison, R. W., Andrews, L. C., and Weber, I. T. (1992) Crystal structure at 1.5-Å resolution of d(CGCICICG), an octanucleotide containing inosine, and its comparison with d(CGCG) and d(CGCGCG) structures, *Biochemistry 31*, 1541−1550.
46. Cleland, W. W. (1992) Low-barrier hydrogen bonds and low fractionation factor bases in enzymatic reactions, *Biochemistry 31*, 317−319.

BI0496743

THE JOURNAL OF BIOLOGICAL CHEMISTRY
Vol. 278, No. 10, Issue of March 7, pp. 8238–8243, 2003
Printed in U.S.A.

A Potent Cell-active Allosteric Inhibitor of Murine DNA Cytosine C^5 Methyltransferase*

Received for publication, September 25, 2002, and in revised form, November 25, 2002
Published, JBC Papers in Press, December 10, 2002, DOI 10.1074/jbc.M209839200

James Flynn‡, Jing-Yuan Fang§, Judy A. Mikovits¶, and Norbert O. Reich‡¶‖

From the ‡Department of Chemistry and Biochemistry and Program in Biochemistry and Molecular Biology, University of California, Santa Barbara, California 93106, the §Shanghai Institute of Digestive Diseases, Shanghai, China, and ¶EpiGenX Pharmaceuticals, Pacific Technology Center, Santa Barbara California, 93111

The major DNA cytosine methyltransferase isoform in mouse erythroleukemia cells, Dnmt1, exhibits potent dead-end inhibition with a single-stranded nucleic acid by binding to an allosteric site on the enzyme. The previously reported substrate inhibition with double-stranded substrates also involves binding to an allosteric site. Thus, both forms of inhibition involve ternary enzyme-DNA-DNA complexes. The inhibition potency of the single-stranded nucleic acid is determined by the sequence, length, and most appreciably the presence of a single 5-methylcytosine residue. A single-stranded phosphorothioate derivative inhibits DNA methylation activity in nuclear extracts. Mouse erythroleukemia cells treated with the phosphorothioate inhibitor show a significant decrease in global genomic methylation levels. Inhibitor treatment of human colon cancer cells causes demethylation of the *p16* tumor suppressor gene and subsequent p16 re-expression. Allosteric inhibitors of mammalian DNA cytosine methyltransferases, representing a new class of molecules with potential therapeutic applications, may be used to elucidate novel epigenetic mechanisms that control development.

The patterns of DNA cytosine methylation in mammals evolve throughout development (1). This essential process regulates imprinted genes, X chromosome inactivation, the inactivation of repetitive elements, and the expression of tissue-specific genes (2, 3). Methylated DNA is recognized by several proteins and assembled into transcriptionally silent chromatin structures. Gene regulatory regions, including normally undermethylated CpG islands, become hypermethylated with age and in tumors, thereby repressing the expression of essential genes (2, 4, 5). Changes in DNA methylation and AdoMet-dependent DNA cytosine methyltransferase (DCMTase)[1] activity appear early in tumorigenesis. These and other observations have motivated and continue to motivate the development of DCMTase inhibitors as potential "epigenetically based" drugs (2, 6, 7). Thus, antisense oligonucleotides that interfere with DCMTase expression inhibit tumor formation (8), and the cancer drug 5-aza-deoxycytidine (5AC; decitabine) functions by inhibiting DCMTase (9, 10). 5AC virtually abolished adenoma formation in mice genetically prone to colon tumors (11). 5AC is a clinically administered mechanism-based inhibitor of DCMTase. Unfortunately, it may be too carcinogenic and mutagenic for most applications (10). Targeting DCMTase function with novel inhibitors has great therapeutic potential, and novel regulators could help elucidate the aspects of epigenetic control that occur throughout development (2, 6, 12).

The major eukaryotic DCMTase, Dnmt1, has been cloned and sequenced from at least five animal sources: mouse, human, chicken, frog, and sea urchin (13–17). Several variants have been identified that arise from separate gene loci and alternatively spliced mRNAs (1, 3). Dnmt1 is the largest DCMTase, with a molecular mass of 184 kDa. The smaller C-terminal domain shares sequence homology with all DCMTases and contains all or the majority of the residues required for catalysis. Mammalian methylation occurs predominately within the context of the CpG dinucleotide. The N-terminal domain contains a phosphorylation site (18) as well as zinc (19), nucleic acid (20–23), and protein-binding elements (24). The large N-terminal domain is likely to play an active role in the complex interplay with several proteins including histone deacetylases and other Dnmts, leading to the active restructuring of chromatin (1). A previous report postulating such protein-protein interactions proposed that the substrate inhibition of Dnmt1 at high DNA concentrations results from the loss of activating Dnmt1-Dnmt1 interactions with adjacent enzyme molecules on the same DNA scaffold (25).

Early evidence indicated that Dnmt1 binds a second DNA molecule at an unidentified allosteric site (20, 21) and that N-terminal domain-derived peptides bind nucleic acids (26). These interactions recently have been characterized in detail (22, 27–29). The N-terminal domain comprising the first 501 amino acids represses the methylation reaction of the human Dnmt1; this repression is relieved upon binding to methylated DNA (23). A similar stimulation was reported for murine Dnmt1 upon the addition of fully methylated double-stranded DNA, again leading to the proposal that the enzyme forms a ternary enzyme-DNA-DNA complex (30). Another form of allosteric Dnmt1 activation, in this circumstance involving single-stranded substrates with the potential of forming transient duplexes, has been described for oligonucleotides containing 5-methylcytosine adjacent to the CpG site that undergoes methylation (31, 32). Many of these nucleic acid-mediated effects appear to depend on the nature of the DNA substrate upon which the enzyme is initially positioned. For example, although poly(dI·dC) and hemimethylated $(CGG/CCG)_{12}$, a 36-bp fragment containing the triplet repeat sequence in which expansion in the *FMR1* gene causes fragile-X syndrome, show complex kinetics consistent with DNA binding to an allosteric site, no such behavior is observed with unmethylated (CGG/

* The costs of publication of this article were defrayed in part by the payment of page charges. This article must therefore be hereby marked "*advertisement*" in accordance with 18 U.S.C. Section 1734 solely to indicate this fact.

‖ To whom correspondence should be addressed: Dept. of Chemistry and Biochemistry, University of California, Santa Barbara, CA 93106. E-mail: reich@mail.chem.ucsb.edu.

[1] The abbreviations used are: DCMTase, DNA cytosine methyltransferase; 5AC, 5-aza-deoxycytidine (decitabine); MEL, mouse erythroleukemia cells; AdoMet, *S*-adenosylmethionine; CRE, cAMP-response element; MSP, methyl-specific PCR; 5-^{m}C, 5-methylcytosine residue.

$CCG)_{12}$ (22, 23). The biological role most frequently invoked for allosteric regulation of Dnmt1 via DNA binding is in the context of "methylation spreading," a process leading to *de novo* DNA methylation of previously ummethylated regions (30, 34–36). This bidirectional spreading, which occurs in newly integrated viral DNA (36), in gene regulatory sequences during X chromosome inactivation (37), and during cellular immortalization (38), in transposed DNA sequences (39), may be a threat to the success of gene therapy (40).

Our interests were to address the mechanism of the well known substrate inhibition that underlies much of the complex kinetics reported for Dnmt1 and to further characterize the interactions of the enzyme with several single-stranded DNA molecules that were previously shown to be poor substrates for the enzyme (41). The enzyme binds these poor substrates with affinities comparable with substrates that are readily methylated (21), and we hypothesized that they might act as dead-end inhibitors. A previous report of nucleic acids that bind Dnmt1 but are poor substrates showed that various single- and double-stranded nucleic acids can act as inhibitors (42). Here we report the mechanism of action of one such single-stranded inhibitor and demonstrate its ability to inhibit methylation *in vitro*.

EXPERIMENTAL PROCEDURES

Materials—S-Adenosyl-L-[*methyl*-^{3}H]methionine (75 Ci/mmol, 1 mCi/ml = 37 GBq) was purchased from Amersham Biosciences. Unlabeled AdoMet (Sigma) was further purified as described (43). Routinely, 125 μM AdoMet stocks were prepared at a specific activity of 5.8×10^3 cpm/pmol. Two lots of poly(dI·dC-dI·dC) were purchased from Amersham Biosciences, with an average length of 6250 and 5000 base pairs. DE81 filters were purchased from Whatman. LipofectAMINE was purchased from Invitrogen. Other standard chemicals and reagents were purchased from Sigma or Fisher Scientific. Oligonucleotides were synthesized by Research Genetics (Huntsville, AL) and HPLC-purified on a Dynamax PureDNA column (Rainin Instrument Co.) according to the manufacturer's specifications. Oligonucleotides were stored in 10 mM Tris, pH 8.0, 1 mM EDTA. The following sequences were prepared (GC-box p^{MET}, LC2, and the antisense sequence (8) have a phosphorothioate backbone; all others contain a deoxyribose backbone; M superscript denotes 5-methylcytosine; the numbers refer to nucleotide length; the recognition CpG dinucleotides are underlined and bold): 30, GC-box^b, d(CTGGATCCTTGCCC**CG**CCCCTTGAATTCCC); 30, GC-box^a, d(GGGAATTCAAGGGG**CG**GGGCAAGGATCCAG); 30, LC2, d(CTGGATCCTTGCC*AAAA*CCCTTGAATTCCC); 30, GC-box^{bMET}, d(CTGGATCCTTGCC^M**CG**CCCCTTGAATTCCC); 30, GC-box^{pMET}, d(CTGGATCCTTGCCC ^{M}**CG**CCCCTTGAATTCCC); 50, GC-box^{cMET}, d(CCTACCCACC-(GC-box b^{MET})-AACCCTCCAC); 22, GC-box^{dMET}, d(ATCCTTGCCC^M**CG**CCCCTTGAAT); 14, GC-box^{eMET}, d(TTGCCC ^{M}**CG**CCCCTT); 30, CRE, d(GGGAATTCAAATGA^M**CG**TCAAAAGGATCCAG); 20, antisense, d(TCTATTTGAGTCTGCCATTT).

Concentrations were determined using calculated coefficients, and the annealing of GC-box$^{a/b}$ was as described previously (41). Dnmt1 was isolated from mouse erythroleukemia cells (MEL cells) as described (41).

Methyltransferase Assays—Filter binding assays monitored the incorporation of tritium-labeled methyl groups into DNA. Reaction and dilution buffers and filter processing were described previously (20). Incubations were at 37 °C for 60 min. Each point represents the average of at least two reactions.

Substrate Inhibition—Initial velocity data were collected with a 6250-base pair poly(dI·dC) and a 30-base pair GC-box$^{a/b}$ substrate. The poly(dI·dC) concentrations were ~2.0, 4.0, 8.0, 16, 35, 80, 160, 250, 400, 700, and 1000 picomolar in duplex DNA; Dnmt1 was 3.0 nM. The GC-box$^{a/b}$ substrate concentrations were (0.20, 0.40, 1.0, 2.0, 4.0, 8.0, 15, 23, and 35 μM); Dnmt1 was 100 nM.

Inhibition with Single-stranded Oligonucleotides—Initial velocity data were collected with poly(dI·dC), AdoMet, GC-box^b, and GC-box^{bMET} at the concentrations indicated in Fig. 2 legend. Dnmt1 was either 3 or 4 nM (see Fig. 2 legend), AdoMet was 10 μM when added as the nonchanging substrate, and poly(dI·dC) was 50 pM when added as the nonchanging substrate. IC_{50} determinations with GC-box^{bMET}, GC-box^{pMET}, GC-box^{cMET}, GC-box^{dMET}, GC-box^{eMET}, and CRE used 4 nM Dnmt1 and 50 pM poly(dI·dC). Oligonucleotide concentrations ranged between 5-fold lower and 5-fold higher than the IC_{50}.

Nuclear Extract Assays—MEL nuclear extracts were prepared as described previously (41). Freshly made nuclear extract (2 μl) was combined with 12.5 μM tritiated AdoMet, 1 nM poly(dI·dC), and varying concentrations of oligonucleotides in a volume of 20 μl at 37 °C. The reaction was stopped after 60 min, and label incorporation into DNA was determined as described (41).

Mouse Erythroleukemia Cell Studies—MEL cells, prepared as described (41) to a density of 10^6/ml, were treated with inhibitors (7.7 μM GC-box^{pMET}, 1.5 μM 5AC, or 18 μM antisense oligonucleotide) along with LipofectAMINE as described by the manufacturer. The mock treatment used TE (Tris, pH 8.0 (10 mM), and EDTA, 1 mM) in place of any inhibitor. The inhibitors or the mock were added only at the initiation of the experiment, and genomic DNA was isolated after 72 and 110 h of cell culture. 5-Methylcytosine content was determined as described (44). Briefly, *Msp*I endonuclease was used to digest the genomic DNA, and the samples were then treated sequentially with calf intestinal alkaline phosphatase, T4 polynucleotide kinase (and [γ-^{32}P]ATP), and P1 nuclease. The ^{32}P end-labeled cytosines, either 5-^{m}CMP or CMP within the CpG of the *Msp*I ends, were separated on cellulose thin layer chromatography plates. A PhophorImager (Amersham Biosciences) was used to visualize and quantify the percent 5-methylcytosine. Each reported result is the average of at least two independent determinations.

Human Colon Cancer Cell Studies—HT29 cells were plated at 50% confluence in six-well plates and treated with 5AC at 1 μM or LipofectAMINE-transfected with either 10 μM GC-box^{bMET} or LC2 control oligonucleotides for 48–72 h. The LC2 control is identical to GC-box^{bMET} with the four central bases converted to adenines. DNA was isolated using the Qiagen blood and cell culture DNA kit (Qiagen) according to the manufacturer's instructions. Methyl-specific PCR (MSP) was performed as described previously (45) using primers described therein. Peripheral blood lymphocytes were used as a positive control for unmethylated *p16*, and peripheral blood lymphocyte DNA, methylated *in vitro* using *Sss*I methylase (New England Biolabs) according to the manufacturer's instructions, was used as a positive control for methylated *p16*. RNA was isolated using Trizol (Invitrogen). cDNA was prepared from 1 μg of RNA using a Superscript II reverse transcription system with random hexamers as primers (Invitrogen). PCR was performed using primers for *p16* designed to cross a splice junction in the gene (GenBank™ accession number L27211), 5′-ATC ATC AGT CAC CGA AGG TC-3′ (sense) and 5′-CCA CAT GAA TGT GCG CTT AG-3′ (antisense), on 1 μl of cDNA product. The reaction was initiated with a 3-min incubation at 94 °C followed by 35 amplification cycles (94 °C for 30 s, 58 °C for1 min, 72 °C for 1 min) and a final 10 min extension step of 10 min yielding a 355-bp product following electrophoresis on a 1.5% agarose gel. The gel was stained with ethidium bromide and photographed. Expression of β-actin was used as a standard for RNA integrity and equal gel loading. Primers for β-actin were 5′-GGA GTC CTG TGG CAT CCA CG-3′ (sense) and 5′-CTA GAA GCA TTT GCG GTG GA-3′ (antisense). Amplification was the same as p16 with the exception of using an annealing temperature of 60 °C and 27 amplification cycles.

RESULTS AND DISCUSSION

The original observation by Linn and co-workers (25) that hemimethylated duplex plasmid DNA and single-stranded DNA are inhibitory at high concentrations was explained with an interesting model in which Dnmt1 associates with itself upon the DNA scaffold at low ratios of DNA to enzyme, thereby activating the enzyme. Monomeric enzyme-DNA complexes are stabilized with excess substrate, thus leading to a loss of the activated form. An alternative explanation for this behavior at high DNA concentrations is the formation of an inhibitory ternary complex involving the enzyme and two or more DNA molecules. Although recent reports provide data consistent with this alternative explanation (23, 30), we sought to provide a simple probe of the underlying mechanism. Fig. 1 shows our results with a large multi-site 6250-bp poly(dI·dC) substrate and a short 30-bp GC-box$^{a/b}$ duplex containing a single CpG site. The GC-box$^{a/b}$ duplex is an excellent substrate for Dnmt1 and contains an Sp1 transcription factor recognition element (41). We and others have demonstrated that poly(dI·dC) shows inhibition at high DNA concentrations (20, 23, 46), which is revealed by the data in Fig. 1. The relative velocities *versus* S/K_m plots conveniently normalize the data between the two

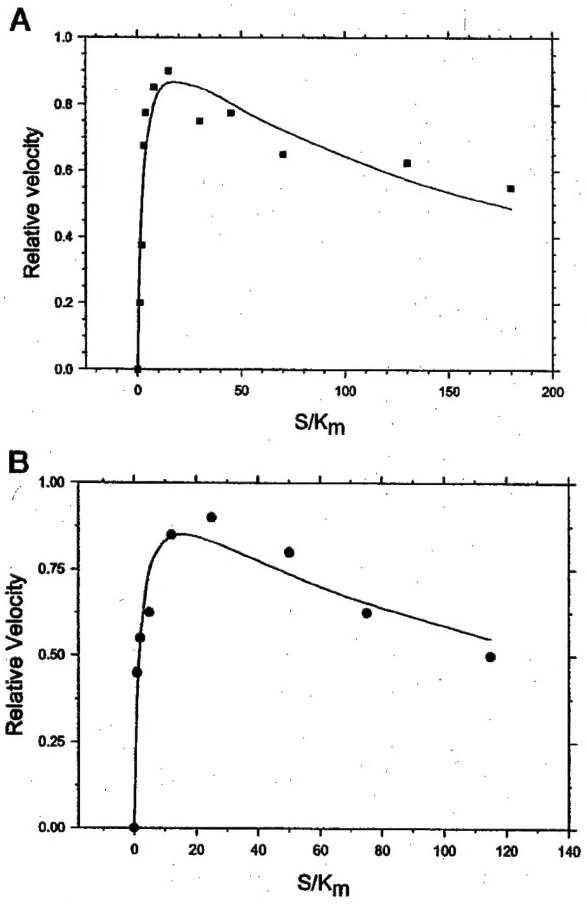

FIG. 1. **DNA substrate inhibition of Dnmt1.** *A*, initial velocity plots of DNA methyltransferase activity with poly(dI·dC:dI·dC) (6250 bp) and GC-box$^{a/b}$ (30 bp). For a direct comparison, the data are expressed in an S/K_m ratio (for DNA). The poly(dI·dC:dI·dC) concentrations were 2.0, 4.0, 8.0, 16, 35, 80, 160, 250, 400, 700, and 1000 pM. Dnmt1 concentration was 3.0 nM. *B* shows data in which GC-box$^{a/b}$ (0.20, 0.40, 1.0, 2.0, 4.0, 8.0, 15, 23, and 35 μM) was used with 100 nM Dnmt1. The lines represent the best fit to the data using a model of simple substrate inhibition (formation of an inactive, ternary enzyme-substrate-substrate complex).

diverse DNA substrates. The short 30-bp duplex nearly matches the footprint of the Dnmt1-DNA complex (20), and we reasoned that this substrate would be precluded from stabilizing the types of complexes proposed by Linn and coworkers (25). As shown in Fig. 1, the GC-box$^{a/b}$ duplex shows the same form of substrate inhibition as the much larger poly(dI·dC). The poorer affinity observed with the 30-bp duplex limited our ability to take the S/K_m ratio as high as with the poly(dI·dC); nevertheless, both sets of data are nicely fit to a standard equation for substrate inhibition, invoking formation of an inhibitory ternary enzyme-DNA-DNA complex (47).

Our results provide compelling support for a mechanism involving the binding of a second double-stranded DNA molecule to an allosteric site on Dnmt1. The observed inhibition with the short duplex DNA (Fig. 1) is unlikely to come from the preferential stabilization of monomeric enzyme forms, because these short substrates were designed to be incapable of stabilizing such complexes under any enzyme concentrations. In this circumstance limited to unmethylated duplexes (poly(dI·dC) or GC-box$^{a/b}$), the binding of a second DNA molecule is inhibitory. We recently confirmed this result with unmethylated DNA and another assay, showing that the ternary enzyme-DNA-DNA complexes dramatically decrease the processive action of the enzyme on multi-site substrates by increasing the off-rate from the substrate DNA.[2] Such an increased off-rate could have the same effect with the single-site substrate (GC-box$^{a/b}$) if the off-rate and methylation rates are comparable. In contrast to these inhibitory allosteric effects, we and others (Ref. 30 and footnote 2) have shown that methylated DNA activates Dnmt1. This occurs in *trans*, with 5-methylcytosine attached to DNA other than that being methylated, and in *cis*, when introduced on the same molecule at positions adjacent to the target methylation sequence (CpG) (31, 48)).[3] It remains unclear whether the activation and inhibition effects are mediated by nucleic acid binding to the same allosteric site.

Dnmt1 shows good activity with single-stranded plasmid-derived substrates (25) and single-stranded oligonucleotides (Refs. 31 and 34, and footnote 3); we previously determined this with single-stranded versions of CRE, a *cis*-regulatory transcriptional element (41). Some single-stranded oligonucleotides are proposed to form transient duplexes that are then acted upon by the enzyme (31); the CRE and GC-box-derived single strands used in our study show no such behavior (41). In contrast to the CRE-derived strands, single-stranded substrates mimicking the GC-box element, showed no detectable activity (41) despite the ability of the enzyme to bind such sequences with good affinity (21). We therefore speculated that the single-stranded GC-box oligonucleotides could act as dead-end inhibitors of the enzyme. We submitted GC-box^{b} single-stranded DNA to a detailed inhibition analysis; the double reciprocal plots are shown in Fig. 2*A*. The pattern of lines intersects far to the left of the *y* axis and is best fit by a standard equation for noncompetitive inhibition. The inhibition constants were determined to be $K_{is} = 3.6 \pm 1.5$ μM and $K_{ii} = 6.8 \pm 1.2$ μM (49). K_{ii} describes the inhibition constant for the enzyme-substrate complex, and K_{is} the inhibition constant for the free enzyme. The K_{ii}/K_{is} ratio is a measure of which binding event is preferred (49), and in this case, its value of 1.9 suggests that this inhibitor slightly favors addition to the free enzyme over the enzyme-DNA complex. Thus, the pattern shows that the free enzyme can bind to single-stranded GC-box^{b}, as can the binary enzyme-poly(dI·dC) complex. In both cases the enzyme is inhibited. The latter ternary complex requires that GC-box^{b} binds to an allosteric site.

Dead-end inhibition with a CpG methylated homolog of GC-box^{b}, GC-box^{bMET}, also exhibited noncompetitive inhibition (Fig. 2*B*). Remarkably, a single 5-^{m}C substitution reduces the inhibition constant associated with the allosteric site 340-fold, as $K_{ii} = 20 \pm 3$ nM. The pattern of lines is visibly less convergent than in Fig. 2*A*, and $K_{ii}/K_{is} = 0.57$. The unmethylated and methylated inhibitors have distinct partitioning preferences as suggested by the changes in binding affinity and K_{ii}/K_{is}. These results strongly suggest that GC-box^{bMET} and poly(dI·dC) can and do bind preferentially to distinct sites on Dnmt1, with the single methyl moiety driving that preference in the favor of the allosteric site.

The initial velocity patterns obtained by varying AdoMet and GC-box^{bMET} concentrations were best fit to a standard equation for competitive inhibition (Fig. 2*C*). The intersection of the fit lines on the 1/velocity axis, $K_{is} = 25 \pm 10$ nM, suggests that GC-box^{bMET} and AdoMet bind competitively to the same poly(dI·dC)-bound form of the enzyme but not necessarily to the same site on the enzyme. The inhibition constants determined for GC-box^{bMET} at the proposed allosteric site, K_{is} in Fig. 2*C* and K_{ii} in Fig. 2*B*, are in good agreement at about 30 nM. In the absence of poly(dI·dC), GC-box^{bMET} binds free enzyme with a dissociation constant of 880 nM (21). Therefore, poly(dI·dC) stabilizes GC-box^{bMET} binding 29-fold.

[2] Z. Svedruzic and N. O. Reich, submitted for publication.
[3] B. Aubol and N. O. Reich, submitted for publication.

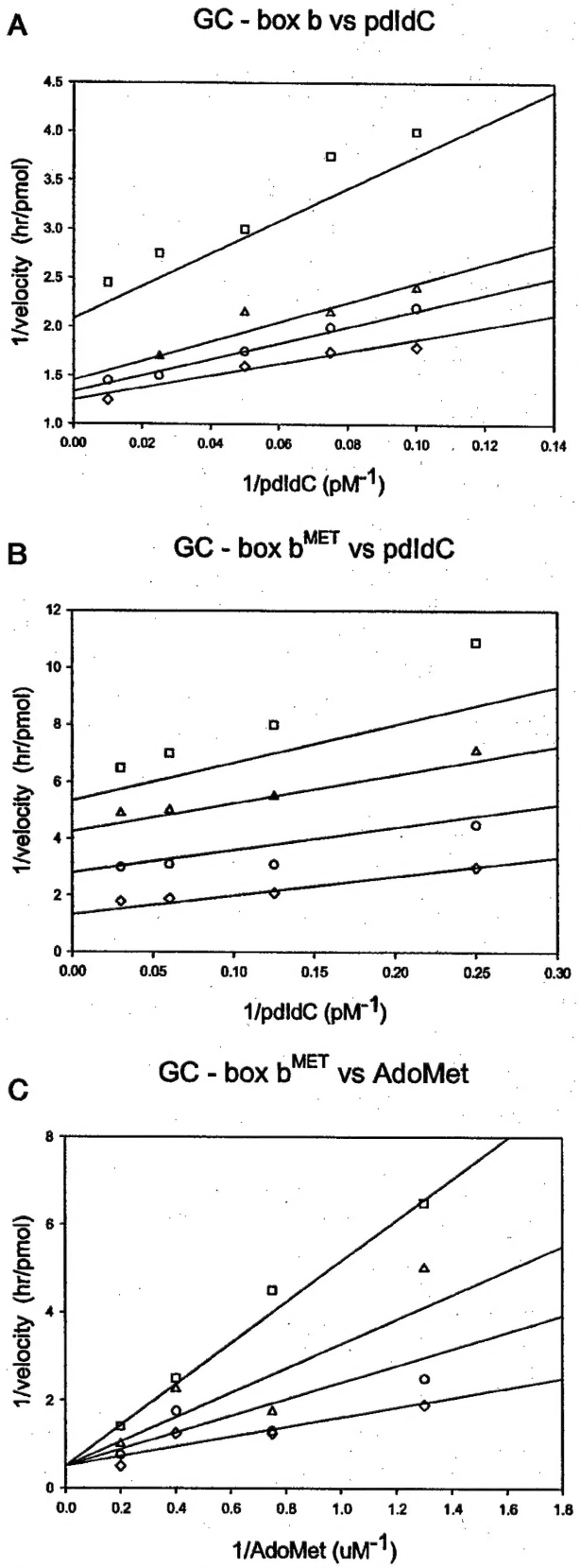

FIG. 2. **Dead-end inhibition of DNA methyltransferase.** *A*, double reciprocal plot of velocity *versus* poly(dI·dC) (10, 13, 20, 40, and 100 pM) with varying GC-box^{b} concentrations: 0 (*diamonds*), 0.75 (*circles*), 1.5 (*triangles*), and 5.0 μM (*squares*). All reactions contained 3.0 nM Dnmt1 and 10 μM AdoMet. Experimental data are shown scattered around lines derived from the fit to the standard noncompetitive equation: $v = V \times S/(K_m \times (1 + I/K_{is}) + S \times (1 + I/K_{ii})$. Increasing concentrations of the nonvaried inhibitor align upward from the *x* axis. *B*, double reciprocal plot of velocity *versus* poly(dI·dC) (1.5, 3.0, 7.5, 15, and 20 pM) with varying GC-box^{bMET} concentrations: 0 (*diamonds*), 30 (*circles*), 60 (*triangles*), and 90 nM (*squares*). All reactions contained 4.0 nM Dnmt1 and 10 μM AdoMet. Experimental data are shown scattered around lines derived from a fit to the standard noncompetitive equation, and increasing concentrations of the nonvaried inhibitor align upward from the *x* axis. *C*, double reciprocal plot of velocity *versus* AdoMet (0.75, 1.5, 3.0, and 6.0 μM) with varying GC-box^{bMET} concentrations: 0, 20, 40, and 80 nM. All reactions contained 4.0 nM Dnmt1 and 50 pM poly(dI·dC). Experimental data are shown scattered around lines derived from a fit to the standard equation for competitive inhibition, $v = V \times S/(K_m (1 + I/K_{is}) + S)$. Increasing concentrations of the nonvaried inhibitor align upward from the *x* axis.

TABLE I

In vitro inhibition analysis of oligonucleotides

The concentration of inhibitor required to achieve 50% inhibition of a control reaction was determined for each and is shown as the IC_{50}. K_{ii} values were estimated from the mechanistic studies in Fig. 2 (ND, not determined). All data were collected in triplicate, and estimated errors are less than 10%.

Name	K_{ii}	IC_{50}
	nM	
GC-box^{b}	6800	ND
GC-box^{bMET}	20	15
GC-box^{pMET}	ND	5
GC-box^{cMET}	ND	30
GC-box^{dMET}	ND	50
GC-box^{eMET}	ND	150
CRE	ND	>300

The binding of these duplex and single-stranded nucleic acids to a site on Dnmt1 distinct from the substrate-binding site is intriguing. The evidence for the existence of such an allosteric site is compelling: (i) the substrate inhibition described in Fig. 1 for both long and short substrates is best explained by the binding of a second DNA molecule; (ii) noncompetitive, dead-end inhibition by single-stranded oligonucleotides (Fig. 2, *A* and *B*) was dramatically enhanced when the inhibitor contained 5-methylcytosine; (iii) no inhibition with either GC-box^{b} or GC-box^{bMET} was observed with two bacterial DNA cytosine methyltransferases, M.*Hha*I and M.*Sss*I (data not shown); (iv) previous product inhibition studies support a Dnmt1-DNA-DNA ternary complex (20, 22, 23, 25); (v) DNA concentrations 10 times higher than K_m produce a second, less mobile band by gel mobility shift assays (20); (vi) short peptides from the N terminus of Dnmt1 have primary sequence similarity to zinc fingers and bind double-stranded DNA, although single-stranded DNA was not tested (24).

Allosteric enzyme regulators provide a novel approach to alter enzyme function and thus to introduce new strategies for drug design (50). Because GC-box^{bMET} is a potent allosteric inhibitor, we sought to define those features that are essential for its activity. Derivatives of GC-box^{bMET} were tested to determine how length, base, and backbone composition affect Dnmt1 inhibition (Table I). The IC_{50}, defined as that concentration of inhibitor that causes 50% inhibition of the methylation reaction with poly(dI·dC), increased 2-fold in going from 30 to 50 nucleotides, being 15 and 30 nM, respectively. Significantly weaker binding was observed with 22 and 14 nucleotide lengths. Thus the enzyme appears to interact with at least 30 nucleotides through this allosteric site. Changing the backbone to a phosphorothioate, GC-box^{pMET}, decreased the IC_{50} from 15 nM for the comparable 30-nucleotide GC-box^{bMET} to 5 nM. This 3-fold better binding could derive from various effects, including altered electrostatics to subtle changes in the allowed conformations of the oligonucleotides. Sequence specificity was demonstrated with CRE^{aMET}, a relatively adenine/thymine-rich element compared with the GC-box inhibitors. CRE^{aMET}

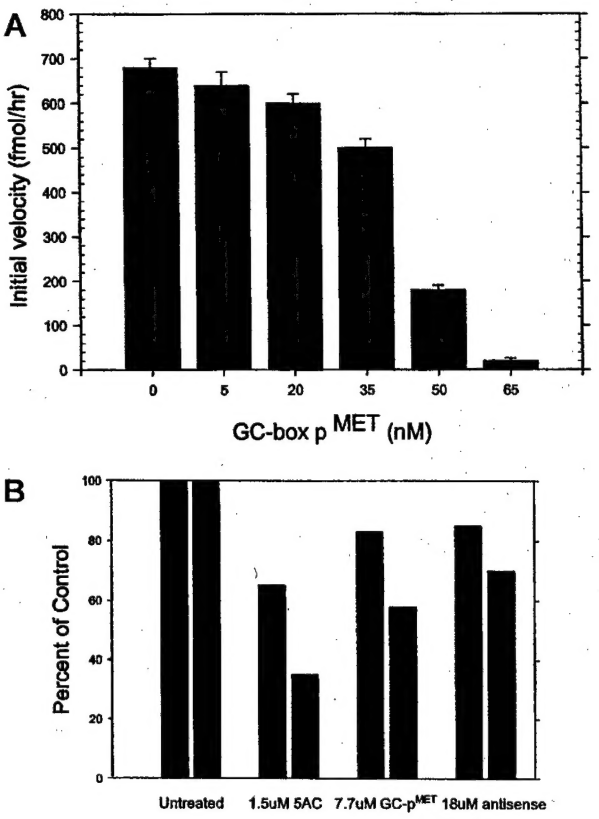

FIG. 3. **DCMTase inhibition by GC-box p^{MET} in nuclear extracts and in MEL cell culture.** *A*, GC-box^{pMET} decreases DCMTase activity in a MEL nuclear extract. Reactions (20 μl) were done in triplicate and contained 2 μl of nuclear extract, 12.5 μM AdoMet, and 1 nM poly(dI·dC). Standard errors are shown. *B*, DCMTase inhibitors decrease the global 5-^{m}C content of genomic DNA. MEL cell cultures were seeded in six-well plates at 2.5×10^4 cells/ml and either mock treated or treated with 1.5 μM 5AC, 7.7 μM GC-box^{pMET}, or 18 μM antisense to Dnmt1. After 72 (*left-hand bars*) and 110 h (*right-hand bars*) incubation, genomic DNA was isolated, and the 5-^{m}C content was determined twice and averaged (20).

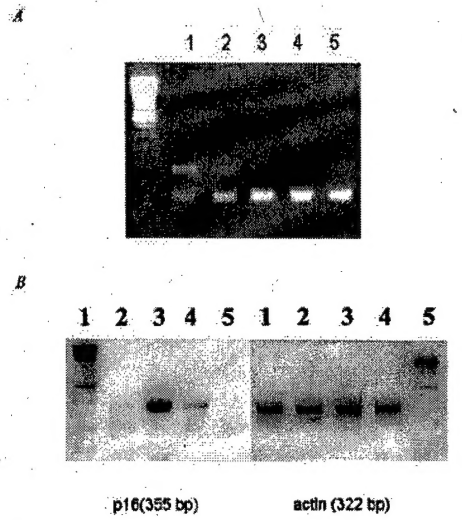

FIG. 4. **Methylation status and expression of p16 in HT29 following treatment with GC-box^{bMET}.** HT29 cells were plated at 50% confluence in six-well plates and treated with 5AC at 1 μM or LipofectAMINE transfected with 10 μM GC-box^{bMET} or LC2 control oligonucleotides for 48–72 h. RNA and DNA were extracted according to standard protocols. DNA was bisulfite-modified, and the methylation pattern of the p16 promoter was determined by MSP using primer specific for methylated DNA. MSP PCR: *A*, *lane 1*, untreated HT29; *lane 2*, LC2 10 μM; *lane 3*, GC-box^{bMET} 10 μM; *lane 4*, 5AC 1 μM; *lane 5*, 5AC 0.1 μM. *B*, RT PCR of p16 expression, *left panel*: *lane 1*, molecular weight marker; *lane 2*, no treatment; *lane 3*, 5AC 1 μM; *lane 4*, GC-box^{bMET} 10 μM; *lane 5*, LC2 10 μM. *Right panel*, actin as an amplification control with the same lane designations as for the *left panel*.

was at least 60-fold less inhibitory than our most potent inhibitor, GC-box p^{MET} (Table I), and showed competitive inhibition against poly(dI·dC) (data not shown). We suggest that CRE^{aMET} and the substrate DNA (poly(dI·dC)) bind the same form of the enzyme, a binding that most likely occurs at the active site. This is supported by our observations that the nonmethylated version of CRE^{aMET} (CRE a) is an excellent substrate for Dnmt1 (41) and that CRE^{aMET} shows competitive inhibition.

Our data provide the first evidence that an allosteric site on Dnmt1 shows DNA sequence preferences, which almost certainly opens up novel regulatory pathways. The data provided here and by others show that one or more allosteric site(s), most likely residing within the N-terminal domain, can bind double- or single-stranded nucleic acids. This binding is highly dependent on methylation status and DNA sequence, as well as on length and backbone composition. Although much needs to be learned about the site within the protein, its interactions with nucleic acids, and its biological role, there can be no question that the function of Dnmt1 is regulated by an allosteric mechanism.

Novel *in vitro* modulators of DCMTase activity could possibly alter genomic methylation patterns, alter gene expression and control the unrestricted proliferation of cancerous cells (3, 6, 51). The epigenetic inactivation of genes is as important a driving force in tumorigenesis as the inactivation of genes by mutation (52). Epigenetic transcriptional repression has been demonstrated in diverse tumor types including tumor suppressor genes, DNA repair genes, cell-cycle genes, and genes involved in invasion and metastasis (5, 12, 52). The re-expression of such genes in tumor cells leads to cell growth suppression and altered sensitivity to existing cancer therapies. However, despite encouraging results with available approaches to alter cellular DNA methylation, there is clearly a need for potent Dnmt1 inhibitors with improved drug characteristics (3, 6, 51). Based on the nanomolar potency of GC-box^{pMET}, its novel mechanism of inhibition, and its phosphorothioate backbone, we sought to determine whether this compound could alter methylation in nuclear extracts as well as in cells. We tested the effectiveness of GC-box^{pMET} in nuclear extracts from MEL cells (41). Potent inhibition of DNA methylation was observed with an IC_{50} of 45 nM (Fig. 3*A*). A direct comparison with our results obtained with purified Dnmt1 (Table I) is complicated by several factors, such as Dnmt1 concentration and allosteric site accessibility. If significant levels of other DCMTase family members exist in MEL nuclear extracts (1, 3), then the inhibitor appears to regulate them also, because methylation activity was potently decreased to background levels.

To test the efficacy of the inhibitor in intact cells, we treated MEL cells with a mock inhibitor solution, 1.5 μM 5AC, 7.7 μM GC-box^{pMET}, or 18 μM of an antisense to Dnmt1 mRNA. The antisense oligonucleotide was previously shown to alter cellular DNA methylation levels and is in Phase II clinical trials for the treatment of cancer (8). Genomic DNA was isolated after 72 and 110 h of cell culture, and the percentage of 5-^{m}C within CpG sites was used to assess genomic methylation levels (44). The 5-^{m}C content decreased in a time-dependent manner in all treatment cases (Fig. 3*B*). A decrease in 5-^{m}C was evident after 110 h using 5AC (Fig. 3*B*). Likewise, GC-box^{pMET} was effective in reducing the 5-^{m}C content, whereas the Dnmt1 antisense oligonucleotide was the least effective. Although it was not as

effective as 5AC under these conditions, GC-box^{pMET} did not appear to damage the cells; 5AC did damage the cells, resulting in significant degradation of cellular DNA. These results on genomic methylation levels were complemented by our characterization of the impact of the inhibitor on the methylation of a specific locus, in which inappropriate methylation was previously shown to cause gene expression changes leading to tumorigenesis. The HT29 human colon cell line was used to examine the ability of LipofectAMINE-transfected GC-box^{bMET} to cause gene-specific demethylation of the tumor suppressor gene, *p16* (12, 53). The aberrant methylation of the CpG island associated with the *p16* gene occurs in diverse human cancers with frequencies up to 48% (lymphoma), 39% (pancreatic), and 37% (colon) (53). Reversal of this methylation with 5AC treatment results in re-expression of p16. MSP was used to determine the methylation status of individual CpG sites (54). Treatment of the HT29 cells with 5AC results in demethylation (Fig. 4*A*, *lane 4*) and expression of p16 (Fig. 4*B*, *lane 3*) and was used as a positive control. A similar experiment performed with LipofectAMINE-transfected GC-box^{bMET} showed specific demethylation of *p16* (Fig. 4*A*, *lane 3*) and re-expression of the gene (Fig. 4*B*, *lane 4*), whereas a control oligonucleotide (LC2, see "Experimental Procedures") had no effect on p16-specific demethylation in HT29 (Fig 4, *A*, *lane 2* and *B*, *lane 5*). The LC2 control results argue persuasively for a specific effect deriving from the inhibitor on the cellular processes leading to the *p16* CpG island methylation.

In conclusion, we and others have previously identified low affinity interactions between Dnmt1 and various nucleic acids (22, 23, 25, 30, 41, 48, 55), effects that predominately involve the active site of the enzyme. Although the underlying mechanisms remain obscure in most of these cases, it is clear that they are distinct from the inhibition described in this report. Cell-active, tight binding, allosteric Dnmt1 inhibitors may form the basis of a new class of cancer drugs. Such therapies are likely to involve treatment with other epigenetically based drugs, such as histone deacetylase inhibitors, and to complement chemotherapies that are vulnerable to methylation-dependent resistance mechanisms (33). Although oncogenic transformation has been reversed with 5AC, allosteric inhibitors can perhaps separate the beneficial effects of gene reactivation from the known cytotoxic effects of 5AC.

REFERENCES

1. Nakao, M. (2001) *Gene* **278,** 25–31
2. Futscher, B. W., Oshiro, M. M., Wozniak, R. J., Holtan, N., Hanigan, C. L., Duan, H., and Domann, F. E. (2002) *Nat. Genet.* **31,** 175–179
3. Robertson, K. D., and Wolffe, A. P. (2000) *Nat. Rev. Genet.* **1,** 11–19
4. Laiho, P., Launonen, V., Lahermo, P., Esteller, M., Guo, M., Herman, J. G., Mecklin, J. P., Jarvinen, H., Sistonen, P., Kim, K. M., Shibata, D., Houlston, R. S., and Aaltonen, L. A. (2002) *Cancer Res.* **62,** 1166–1170
5. Wajed, S. A., Laird, P. W., and DeMeester, T. R. (2001) *Ann. Surg.* **234,** 10–20
6. Szyf, M. (2001) *Trends Pharmacol. Sci.* **22,** 350–354
7. Brown, R., and Strathdee, G. (2002) *Trends Mol. Med.* **8,** (suppl.) S43–S48
8. Szyf, M., Ramchandani, S., MacLeod, A. R., Pinard, M., and von Hofe, E. (1997) *Proc. Natl. Acad. Sci. U. S. A.* **94,** 684–689
9. Jones, P. A., Taylor, S. M., and Wilson, V. L. (1983) *Recent Results Cancer Res.* **84,** 202–211
10. Jones, P. A., and Laird, P. W. (1999) *Nat. Genet.* **21,** 163–167
11. Laird, P. W., Jackson-Grusby, L., Fazeli, A., Dickinson, S. L., Jung, W. E., Li, E., Weinberg, R. A., and Jaenisch, R. (1995) *Cell* **81,** 197–205
12. Jones, P. A., and Baylin, S. B. (2002) *Nat. Rev. Genet.* **3,** 415–428
13. Bestor, T. H. (1988) *Gene* **74,** 9–12
14. Yen, R.-W. C., Vertino, P. M., Nelkin, B. D., Yu, J. J., El-Eeiry, W., Cumaraswamy, A., Lennon, G. G., Trask, B. J., Celano, P., and Baylin, S. B. (1992) *Nucleic Acids Res.* **20,** 2287–2291
15. Tajima, S., Tsuda, H., Wakabayashi, N., Asano, A., Mizuno, S., and Nishimoi, K. (1995) *J. Biochem.* **117,** 1050–1057
16. Kimura, H., Ishihara, G., and Tajima, S. (1996) *J. Biochem.* **120,** 1182–1189
17. Aniello, F., Locascio, A., Fucci, L., Geraci, G., and Branno, M. (1996) *Gene* **178,** 57–61
18. Glickman, J. F., Pavlovich, J. G., and Reich, N. O. (1997) *J. Biol. Chem.* **272,** 17851–17857
19. Bestor, T. (1992) *EMBO J.* **11,** 2611–2617
20. Flynn, J., and Reich, N. O. (1998) *Biochemistry* **37,** 15162–15169
21. Flynn, J., Azzam, R., and Reich, N. O. (1998) *J. Mol. Biol.* **279,** 101–116
22. Bacolla, A., Pradhan, S., Roberts, R. J., and Wells, R. D. (1999) *J. Biol. Chem.* **274,** 33011–33019
23. Bacolla, A., Pradhan, S., Larson, J. E., Roberts, R. J., and Wells, R. D. (2001) *J. Biol. Chem.* **276,** 18605–18613
24. Chuang, L. S. H., Ian, H.-I., Koh, T.-W., Ng, H.-H., Xu, G., and Li, B. F. L. (1997) *Science* **277,** 1996–2000
25. Hitt, M. M., Wu, T.-L., Cohen, G., and Linn, S. (1988) *J. Biol. Chem.* **263,** 4392–4399
26. Wade, P. A., Wolffe, A. P., and Jones, P. L. (2001) *Proc. Natl. Acad. Sci. U. S. A.* **96,** 5894–5896
27. Pradhan, S., Bacolla, A., Wells, R. D., and Roberts, R. J. (1999) *J. Biol. Chem.* **274,** 33002–33010
28. Kim, G. D., Ni, J., Kelesoglu, N., Roberts, R. J., and Pradhan, S. (2002) *EMBO J.* **21,** 4183–4195
29. Jeltsch, A., Christ, F., Fatemi, M., and Roth, M. (1999) *J. Biol. Chem.* **274,** 19538–19544
30. Fatemi, M., Hermann, A., Pradhan, S., and Jeltsch, A. (2001) *J. Mol. Biol.* **309,** 1189–1199
31. Christman, J. K., Sheikhnejad, G., Marasco, C. J., and Sufrin, J. R. (1995) *Proc. Natl. Acad. Sci. U. S. A.* **92,** 747–7351
32. Baker, D. J., Laayoun, A., Smith, S. S., Lingeman, R. G., and Riley, J. (1994) *J. Mol. Biol.* **243,** 143–151
33. Soengas, M. S., Capodieci, P., Polsky, D., Mora, J., Esteller, M., Opitz-Araya, X., McCombie, R., Herman, J. G., Gerald, W. L., Lazebnik, Y. A., Cordon-Cardo, C., and Lowe, S. W. (2001) *Nature* **409,** 207–211
34. Tollefsbol, T. O., and Hutchison, C. A., III (1997) *J. Mol. Biol.* **269,** 494–504
35. Orend, G., Kuhlmann, I., and Doerfler, W. (1991) *J. Virol.* **65,** 4301–4308
36. Toth, M., Müller, U., and Doerfler, W. (1990) *J. Mol. Biol.* **214,** 673–683
37. Barlow, D. P. (1995) *Science* **270,** 1610–1613
38. Vertino, P. M., Yen, R.-W. C., and Baylin, S. B. (1996) *Mol. Cell. Biol.* **16,** 4555–4565
39. Martienssen, R. (1998) *Trends Genet.* **14,** 263–264
40. Bestor, T. (2001) *J. Clin. Invest.* **105,** 409–411
41. Flynn, J., Glickman, J. F., and Reich, N. O. (1966) *Biochemistry* **35,** 7308–7315
42. Bolden, A., Ward, C., Siedlecki, J. A., and Weissbach, A. (1984) *J. Biol. Chem.* **259,** 12437–12443
43. Reich, N. O., and Mashhoon, N. (1990) *J. Biol. Chem.* **265,** 8966–8970
44. Cedar, H., Solage, A., Glaser, G., and Razin, A. (1979) *Nucleic Acids Res.* **6,** 2125–2132
45. Herman, J. G., Graff, J. R., Myohanen, S., Nelkin, B. D., and Baylin, S. B. (1996) *Proc. Natl. Acad. Sci. U. S. A.* **93,** 9821–9826
46. Pedrali-Noy, G., and Weissbach, A. (1986) *J. Biol. Chem.* **261,** 7600–7602
47. Segel, I. (1975) *Enzyme Kinetics*, John Wiley and Sons, New York
48. Carotti, D., Funiciello, S., Palitti, F., and Strom, R. (1998) *Biochemistry* **37,** 1101–1108
49. Spector, T., and Cleland, W. W. (1981) *Biochem. Pharmacol.* **30,** 1–7
50. Phan, J., Steadman, D. J., Koli, S., Ding, W. C., Minor, W., Dunlap, R. B., Berger, S. H., and Lebioda, L. (2001) *J. Biol. Chem.* **276,** 14170–14177
51. Brown, R., and Strathdee, G. (2002) *Expert. Opin. Investig. Drugs* **11,** 747–754
52. Esteller, M., and Herman, J. G. (2002) *J. Pathol.* **196,** 1–7
53. Esteller, M., Gonzalez, S., Risques, R. A., Marcuello, E., Mangues, R., Germa, J. R., Herman, J. G., Capella, G., and Peinado, M. A. (2001) *J. Clin. Oncol.* **19,** 299–304
54. Paz, M. F., Avila, S., Fraga, M. F., Pollan, M., Capella, G., Peinado, M. A., Sanchez-Cespedes, M., Herman, J. G., and Esteller, M. (2002) *Cancer Res.* **62,** 4519–4524
55. Bigey, P., Knox, J. D., Croteau, S., Bhattacharya, S. K., Theberge, J., and Szyf, M. (1999) *J. Biol. Chem.* **274,** 4594–4606